CHAPTER 3

MODELLING A DELETION OF THE HUMAN REGION 21q11.2–q21.1 IN MICE

3.1 GENERAL OVERVIEW

Haploinsufficiency of human chromosome 21 results in a rare condition known as Monosomy 21. Complete Monosomy 21 typically results in prenatal death, and thus most cases described are partial or mosaic. Patients with Monosomy 21 display a variety of clinical features, including intellectual disability, craniofacial, skeletal and/or cardiac abnormalities, and respiratory complications. In addition, partial deletions of the long arm of human chromosome 21 have also been observed in several types of solid tumours. To search for dosage-sensitive genes involved in these human pathologies, we used chromosome engineering to generate a monosomic mouse model carrying a deletion of the *Lipi* to *Usp25* interval, syntenic with 21q11.2–q21.1 in humans. Haploinsufficiency for the six genes in this interval resulted in no gross morphological defects. Behavioural analysis including open field and measures of anxiety and social interaction were normal in monosomic mice. They did, however, display impaired memory retention compared to control animals, which models the intellectual disability observed in patients with Monosomy 21. Moreover, when fed a high-fat diet (HFD), monosomic mice exhibited a significant increase in fat mass/fat percentage estimate compared with controls, severe fatty changes in their livers, and thickened subcutaneous fat. Thus genes within the *Lipi–Usp25* interval are involved in memory retention and the regulation of fat deposition.

3.2 INTRODUCTION

3.2.1 OVERVIEW OF HUMAN CHROMOSOME 21

Chromosome 21 is the smallest human autosome (Hattori 2000). This acrocentric chromosome spans almost 47 Mb of DNA and corresponds to about 1 – 1.5% of the genome (Hattori 2000). According to the current Ensembl annotation (Human GRChr37), chromosome 21 and contains 232 known protein-coding genes, 7 novel protein-coding genes and 141 pseudogenes. The genomic regions of human chromosome 21 show synteny to mouse genomic regions located on chromosomes 16, 17 and 10 (Hattori 2000). Analysis of the DNA sequence of human chromosome 21 revealed that 81% of known human genes overlapped with mice genes by at least one exon (Frazer 2001).

3.2.2 BRIEF DESCRIPTION OF GENES MAPPED TO THE HUMAN REGION 21q11.2–q21.1

The human region 21q11.2–q21.1 spans 1.7 Mb and contains only eight genes (*LIPI*, *RBM11*, *ABCC13*, *HSPA13*, *SAMSN1*, *AF1651138.1*, *NRIP1*, and *USP25*). Six of these genes, namely *LIPI*, *RBM11*, *HSPA13*, *SAMSN1*, *NRIP1* and *USP25*, are conserved between human and mouse.

The lipase, member 1 (*LIPI*) gene consists of 10 exons and is expressed only in the testis (Wen 2003). The *LIPI* gene encodes a 460 amino acid phospholipase that hydrolyzes phosphatidic acid to produce lysophosphatidic acid (Hiramatsu 2003). Exon sequencing of *LIPI* identified a single nucleotide polymorphism (SNP) (C55Y) in two patients with hypertriglyceridemia, suggesting that this missense mutation might be a causal factor for hypertriglyceridemia. Also, at least one other SNP was found to be associated with variation in plasma cholesterol in unrelated populations (Wen 2003).

The RNA binding motif protein 11 like (*RBM11*) gene consists of 5 exons and is expressed only in the testis (Brun 2003). The full-length isoform of RBM11 (RBM11a) has an RNA recognition motif (a putative RNA-binding domain) that is known to bind single-stranded RNAs (Brun

2003). Two truncated isoforms of RBM11 (RBM11b and RBM11c) are devoid of an RNA recognition motif, and thus are unable to bind single-stranded RNAs (Brun 2003).

The ATP-binding cassette, sub-family C (CFTR/MRP), member 13 (*ABCC13*) pseudogene consists of 14 exons and is expressed in a variety of tissues, including brain, placenta, lung, liver, pancreas, ovary, bone marrow, and in the digestive system, from ileum to rectum, with especially high expression detected in the colon (Yabuuchi 2002). *ABCC13* encodes a 325 amino acid protein that consists of four transmembrane domains homologous to ABCC1 (MRP1), ABCC2 (MRP2), ABCC3 (MRP3) and ABCC6 (MRP6) proteins, but is devoid of Walker A, Walker B, and signature C motifs, and thus results in production of a non-functional ABC protein (Yabuuchi 2002). *ABCC13* belongs to the superfamily of genes encoding ATP-binding cassette (ABC) transporters that are involved in the transport of different molecules across membranes and modulation of ion channels. More specifically, *ABCC13* is a member of the multidrug resistance-associated protein (MRP, ABCC) subfamily of genes that play a role in multidrug resistance (Yabuuchi 2002).

The heat shock protein 70kDa family, member 13 (*HSPA13*) gene (previously known as *STCH*) consists of 5 exons and is constitutively expressed in a variety of tissues, including heart, brain, placenta, lung, liver, skeletal muscle, kidney and pancreas (Otterson 1994). *HSPA13* encodes a 471 amino acid protein that associates with microsome membranes and contains an ATPase domain that shows activity independent of peptide stimulation. HSPA13 belongs to the heat shock protein 70 family, of which members are involved in processing and transport of cytosolic and secretory proteins and disposal of denaturated or misfolded proteins (Otterson 1994). However, in contrast to the other members of the family, HSPA13 is not inducible by heat shock (Otterson 1994).

The SAM domain, SH3 domain and nuclear localization signals 1 (*SAMSN1*) gene (previously known as *HACS1*) consists of 8 exons and is highly expressed in immune tissues and haematopoietic cells, and shows low level expression in many other tissues, including heart, brain, placenta and lung (Claudio 2001). *SAMSN1* encodes a 441 amino acid protein that consists

of an SH3 motif and a SAM domain that are found in adaptor proteins that are involved in signalling pathways, and thus seems to be involved in cytoplasmic signal transduction in cells (Claudio 2001). *SAMSN1* may potentially play a role in the development of haematopoietic tumours, as it is mapped to the 21q11.2 region that is frequently disrupted by translocation events (Mitelman 1997).

The nuclear receptor interacting protein 1 (*NRIP1*) gene consists of 3 exons and is expressed in a variety of tissues, including breast, bone, lung, cervix, ovary, placenta, liver and fibroblast (Cavailles 1995). *NRIP1* encodes a 1158 amino acid protein that contains an amphipathic α-helix that is found in proteins that are involved in ligand-dependent transcription stimulation by nuclear receptors (Cavailles 1995). In fact, NRIP1 modulates the transcriptional activity of the oestrogen receptor by interacting with the hormone-dependent activation domain AF2 of this receptor (Cavailles 1995).

The ubiquitin-specific processing protease 25 (*USP25*) gene consists of 25 exons (Valero 1999). USP25 encodes 3 protein isoforms that are generated by alternative splicing (Bosch-Comas 2006). The USP25a isoform is expressed in a variety of tissues, including brain, heart, kidney, liver, lung, prostate, testis, spleen, thymus, and skeletal muscle (Bosch-Comas 2006). The USP25b isoform is expressed in all the aforementioned tissues except skeletal muscle, however, its level of expression is much lower than that of USP25a (Bosch-Comas 2006). In contrast, the USP25m isoform has a very restricted expression pattern, and can only be detected in heart and skeletal muscle (Bosch-Comas 2006). USP25 belongs to the ubiquitin-specific processing protease (UBP) subfamily of deubiquitinating enzymes that rescue proteins from degradation by the 26S proteasome (Valero 1999). Moreover, the USP25m isoform seems to regulate muscle differentiation and functioning, because it interacts with sarcomeric proteins (Bosch-Comas 2006).

3.2.3 MONOSOMY 21 SYNDROME

The triplication of chromosome 21 (or a subset of genes mapped to the long arm of this chromosome) is responsible for Down syndrome. In contrast, haploinsufficiency of genes on human chromosome 21 results in Monosomy

21. Only partial or mosaic monosomies of chromosome 21 have been diagnosed in living individuals, and thus it is believed that complete monosomy of chromosome 21 results in prenatal death (Joosten 1996; Mori 2004). Clinical phenotypes observed in patients with partial monosomies of chromosome 21 are very heterogeneous. Some patients show only mild to moderate intellectual disability, and have no other apparent dysmorphic or congenital malformations (Wakui 2002; Tinkel-Vernon 2003), while others are diagnosed with a variety of severe clinical symptoms, such as intellectual disability, microcephaly, epilepsy, craniofacial, skeletal, cardiac and/or renal abnormalities, and respiratory difficulties (Chettouh 1995; Riegel 2005; Lyle 2008; Katzaki 2010; Lindstrand 2010; Roberson 2010).

To date, four comprehensive studies have been performed using array comparative genomic hybridization (aCGH) and high-density single nucleotide polymorphism (SNP) genotyping to define the breakpoint regions present in patients with Monosomy 21 and to correlate these breakpoints with phenotype (Lyle 2008; Katzaki 2010; Roberson 2010; Lindstrand 2010).

Array comparative genome hybridization performed by Lyle *et al* identified eight new partial monosomies of chromosome 21 and refined the mapping of three previously described ones (Lyle 2008). All the partial Monosomy 21 cases had unique breakpoints and varied in size, ranging from 1.48 to 18.2 Mb. The identified partial monosomies were subsequently grouped into three broad regions of human chromosome 21 on the basis of observed monosomy phenotype in patients. Deletions within/of the "centromeric" region, from the centromere to around 31.2 Mb, were associated with a severe phenotype, including profound intellectual disability and a variety of craniofacial malformations. No cases with a deletion spanning the entire "medial" region, from 31.2 to 36 Mb, were identified. Only one patient with a partial aneuploidy of the medial region was reported, and this patient had a severe phenotype. The apparent absence of patients carrying a deletion spanning the entire medial region might suggest that haploinsufficiency for genes in this interval results in prenatal death. Deletions within/of the "telomeric" region, from around 36 – 37.5 Mb to the telomere, were associated with a milder phenotype, including mild to moderate intellectual disability, and either the complete absence of craniofacial

malformations or the presence of only minor craniofacial abnormalities (Lyle 2008).

Array comparative genome hybridization performed by Katzaki *et al* identified three new patients with partial monosomies of chromosome 21, spanning the 21q22.11–q22.12 region (Katzaki 2010). All three new cases were diagnosed with severe developmental retardation, dysmorphic malformations, behavioural problems, and thrombocytopenia. Subsequently, they compared clinical symptoms observed in these three new cases with clinical features previously reported in six other patients with the overlapping 21q22.11–q22.12 deletions. They concluded that two potential clinical phenotypes related to the 21q22 microdeletions (including the *RUNX1* gene) could be defined, namely syndromic thrombocytopenia with developmental and growth retardation and thrombocytopenia with/without mild dysmorphic abnormalities (Katzaki 2010).

High-density single nucleotide polymorphism genotyping performed by Robertson *et al* identified ten new partial monosomies of chromosome 21 (Roberson 2010). These cases were divided into two cohorts. Cohort A consisted of three patients that had relatively mild phenotypes characterized by intellectual disability (mild to moderate) and the presence of only a few dysmorphic abnormalities. Cohort B consisted of seven patients that had more severe phenotypes characterized by intellectual disability (moderate to severe, if the severity was assessed), and the presence of multiple congenital anomalies, including craniofacial, cardiac and skeletal defects. They also collected and included information about twelve additional cases of partial Monosomy 21 obtained from the Database of Chromosomal Imbalance and Phenotype in Humans using Ensembl Resources (DECIPHER) (Firth 2009) and commented on three cases described previously by Lindstrand *et al* (Lindstrand 2010; Roberson 2010). The data obtained from all these cases were classified and interpreted according to their locations within the “centromeric”, “medial” or “telomeric” regions of human chromosome 21 described previously by Lyle *et al* (Lyle 2008; Roberson 2010).

Four new cases, two DECIPHER cases and two Lindstrand *et al* cases of partial Monosomy 21 were mapped to/within the “centromeric” region of

chromosome 21 (Roberson 2010). In contrast to Lyle *et al*, they observed that not all of their cases with deletions of/within the “centromeric” region had a severe phenotype. For example, one of their patients with a deletion spanning the entire “centromeric” region was diagnosed with only mild dysmorphia and an absence of any intellectual, cardiac or renal defects (Roberson 2010). It is worth noticing that one of the cases described by Lindstrand *et al* had a large deletion within the “centromeric” region of chromosome 21 spanning approximately 14 Mb but also did not show a severe clinical phenotype, and was diagnosed with normal to late speech development, normal to mildly delayed social, emotional and cognitive development and some abnormalities in gross and fine motor functions (Lindstrand 2010). Robertson *et al* hypothesised that, perhaps, deletions or translocations of chromosomes other than 21 might contribute to the variety of observed phenotypes in patients with deletions of/within the “centromeric” region.

Four new cases, three DECIPHER cases and two Lindstrand *et al* cases of partial Monosomy 21 were mapped to/within the “medial” region of chromosome 21 (Roberson 2010). In addition to two DECIPHER cases that had deletions that spanned almost the entire “medial” region of chromosome 21, two new cases and two Lindstrand *et al* cases had deletions that substantially overlapped with the “medial” region of chromosome 21. The presence of cases that had such large deletions of the “medial” region is in contrary to the finding of Lyle *et al*, who identified only one patient with a small partial deletion of the “medial” region of chromosome 21, and questions the Lyle *et al* hypothesis that deletions of the “medial” region are not compatible with life.

Six new cases and eight DECIPHER cases of partial Monosomy 21 were mapped to/within the “telomeric” region of chromosome 21 (Roberson 2010). In agreement with Lyle *et al,* deletions of/within the “telomeric” region were the most prevalent, and patients with such deletions were diagnosed with a less severe range of clinical features (Roberson 2010).

Lindstrand *et al* suggested that deletions spanning the *ITSN1* gene might form a critical region of intellectual disability, and deletions spanning the *KCNE1*, *RCAN1*, *CLIC6* and *RUNX1* genes might form a critical region of severe cardiac abnormalities (Lindstrand 2010). Nevertheless, some of

Robertson *et al* new cases, DECIPHER cases and Lyle *et al* cases that were diagnosed with intellectual disability and/or severe cardiac malformations, had deletions that did not span any of the above genes, which stresses the importance of searching for additional genes that are responsible for the clinical phenotypes observed in Monosomy 21 patients (Roberson 2010).

3.2.4 MOUSE MODELS OF MONOSOMY 21 SYNDROME

In parallel with human genetics approaches, monosomic mouse models have been generated to facilitate the identification of dosage-sensitive genes involved in the clinical features observed in patients with Monosomy 21 (Olson 2004; Besson 2007; Olson 2007; Yu 2010). Synteny exists between human chromosome 21 (HSA21) and mouse chromosomes 16 (MMU16), 17 (MMU17) and 10 (MMU10). Specifically, about 23.2 Mb of human chromosome 21, from 21q11.2 to 21q22.3, is homologous to C3.1–C4 on MMU16, 1.1 Mb of 21q22.3 is homologous to the B1 band on MMU17 and 2.3 Mb of the 21q22.3 region is syntenic to C1 on MMU10.

A mouse model carrying a heterozygous deletion of MMU16, syntenic to the human region 21q22.12–q22.3 displayed a significant reduction in both overall brain and hippocampus volume and in body size, but had a notably larger cerebellum, and a higher density of both Purkinje cells and granule cells (Olson 2007). Nevertheless, these changes did not show any correlation with abnormal functioning of the hippocampus measured in the Morris water maze assay or by electrophysiology (Olson 2007), suggesting that this region of mouse chromosome 16 might be excluded from further searches for a causative gene (or genes) for partial Monosomy 21-associated intellectual disability.

A mouse model carrying a heterozygous deletion of MMU10, syntenic to the distal part of human region 21q22.3 located between the *PRMT2* and *COL6A1* genes, showed no gross morphological or behavioural anomalies. However, it exhibited an increased inflammatory reaction after intranasal lipopolysaccharide (LPS) administration, an impaired airway response, and an enhanced secretion of pro-inflammatory cytokines (Besson 2007). These

results suggested that some genes in the deleted region might be responsible for the regulation of lung function and inflammation (Besson 2007).

In contrast, a mouse model carrying a heterozygous deletion of MMU10, syntenic to the human region located between the *PRMT2* and *PDXK* genes, showed both impairment in spatial learning and memory when assessed in the Morris water maze tasks, and in context-associated learning when examined by the contextual fear conditioning test (Yu 2010). Interestingly, 13 out of 41 syntenic genes located on mouse chromosome 10, namely the genes located between the *Prmt2* and *Col6a1* genes, could be excluded as candidate genes for partial Monosomy 21-associated intellectual disability, as heterozygous deletion of these genes did not result in learning impairment in mice (Besson 2007).

A mouse model carrying the deletion of the region of mouse chromosome 17 syntenic to the human region located between the *ABCG1* and *RRP1B* genes displayed impairment in context-associated learning when examined by the contextual fear conditioning test (Yu 2010), suggesting that a causative gene (or genes) for partial Monosomy 21-associated intellectual disability might be among the 19 syntenic genes located on mouse chromosome 17.

3.2.5 INCREASED FREQUENCY OF TUMOUR FORMATION IN PATIENTS WITH DELETIONS OF THE PROXIMAL END OF THE LONG ARM OF CHROMOSOME 21

Apart from the association of partial deletions of human chromosome 21 with Monosomy 21, partial loss of the proximal end of the long arm of chromosome 21 has been observed in several types of solid tumours, including cancers of the ovary, stomach, breast, oral cavity and bone (Cliby 1993; Ohgaki 1998; Yamamoto 2003; Aoki 2005; Chen 2005; dos Santos Aguiar 2007).

In a search for candidate tumour suppressor genes (TSGs), Cliby *et al* analysed 37 epithelial ovarian tumours for loss of heterozygosity (LOH) using 70 polymorphic markers that were distributed along all human autosomal chromosome arms, except for the short arms of acrocentric chromosomes.

They reported a frequency of LOH greater than 35% for several chromosome arms, including the long arm of human chromosome 21 (21q) (Cliby 1993).

Ohgaki *et al* studied 142 breast tumours for LOH using 11 polymorphic microsatellite markers distributed along the long arm of chromosome 21. They found LOH for single or multiple markers in 31% of analysed tumours. The highest LOH was identified for the 21q21 region, suggesting the presence of at least one candidate TSG within this region (Ohgaki 1998).

Dos Santos Aguiar *et al* studied 41 paediatric osteosarcomas (OSs) by comparative genomic hybridization (CGH). They observed a broad range of both gains and losses of different chromosomal arms. Interestingly, they found chromosome 21 abnormalities in 70% of analysed tumours, with losses being much more prevalent than gains. Of the losses, the deletion of the 21q11.2–q21 region was the most frequently detected, suggesting the possible existence of candidate TSGs in this region that might be involved in the development of OSs (dos Santos Aguiar 2007).

Yamamoto *et al* analysed 40 primary oral squamous cell carcinomas (SCCs) for LOH using 30 polymorphic microsatellite markers distributed along the long arms of chromosomes 2, 3 and 21. They reported a frequency of LOH greater than 20% for several markers mapping to all three studied chromosome arms, including increased LOH for markers mapping to the chromosome region 21q11.1 (52.4% frequency of LOH), 21q21 (21.6% frequency of LOH) and 21q22.1 (22.2% frequency of LOH). Their finding suggests that the existence of candidate TSGs in the 21q11.1–q22.1 region are likely to play a role in the development of SCCs (Yamamoto 2003).

Following up on Yamamoto *et al* results, Chen *et al* analysed 43 additional primary oral squamous cell carcinomas (OSCCs) for LOH using 12 polymorphic microsatellite markers distributed along the 21q11.1–q21.1 region. The highest LOH (60%) was observed in two separate areas of the 21q11.1–q21.1 region, suggesting the existence of at least two candidate TSGs in the 21q11.1–q21.1 region that might account for the development of OSCC (Chen 2005).

Sakata *et al* studied 45 differentiated stomach adenocarcinomas for LOH using 10 polymorphic microsatellite markers distributed along the long

arm of human chromosome 21. They found LOH for single or multiple markers in 44% of analysed adenocarcinomas. They also suggested the existence of at least two candidate TSGs on 21q (one mapping to the 21q21 region and the other to the 21q22.1 region) that might be responsible for the development of differentiated stomach tumours (Sakata 1997).

Aoki *et al* conducted a genome-wide linkage analysis using 392 polymorphic microsatellite markers distributed along the entire genome on a group of 170 Japanese sib-pairs diagnosed with stomach cancer. They found that the 1p32, 2q33–q35, 11p13–p14 and 21q21 chromosomal regions showed evidence for linkage with multipoint logarithm of odds (LOD) scores greater than 1.18, corresponding to $P<0.01$ (Aoki 2005). Subsequently, they selected 66 genes that mapped to the 21p11–q22 region and carried out a case-control study using 126 SNPs (Aoki 2005). They identified five SNPs in the stress 70 protein chaperon family member (*STCH*) gene to be significantly associated with stomach cancer ($P<0.05$).

Yamagata *et al* analysed 20 stomach tumour and 20 stomach non-tumour samples for somatic mutations in the *STCH* gene using direct sequencing (Yamagata 2008). They found a heterozygous deletion spanning a 12 bp of the *STCH* gene in one of the 20 analysed sample pairs. This mutation caused a deletion of four amino acids in the conserved ATP-binding domain, which subsequently resulted in the loss of ATP-binding function of the STCH protein. They also showed that cells containing a mutated version of the STCH protein were not sensitive to tumour necrosis factor related apoptosis-inducing ligand (TRAIL)-induced cell death, so the *STCH* gene seems to be involved in cell proliferation and survival, and thus might be regarded as a candidate gene conferring susceptibility to stomach cancer (Yamagata 2008).

Moreover, loss of heterozygosity at chromosome 21q has been a recurrently observed alternation found in lung cancer (Sato 1994; Kohno 1998; Groet 2000; Yamada 2008).

In a search for tumour suppressor candidate genes, Sato *et al* analysed 41 squamous lung cell carcinomas and 119 lung adenocarcinomas for LOH on all human autosomal chromosome arms using Southern blot analysis. In squamous lung cell carcinomas they reported a significant

frequency of LOH for several chromosome arms, including the long arm of human chromosome 21 (21q) ($P<0.05$), suggesting the possible existence of candidate TSGs in this region that might play a role in the development of squamous lung cell carcinoma.

Groet *at al* analysed 34 informative non-small cell lung carcinomas for LOH using 4 polymorphic microsatellite markers distributed along a 4.5 Mb segment of the 21q11.1–q21.1 region. They found LOH of the entire segment in 13 and partial LOH of the segment in two studied carcinomas. Analysis of the endpoints of two partial LOHs of the 21q11.1–q21.1 region enabled them to exclude the *STCH* and *NRIP1* genes from further candidate TSG analysis, as none of these genes were deleted in any of these tumours. Within the overlapping region for both entire and partial deletions of the 21q11.1–q21.1 region they identified a novel gene, *USP21* (currently known as *USP25*), encoding an ubiquitin-specific protease. Subsequently, they performed direct cycle sequencing of the *USP21* gene in all the 34 tumour samples, but found no mutations in any functional domains of the gene. Thus they concluded that the *USP21* gene is unlikely to be a TSG, and further analysis is required to search for a candidate TSG that might play a role in the development of non-small cell lung carcinoma.

Yamada *et al* analysed 85 lung cancer lines for the presence of a homozygous deletion in the 21q11.1–q21.1 region using 12 sequence-tagged site (STS) markers. They found that one non-small cell lung carcinoma line had a homozygous deletion encompassing the region from *LIPI* to *C21orf34* inclusively. They further analysed the *SAMSN1* and *USP25* genes, as these genes are the only genes mapped within the deletion that showed detectable expression in normal lung cells and frequent down-regulation in lung cancer cell lines, as judged by Northern blot analysis. Polymerase chain reaction-single strand conformation polymorphism (PCR-SSCP) analysis did not find any mutations in the *SAMSN1* gene in any of the analysed lung cancer cell lines and tumours, suggesting that the *SAMSN1* gene is unlikely to be a TSG. Also, transfection of a cancer cell line carrying a homozygous deletion of the 21q21.1 region with expression vectors for either the *SAMSN1* or *USP25* gene did not result in cell growth inhibition measured with an MTT

(3-(4,5-Dimethylthiazol-2-yl)-2,5-diphenyltetrazolium bromide) assay, and thus did not provide any evidence for the tumour suppression function of any of these genes. In addition, they observed frequent downregulation of *let-7c*, *miR-125b-2* and *miR-99a* in human lung cancer cell lines and lung tumours, and so they transfected a cancer cell line carrying a homozygous deletion of the 21q21.1 region with expression vectors for either of these miRNAs, but did not observe cell growth inhibition measured with an MTT assay, and thus did not obtain any evidence for the tumour suppression function of any of these miRNAs in lung carcinoma.

Kohno *et al* analysed 12 small cell lung carcinoma (SCLC) and 20 non-small cell lung carcinoma (NSCLC) lines using Southern and Northern blot analysis to detect mutations in the *ANA* (abundant in neuroepithelium area) gene that is mapped within the 21q11.2–q21.1 region. They identified homozygous deletion of the *ANA* gene in one of the NSCLC lines. Next, they analysed 18 SCLCs and 47 SCLCs for LOH, and detected LOH for 7 SCLCs and 24 SCLCs. Finally, they showed that PCR-SSCP analysis did not find any somatic mutations in the *ANA* gene in any of the 6 SCLC and 23 SCLC lines that were previously identified with LOH, and concluded that the *ANA* gene is unlikely to play a role in the development of lung cancer.

Moreover, the importance of chromosome 21q in cancer pathogenesis was strengthened by the dataset released by the Cancer Genome Project (http://www.sanger.ac.uk/cgi-bin/genetics/CGP/cghviewer/CghHome.cgi). This dataset catalogued the structural genomic variations in almost 800 cancer cell lines and revealed the presence of deletions in 50 cell lines in the chromosomal region 21q11.2–q21.1. These deletions mainly encompassed the *SAMSN1* and *USP25* genes, which have previously been reported as being down-regulated in human lung cancer (Yamada 2008), the *NRIP1* gene that encodes a ligand-dependent co-repressor that limits retinoic acid (RA) mediated tumour cell differentiation of embryonal carcinoma (the pluriopotent stem cells of testicular germ cell tumours) (Heim 2007), and the *LIPI* gene that shows a high expression in Ewing family tumours (EFT) (Foell 2008).

In summary, on the one hand, the decreased incidence of solid tumours in patients with Down syndrome (Hasle 2000) and recurrently observed partial losses of the long arm of chromosome 21 in patients diagnosed with different types of solid tumours, strongly suggest the existence of TSGs or growth control genes on chromosome 21q that still await discovery. On the other hand, the existence of a potential causative link between cancer and Monosomy 21 seems to be questionable. Firstly, none of the clinical data currently available for Monosomy 21 patients carrying "centromeric" deletions reports any cases in which tumours were diagnosed (Wakui 2002; Tinkel-Vernon 2003, Lyle 2008; Roberson 2010; Lindstrand 2010). Secondly, there is no clinical data suggesting that any of the patients carrying a deletion of the proximal end of the long arm of chromosome 21 who were diagnosed with cancer displayed any of the clinical features identified in patients with Monosomy 21 (Cliby 1993; Ohgaki 1998; Yamamoto 2003; Aoki 2005; Chen 2005; dos Santos Aguiar 2007). However, the potentially increased risk of cancer development in individuals with Monosomy 21 cannot be excluded, as the medical history of Monosomy 21 patients is not known beyond the initial clinical evaluation, and so the possible occurrence of tumours in individuals with Monosomy 21, especially later in their lives, might have be missed. Also, it cannot be excluded that some of the patients diagnosed with tumours might actually present some of the phenotypic abnormalities that are characteristic for Monosomy 21 individuals, but that this was not noticed or taken into account at the time of diagnosis. Thus, to be able to answer the question about the existence of a potential causative link between cancer and Monosomy 21, it is necessary to both follow the medical history of Monosomy 21 patients carrying "centromeric" deletions throughout their lives, and to re-examine all patients carrying a deletion of or within the proximal end of chromosome 21 (who at some point developed cancer) for the presence of any clinical manifestations observed in Monosomy 21 patients.

3.2.6 GENERATION OF A NEW MOUSE MODEL OF MONOSOMY 21 SYNDROME

To our knowledge all currently available mouse models for Monosomy 21 provide phenotypic data only on the deletions that are syntenic to human regions located between 21q21.3 and the telomere (Besson 2007; Olson 2007; Yu 2010). Thus the contribution of additional regions/genes to the development of clinical features observed in patients with Monosomy 21 remains unclear. Also, to date no mouse models have been generated to investigate the contribution of genes mapped to the proximal end of human chromosome 21 to the development of different types of cancer. To this end, we used chromosome engineering to generate a new mouse model of Monosomy 21, $Df^{Lipi\text{-}Usp25}$, carrying a deletion syntenic to 21q11.2–q21.1 in human, to assess the contribution of the six genes conserved between human and mouse that are mapped within this 1.6 Mb interval to the development of clinical features diagnosed in patients with Monosomy 21 and different types of cancer.

It should be mentioned that the approach we have taken to investigate the contribution of a deletion of the *Lipi–Usp25* region to the formation of different types of tumour does not exactly recapitulate the situation that occurs in humans. Namely, in humans cancer formation takes place during the individual's life, with a deleterious mutation initially occurring in a single somatic cell that is subsequently clonally expanded. However, our monosomic mice carry a germline deletion of the *Lipi–Usp25* region, and so the mutation is present in all body cells throughout both pre- and postnatal development. This might potentially cause the development of different clinical manifestations or accelerate the progression of cancer development.

3.3 RESULTS

3.3.1 GENERATION OF MONOSOMIC MICE FOR THE 1.6 Mb *Lipi–Usp25* REGION

The *Lipi* and *Usp25* genes are located at the proximal and distal ends of a 1.6 Mb region in the C3.1 band of mouse chromosome 16 (MMU16), which is syntenic to the human region 21q11.2–q21.1 (**Figure 3.1A**). This region on human chromosome 21 (HSA21) contains eight genes (NCBI build h36), whereas the syntenic region in MMU16 contains only 6 genes (NCBI build m37) (**Figure 3.1B**) orthologous to their HSA21 counterparts, as there are no murine orthologs of *ABCC13* and *AF165138.1*. The *Lipi–Usp25* deletion was generated using chromosomal engineering (Zheng 1999) as described in Material and Methods (**Figure 3.2A**). Briefly, E14tg2a ES cells were sequentially electroporated with targeting vectors containing a portion of the *Hprt* selection cassette (5' or 3'*Hprt*), a *loxP* site and a coat colour marker (agouti or tyrosinase). The targeting vector containing the 5'*Hprt* cassette (MICER clone: MHPN69h23) (Adams 2004) was inserted proximal to *Lipi* and the targeting vector containing the 3'*Hprt* cassette (pUSP-3HPAg) was inserted distal to *Usp25* (**Figure 3.2A**). The correct insertion of both targeting vectors was confirmed by Southern blot analysis on *Stu*I- or *Bam*HI-digested gDNA extracted from ES clones selected either in G418 or puromycin using a 5′ and 3′ Southern external probe, respectively (**Figure 3.2A, 3.2B**). Double-targeted clones in which both targeting vectors were inserted on the same chromosome (*cis*) were electroporated with a Cre-expression vector, and subsequently selected in a medium containing hypoxanthine, aminopterin and thymidine (HAT) to isolate ES clones carrying a chromosomal deletion generated via recombination of the *loxP* sites (**Figure 3.2A**). The deletion allele was designated $Df^{Lipi\text{-}Usp25}$ (alternatively named *Ms(Lipi-Usp25)1Dja*, and abbreviated as *Ms1Dja*). The presence of the deletion in *Hprt*-resistant ES clones was confirmed by FISH (**Figure 3.2C**). The positive ES clones were used to generate chimaeras, which transmitted $Df^{Lipi\text{-}Usp25}$ to their progeny.

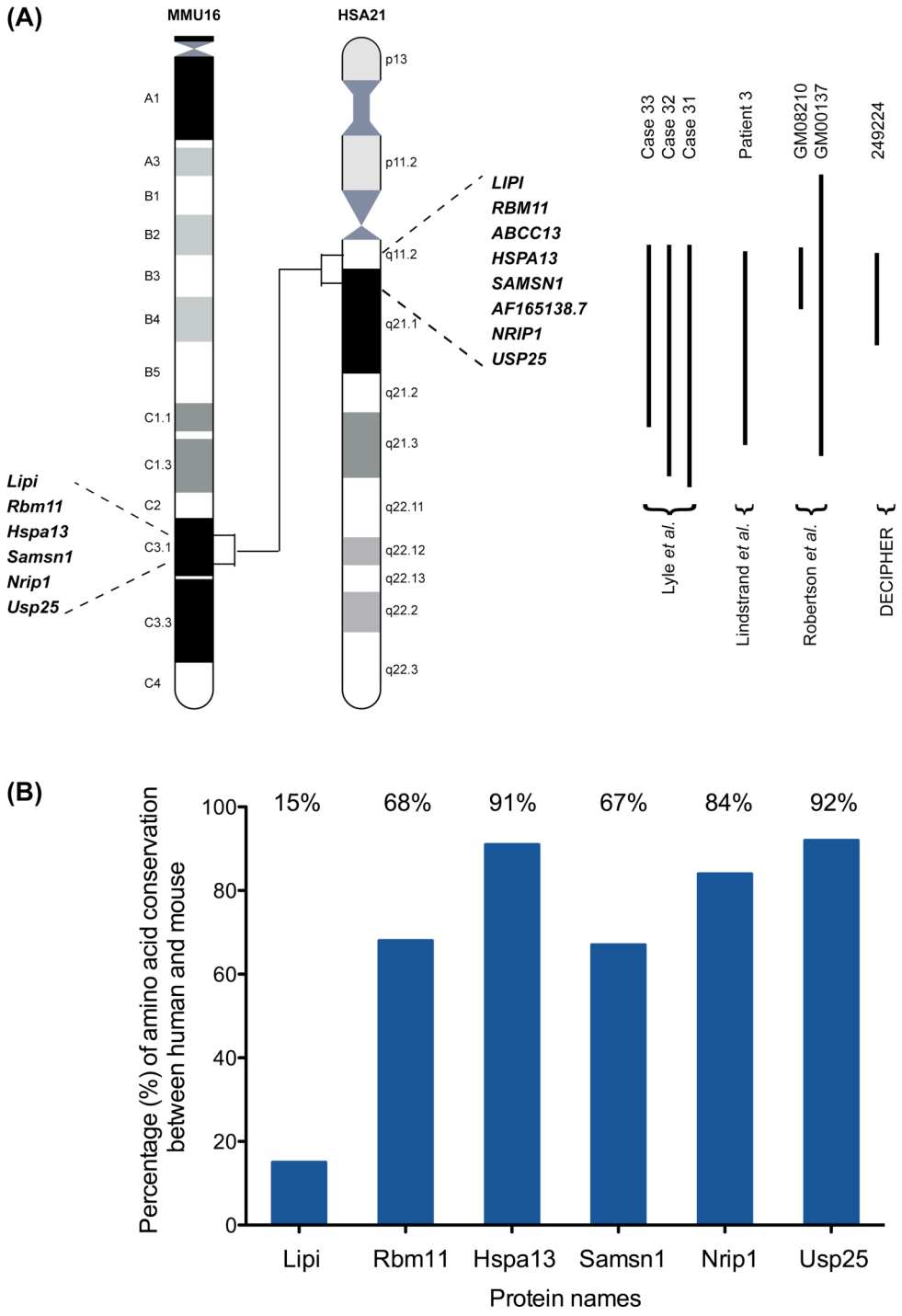

Figure 3.1. (A) Schematic representation of the q11.2–q21.1 interval on HSA21 and the syntenic region in the C3.1 band on MMU16. Genes that mapped to the human 21q11.2–q21.1 region (NCBI build h36) and the C3.1 band on MMU16 (NCBI build m37) are listed. Studies describing partial Monosomy 21 patients with deletions involving the 21q11.2–q21.1 region (as indicated by the length of the black line) are shown. **(B)** The percentage of amino acid conservation for genes within the interval between human and mouse is shown (NCBI build h36). These calculations are based on the longest Ensembl transcript.

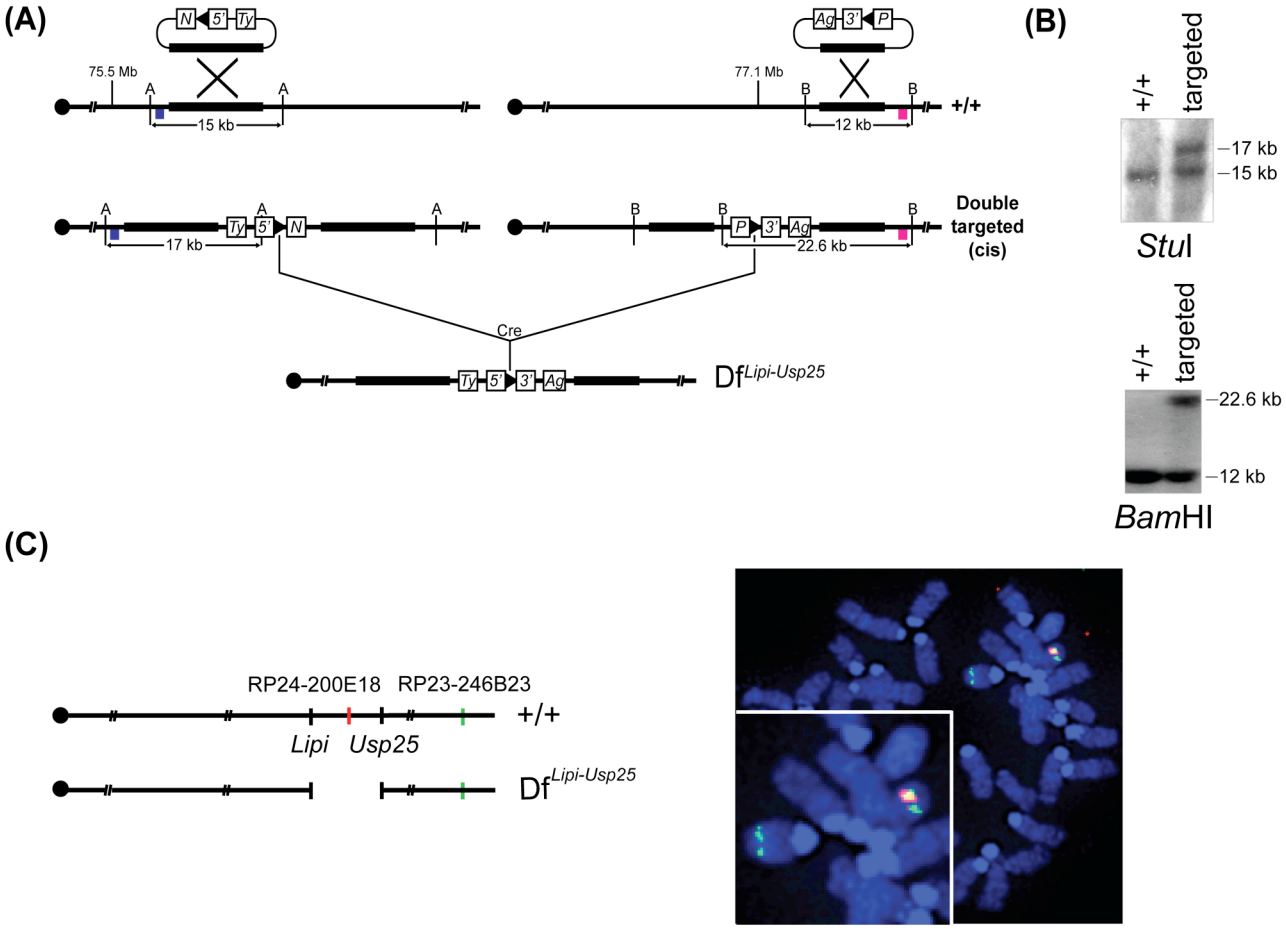

Figure 3.2. Generation of a 1.6 Mb deletion between the *Lipi* and *Usp25* loci using Cre/*loxP*-mediated chromosomal engineering. (A) Strategy to generate the chromosomal rearrangement (NCBI build m37). The targeting vectors containing a *loxP* site (arrowhead), a selectable antibiotic resistance gene (*N* or *P*), a coat colour marker (*Ty* or *Ag*) and part of the *Hprt* gene (5′ or 3′) were integrated successively in the *Lipi* locus and the *Usp25* locus. The coloured boxes (blue and pink) indicate the location of the probes (5' and 3', respectively) used for Southern blotting. A, *Stu*I; B, *Bam*HI; 5', 5'*Hprt*; 3', 3'*Hprt*; *N*, neomycin-resistance gene; *P*, puromycin-resistance gene; *Ty*, tyrosinase minigene, *Ag*, K-14 agouti gene. **(B)** The targeting events were checked by Southern analysis showing an additional *Stu*I fragment of 17 kb compared with the wildtype allele (15 kb) for the *Lipi* locus and an additional *BamH*I fragment of 22.6 kb compared with the wildtype allele (12 kb) for the *Usp25* locus. **(C)** Interphase FISH analysis with BAC probes that map in the region of the deletion (red) and outside (green). Chromosomes from the ES cells double-targeted in *cis* ($Df^{Lipi\text{-}Usp25}$) showed two green and only one red signal due to the deletion of the *Lipi–Usp25* region, while chromosomes from the wildtype ES cells showed two green and two red signals.

3.3.2 HOMOZYGOUS DELETION OF THE *Lipi–Usp25* REGION RESULTS IN EMBRYONIC LETHALITY

Heterozygous (monosomic) $Df^{Lipi\text{-}Usp25}$ mice were viable, fertile and did not show any overt phenotypical abnormalities. To check if wildtype, heterozygous and homozygous offspring were born at normal Mendelian ratios, monosomic $Df^{Lipi\text{-}Usp25}$ mice were intercrossed. Genotyping of 47 progeny did not recover any homozygous (nullisomic) $Df^{Lipi\text{-}Usp25}$ mice (**Figure 3.3A**), showing that the nullisomic deletion resulted in prenatal death. In order to establish the time of death, embryos from monosomic intercrosses were collected at different timepoints during gestation (E14.5, E12.5, E11.5 and E10.5; **Figure 3.3A**). No nullisomic embryos were found at E14.5 (0/32 embryos, P=0.0011) and E11.5 (0/20 embryos, P=0.0098), and only one very necrotic nullisomic embryo was found at E12.5 (1/40 embryos, P=0.0010) (**Figure 3.3A**). Also, there was an increased incidence of embryo resorption between E10.5 and E12.5. Nullisomic embryos were identified at E10.5 at low but still within normal Mendelian ratios (8/52 embryos, P=0.1093), indicating that the majority of embryonic lethality in the nullisomic embryos happened on or before E10.5 (**Figure 3A**). Morphological analysis showed that all nullisomic embryos were markedly smaller than their monosomic and wildtype littermates (**Figure 3.3B**), suggesting developmental retardation. To reveal the reason for embryonic lethality, the nullisomic embryos, as well as their heterozygous and wildtype littermates harvested at E10.5 and E12.5, were analysed histopathologically (**Figure 3.3C, 3.3D**). The hematoxylin and eosin staining showed an increase in the number of apoptotic cells in the neural tube of the nullisomic embryos compared to the monosomic and wildtype littermates (**Figure 3.3C**). To confirm this increased apoptosis, immunostaining was performed using cleaved caspase-3 (Asp175), an apoptotic marker (**Figure 3.3D**). Cleaved caspase-3-positive cells indicated that apoptosis was much more prevalent in the neural tube of the nullisomic embryos compared to the monosomic and wildtype littermates collected at E10.5 (**Figure 3.3D**). In contrast, very few cells labelled by cleaved caspase-3 were present in the neural tube of the nullisomic embryo collected at E12.5 compared to nullisomic embryos harvested at E10.5

(**Figure 3.3D**). Instead, empty areas in the neural tube of the E12.5 nullisomic embryos were observed, suggesting that the apoptotic cells were degraded in the neural tube by E12.5 (**Figure 3.3D**). This indicates that the majority of embryonic lethality in the nullisomic embryos was mostly due to degeneration of the neural tube.

(A)

Litters	Age	+/+	$Df^{Lipi\text{-}Usp25}/+$	$Df^{Lipi\text{-}Usp25}/Df^{Lipi\text{-}Usp25}$	P
8	E10.5	16	28	8	0.1093
3	E11.5	10	10	0	0.0098
7	E12.5	19	20	1	0.0010
5	E14.5	17	15	0	0.0011
7	P21	16	31	0	0.0001

(B)

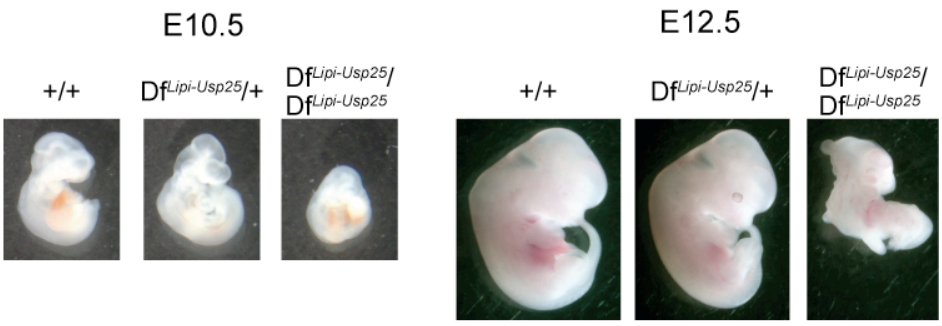

(C)

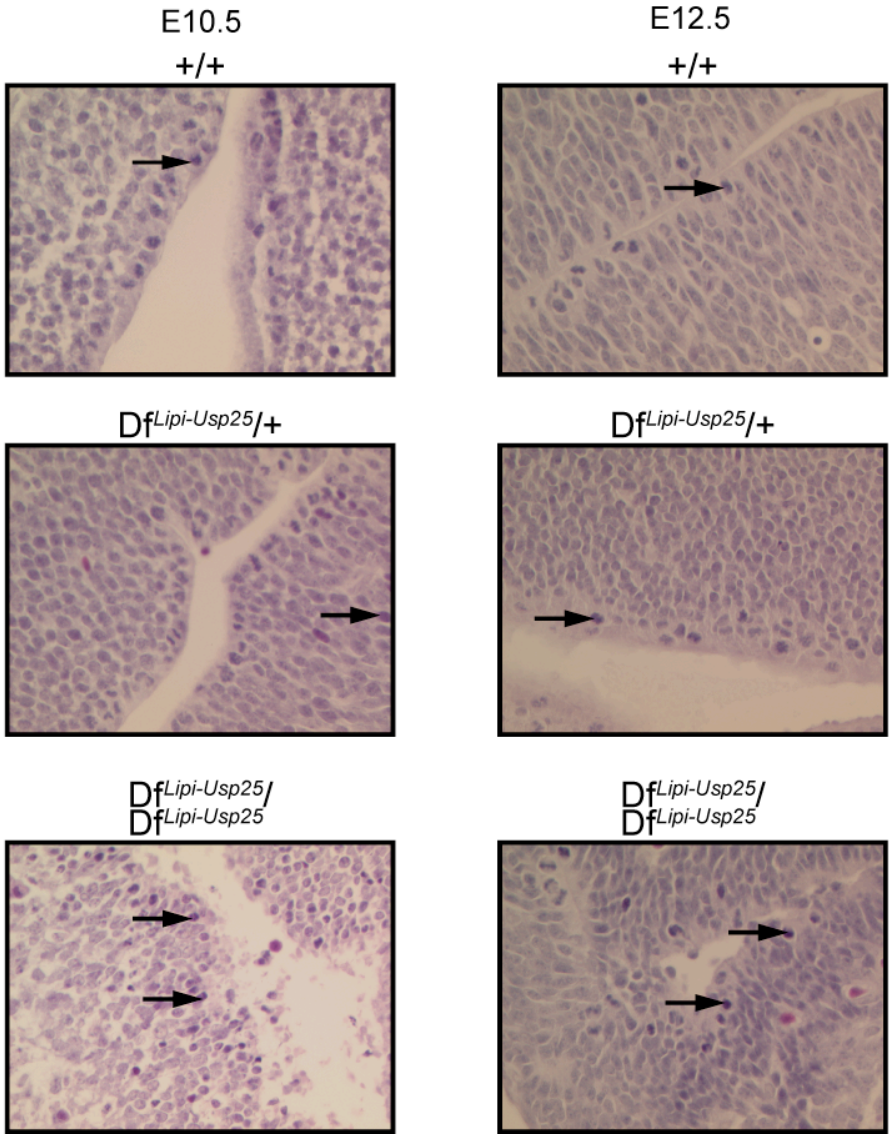

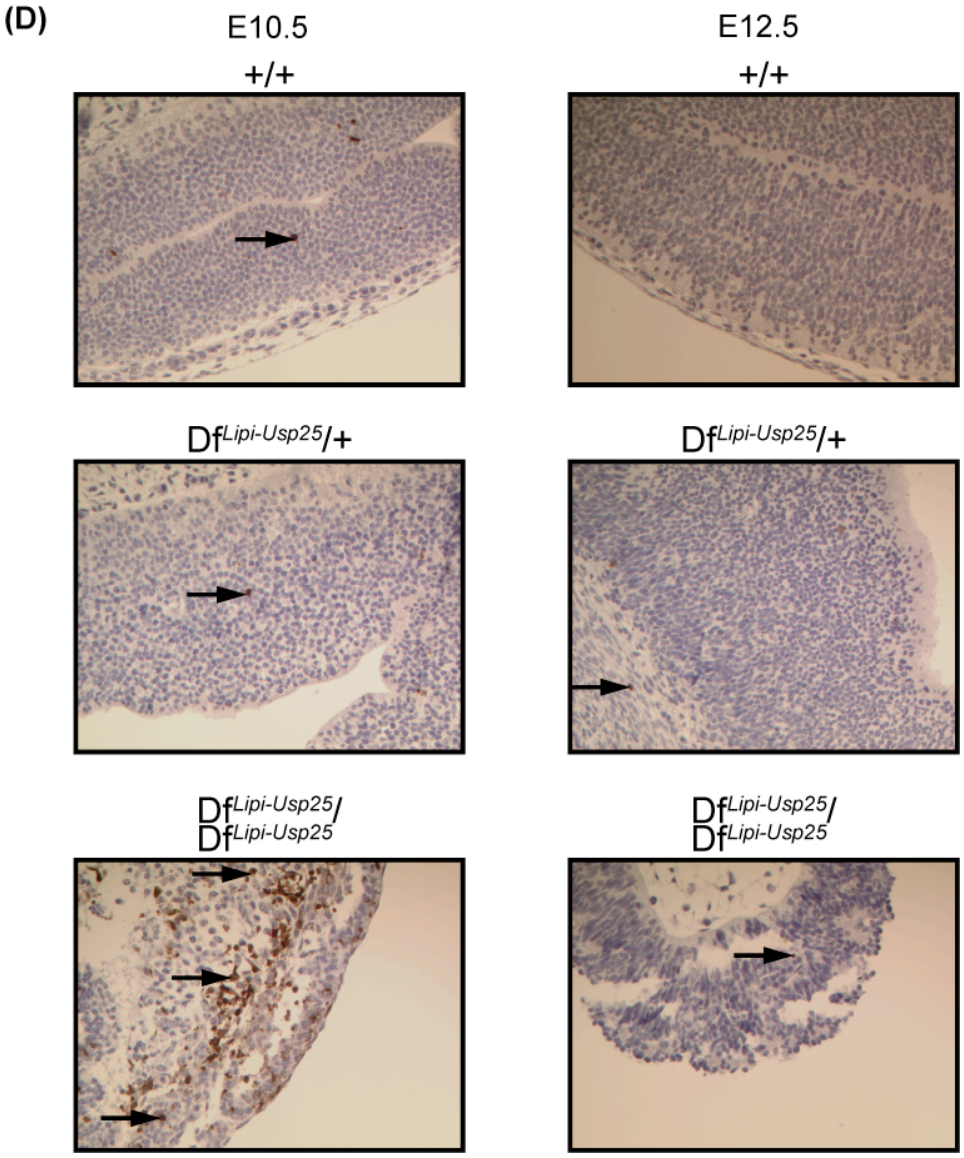

Figure 3.3. Embryonic lethality of mice homozygous for the *Lipi–Usp25* deletion. **(A)** Genotyping of E10.5, E11.5, E12.5 and E14.5 embryos, and P21 (3-week old) mice from monosomic $Df^{Lipi\text{-}Usp25}$ intercrosses. Experimental data was statistically analysed using the Chi-square test. **(B)** Photos of wildtype (+/+), monosomic ($Df^{Lipi\text{-}Usp25}$/+) and nullisomic ($Df^{Lipi\text{-}Usp25}$/ $Df^{Lipi\text{-}Usp25}$) embryos collected at E10.5 and E12.5. Longitudinal measurements are 4 mm, 4 mm and 2.7 mm for the wildtype, monosomic and nullisomic embryos collected at E10.5 respectively. Longitudinal measurements are 9 mm, 9 mm and 4.7 mm for the wildtype, monosomic and nullisomic embryos collected at E12.5 respectively. **(C)** Haematoxylin and eosin-stained sections of neural tubes from wildtype, monosomic and nullisomic embryos collected at E10.5 and E12.5. Dark purple staining indicates apoptotic cells (indicated by arrows). **(D)** Immunohistochemical analysis using a cleaved caspase-3 (Asp175) antibody showed a markedly increased number of apoptotic cells (brown staining; indicated by arrows) in the neural tube of nullisomic embryos collected at E10.5. Note also the empty spaces in the neural tube of nullisomic embryos collected at E12.5 compared to the intact structure of the neural tube of wildtype and monosomic embryos. Images are representative and taken at x200 magnification.

3.3.3 PHENOTYPIC ANALYSIS OF MONOSOMIC MICE

To determine whether clinical features diagnosed in patients with Monosomy 21 syndrome can be observed in the heterozygous (monosomic) *Df*$^{Lipi\text{-}Usp25}$ mice, 14 monosomic mice and 14 wildtype littermates (controls) fed on a high-fat diet (HFD) from the age of 4 weeks were subjected to a series of tests designed to analyse their morphology, behaviour, motor skills, neuromuscular function, pain perception, hearing, metabolism and haematology. Tests were carried out between 4 and 16 weeks of age, depending on the specific test. See **Material and Methods Table 2.4** for a short summary of the phenotypic tests performed; the results for each of the tests can be found at the Wellcome Trust Sanger Institute Mouse Resources Portal under the name Mdel (http://www.sanger.ac.uk/mouseportal/).

3.3.3.1 PHENOTYPIC ANALYSIS OF MONOSOMIC MICE REVEALS THAT LOSS OF ONE COPY OF THE *Lipi–Usp25* REGION DOES NOT AFFECT GENERAL MORPHOLOGY, MOTOR OR NEUROMASCULAR FUNCTION

The monosomic mice were viable, fertile and did not show any overt phenotype upon observation. They showed no gross motor or neurological abnormalities and a similar level of pain perception, muscle strength and hearing compared with the control animals (wildtype littermates) (**Table 3.1**).

The general dysmorphology and eye morphology tests found a difference between the controls and monosomic mice with respect to eye pigmentation (**Table 3.1**). Pigmentation of the eyes was observed in albino monosomic mice and abnormal iris pigmentation observed in albino monosomic males. However, this can be explained by the presence of coat colour markers (agouti and tyrosinase) present in the constructs used for gene-targeting in the ES cells. Thus it was concluded that the monosomic mice did not suffer pigmentation dysmorphology.

Table 3.1. Short summary of the results obtained from phenotypic tests performed on 14 monosomic *Df*$^{Lipi\text{-}Usp25}$ mice and 14 wildtype littermates fed on a high-fat diet.

Time	Name of the test	Result
Weekly; from 4-week old	Weighting mice	No significant changes
4-week old	Hair dysmorphology	No significant changes
6-week old	Hair follicle cycling	No significant changes
9-week old	Open field	No significant changes
9-week old	Modified SHIRPA	No significant changes
9-week old	Grip strength	No significant changes
10-week old	Dysmorphology	Significant changes in both monosomic males and females compared to their wildtype littermates
10-week old	Hot plate	No significant changes
12-week old	Indirect calorimetry	No significant changes
13-week old	Glucose tolerance	No significant changes
14-week old	Auditory brainstem response	No significant changes
14-week old	Dual energy X-ray absorptiometry (DEXA)	Significant changes in both monosomic males and females compared to their wildtype littermates
14-week old	X-ray imaging	No significant changes
15-week old	Core temperature stress	No significant changes
15-week old	Eye morphology screen	Significant changes in both monosomic males and females compared to their wildtype littermates
16-week old	Heart weights	No significant changes
16-week old	Haematology panel	No significant changes
16-week old	Plasma chemistry panel	No significant changes

3.3.3.2 BEHAVIOURAL PHENOTYPING OF MONOSOMIC MICE REVEALS THAT LOSS OF ONE COPY OF THE *Lipi–Usp25* REGION IS ASSSOCIATED WITH A DEFICIT IN MEMORY RETENTION

Even though no differences were observed in the monosomic mice upon open field testing, as no significant changes in locomotion, habituation and fear/anxiety responses to a novel environment between monosomic and control mice were observed (**Table 3.1, Figure 3.4A-D**), we decided to explore further their behaviour and cognition.

12 monosomic mice and 12 wildtype littermate controls fed on a normal-fat diet (NFD) were used in an elevated plus maze test of anxiety and a social recognition paradigm with a long-term social memory component. Both monosomic and wildtype animals showed a preference for the closed arm compared to the open arm of the elevated plus maze, as measured by the amount of time spent in the open arm and the number of entries into the open and closed arm (**Figure 3.5A, 3.5B, 3.5C**; two-way ANOVA: repeated measures for *Trial*, $F_{4,64}$=25.86, P<0.0001, effect for *genotype* $F_{1,64}$=11.26, P=0.943). The social recognition test showed that the monosomic animals were able to recognise two different (sedated) male stimulus animals (mouse A and mouse B) (**Figure 3.6A**; two-way ANOVA: repeated measures for *Trial*, $F_{4,64}$=25.86, P<0.0001, trial 4 versus trial 5, P<0.05, *post hoc* analysis). Both groups of mice had similar initial levels of investigation and spent increasingly lower amounts of time investigating the repeatedly presented stimulus animal (mouse A) (**Figure 3.6A**; two-way ANOVA effect for *genotype* $F_{1,64}$=11.26, P=0.943, interaction *Trial* x g*enotype* $F_{4,64}$=1.762, P=0.1475). Both of these results suggest normal levels of anxiety and social interaction. However, when subjected to a 24-hour social memory retention test, monosomic mice were incapable of distinguishing a familiar stimulus animal (mouse A) from an unfamiliar one (mouse C) (**Figure 3.6B**; ratio of investigation het versus wt, P<0.05 compared with the two-tailed Student's *t*-test). Wildtype animals, in contrast, retained the memory of the familiar stimulus animal (mouse A) and investigated it less frequently.

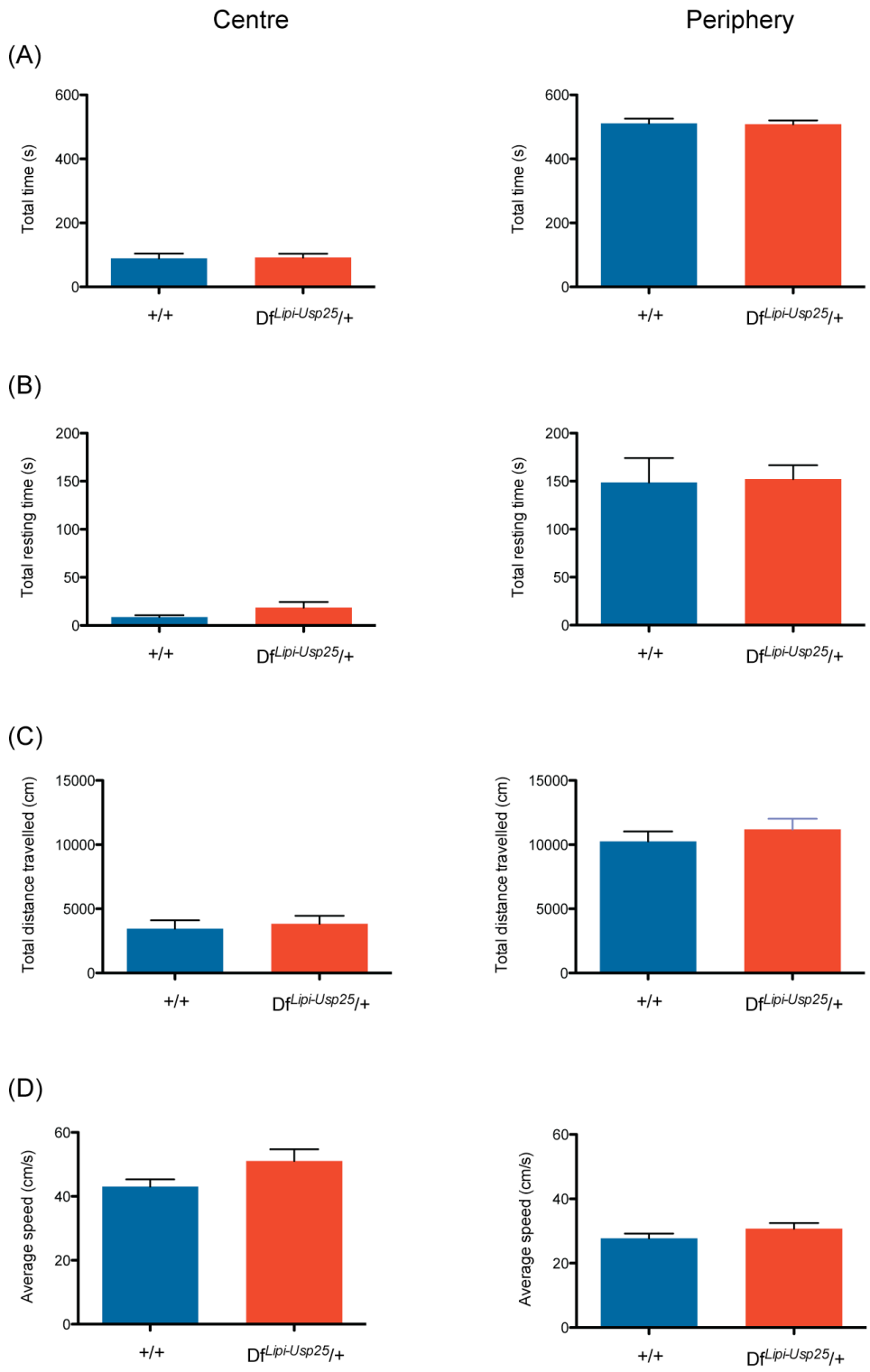

Figure 3.4. Open field results recorded at centre and periphery for 14-week old control (+/+) and monosomic (*Df*$^{Lipi\text{-}Usp25}$/+) littermates. (A) Total time (s, seconds). **(B)** Total resting time (s, seconds). **(C)** Total distance travelled (cm, centimetres). **(D)** Average speed (cm/s, centimetres/seconds). Data was statistically analysed using the two-tailed parametric Welsch's *t*-test. 7 males and 7 females were analysed per genotype.

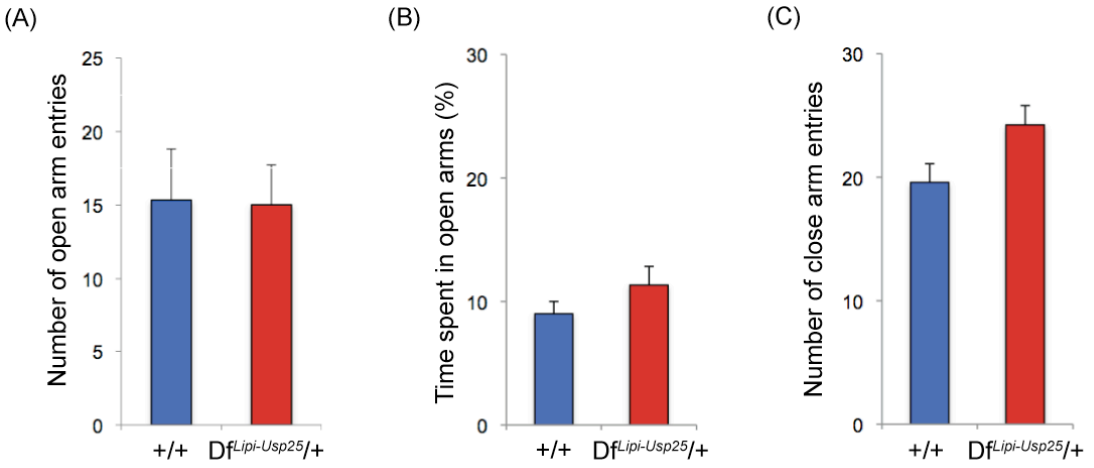

Figure 3.5. Elevated plus maze results recorded at open and close arm for 14-week old control (+/+) and monosomic (*Df*$^{Lipi\text{-}Usp25}$/+) male littermates. (A) Percentage of time spent in the open arms. **(B)** Number of entries into the open arms. **(C)** Number of entries into the closed arms. Both monosomic (*Df*$^{Lipi\text{-}Usp25}$/+) and control (+/+) mice spent similar amount of time in the open arms and had comparable number of entries into the open and closed arms. Data was statistically analysed using the two-tailed Student's *t*-test. 12 males were analysed per genotype.

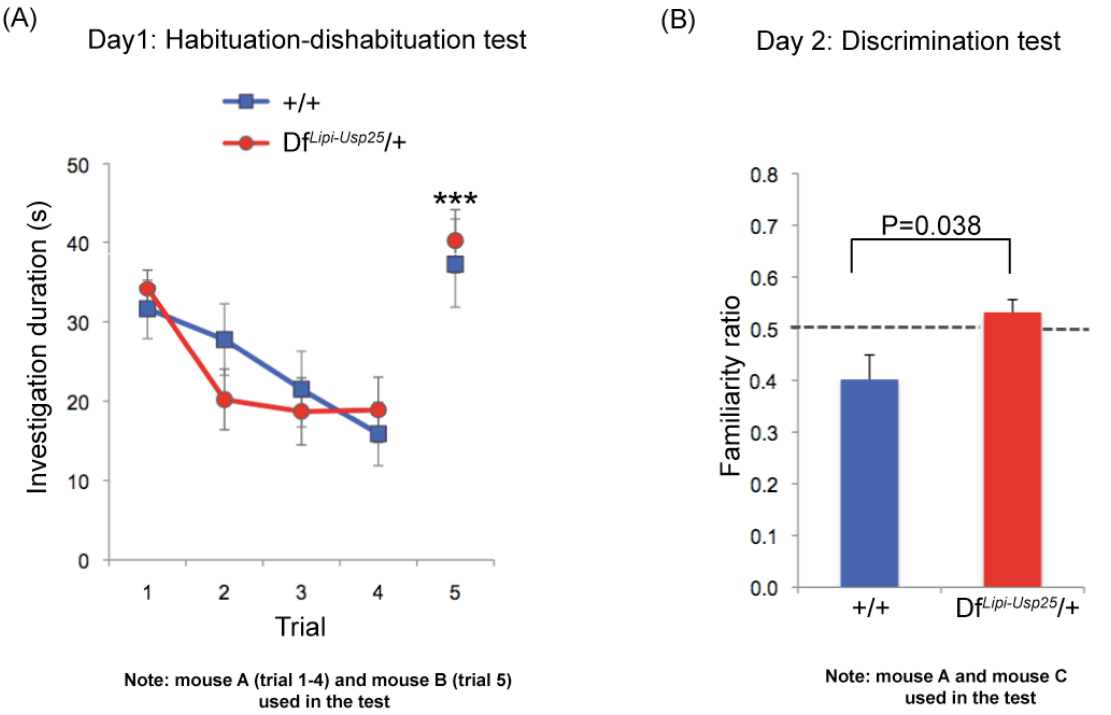

Figure 3.6. Social recognition test. (**A)** Habituation-dishabituation test. Both monosomic (*Df*$^{Lipi\text{-}Usp25}$/+) (n=10) and control (+/+) (n=8) mice recognised two different stimulus animals (mouse A and mouse B), as shown by the decline in the investigation time over trials 1 to 4 when they were repetitively presented the same (familiar) stimulus animal (mouse A) and an increase in the investigation time on trial 5 when they were presented with a novel stimulus animal (mouse B) (trial 4 versus trial 5, *** P<0.0001, *post-hoc* analysis after two-way ANOVA). **(B)** Discrimination test. 24 hours after the habituation-dishabituation test. When given a choice between the familiar stimulus mouse (mouse A, that is the mouse used for trials 1 to 4 on day 1) and a new unfamiliar mouse (mouse C), control mice spent significantly less amount of time investigating the familiar stimulus mouse (mouse A) than the unfamiliar one (mouse C). *Df*$^{Lipi\text{-}Usp25}$/+ did not recognise the familiar from the unfamiliar animal, shown by a familiarity ratio close to 0.5 ("chance", dotted line). Control animals had a significantly smaller familiarity ratio than *Df*$^{Lipi\text{-}Usp25}$/+ mice (two-tailed Student's *t*-test). Five animals (two mutants and three wildtypes) were taken out of the analysis because of their low investigation times (less than 10 seconds on trial 1).

3.3.3.3 ANALYSIS OF THE BODY COMPOSITION OF MONOSOMIC MICE REVEALS THAT LOSS OF ONE COPY OF THE *Lipi–Usp25* REGION RESULTS IN INCREASED FAT DEPOSITION

Analysis of the metabolic related measurements obtained from the dual-energy X-ray absorptiometry (DEXA) scan showed that 14-week old monosomic mice fed on a HFD exhibited a statistically significant increase infat mass and fat percentage estimate (**Table 3.1, Figure 3.7A, 3.7B**).

However, no significant differences in lean mass were observed compared to their wildtype littermates (**Table 3.1, Figure 3.7C**). Interestingly, the average weights of the monosomic mice were not statistically different when compared to the wildtype littermates (**Table 3.1, Figure 3.7D**). However, despite the increased level of fat deposition in monosomic mice, indirect calorimetry did not reveal any significant metabolic differences between the monosomic mice and the controls. In particular, no changes in food intake were observed (**Table 3.1**). Moreover, glucose tolerance tests, as well as the analysis of whole blood and plasma clinical chemistry parameters, including the analysis of the cholesterol, non-esterified free fatty acids, low and high density lipoproteins, triglycerides, and glucose level, did not show any significant differences between the monosomic mice and the wildtype littermates that could explain the observed increase in fat deposition in the monosomic mice (**Table 3.1**).

Finally, as both monosomic mice and the control mice (their wildtype littermates) were on a mixed C57BL/6Jc-/c- – 129P2/OlaHsd genetic background, wildtype C57BL/6Jc-/c- and 129P2/OlaHsd mice fed on a HFD were analysed to evaluate whether these mouse strains were prone to a HFDinduced increase in fat deposition (**Figure 3.8**). Both wildtype C57BL/6Jc/c and 129P2/OlaHsd mice showed much lower fat percentage estimate compared to both monosomic mice and controls (**Figure 3.8**), hence confirming that the HFD-induced increase in fat deposition observed in the monosomic mice was not due to their genetic background.

Thus taken together, we conclude that, whilst monosomy of the *Lipi–Usp25* region does not have a dramatic impact on morphology, motor skills, whole-body metabolism and haematology, it does affect memory retention and the deposition and/or metabolism of fat.

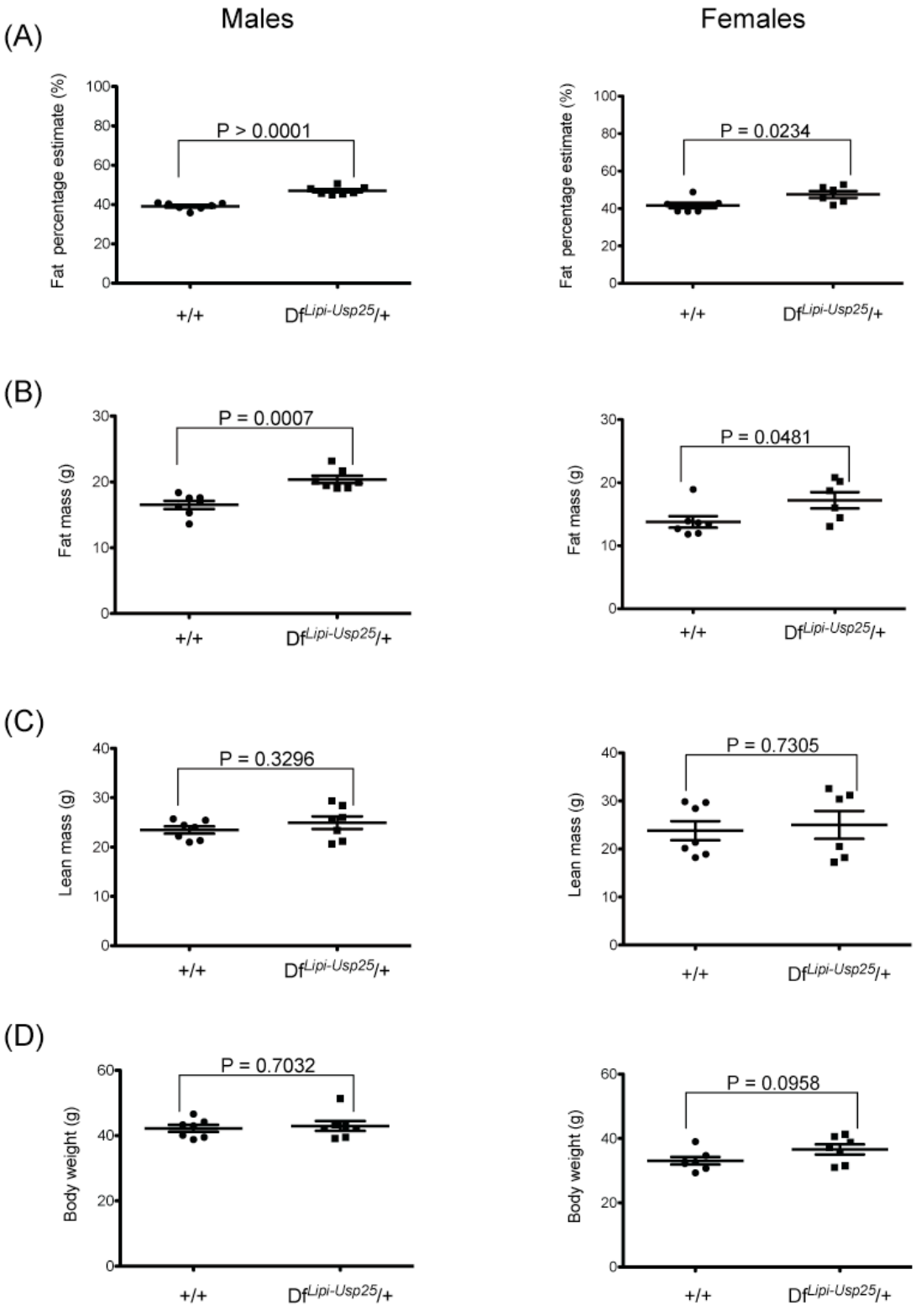

Figure 3.7. DEXA and body weight analysis of 14-week old control (+/+) and monosomic (*Df*$^{Lipi\text{-}Usp25}$/+) littermates fed a high-fat diet. (A) DEXA results showing fat percentage estimate in male and female littermates. **(B)** DEXA results showing fat mass in male and female littermates. **(C)** DEXA results showing lean mass in male and female littermates. **(D)** Body weight results in male and female littermates. Data was statistically analysed using the two-tailed Student's *t*-test. 7 males and 7 females were analysed per genotype.

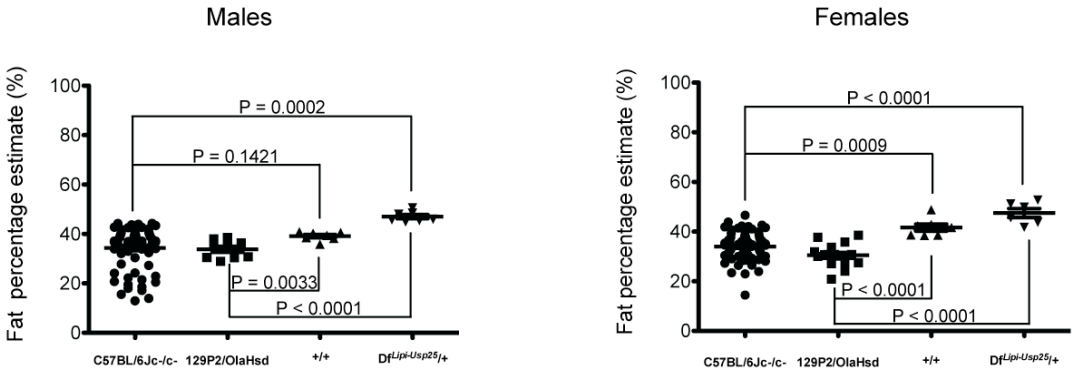

Figure 3.8. Comparison of fat percentage estimate of 14-week old wildtype C57BL/6Jc-/c- and 129P2/OlaHsd mice with control (+/+) and monosomic (*Df*$^{Lipi\text{-}Usp25}$/+) littermates fed on a high-fat diet. Data was obtained from DEXA analysis and statistically analysed using the two-tailed Student's *t*-test.

3.3.4 INCREASED BODY FAT PERCENTAGE IN MONOSOMIC MICE FED ON A HIGH-FAT DIET

Following the preliminary DEXA results, which suggested that the monosomic mice fed on a HFD exhibited a statistically significant increase in fat mass and fat percentage estimate, additional monosomic mice and littermate controls fed on a HFD were analysed by DEXA analysis at additional time points, namely at 8 and 25 weeks. As expected, both monosomic and control mice showed a gradual increase in fat mass and fat percentage estimate with age (**Figure 3.9A, 3.9B, 3.10A, 3.10B**). However, the monosomic mice showed a significantly higher increase in fat mass and fat percentage estimate compared to controls at both 8 and 25 weeks of age (**Figure 3.9A, 3.9B, 3.10A, 3.10B**).

Interestingly, lean mass was significantly decreased in 8-week old monosomic males compared to the controls (**Figure 3.9C**). No significant alterations in lean mass were observed in 8-week old monosomic females and in 25-week old monosomic mice compared to the controls (**Figure 3.9C, 3.10C).**

Next the average weight of the two groups of mice at each time point was compared to see if the increase in fat mass and fat percentage estimate was reflected in the overall body weight gain (**Figure 3.9D, 3.10D**). Average

body weight was significantly increased in 8-week old monosomic females compared to the controls (**Figure 3.9D**). No statistically significant differences in body weights were observed in 8-week old monosomic males compared to the controls (**Figure 3.9D**). However, both 25-week old monosomic males and females exhibited a statistically significant increase in their body weights compared to the controls (**Figure 3.10D, 3.11A, 3.11B**). The body weight gain observed in 25-week old monosomic mice is most likely due to their increased fat deposition as their lean mass was not significantly changed compared to the controls (**Figure 3.10C**).

3.3.5 INCREASED FAT DEPOSITION IN MONOSOMIC MICE IS HIGH-FAT DIET-INDUCED

In order to check if the HFD was the causal factor for the increase in fat deposition, monosomic mice and controls fed on a NFD were subjected to the DEXA analysis at 8 and 25 weeks of age (**Figure 3.9A–D, 3.10A–D**). At 8 week of age, only the monosomic males showed a statistically significant increase in fat mass, while both monosomic males and females exhibited a statistically significant increase in fat percentage estimate compared to the littermate controls (**Figure 3.9A, 3.9B**). However, the increase in fat percentage estimate was much more obvious in monosomic mice fed on a HFD (**Figure 3.9A**). In contrast, 25-week old monosomic mice fed on a NFD did not show a statistically significant increase in fat mass or fat percentage estimate compared to the controls (**Figure 3.10A, 3.10B**).

Interestingly, lean mass was significantly decreased in 8-week old monosomic females compared to their littermate controls (**Figure 3.9C**). No statistically significant alterations in lean mass were observed in 8-week old monosomic females and in both 25-week old monosomic males and females compared to the controls (**Figure 3.9C, 3.10C**).

Next, the average body weights of 8- and 25-week old monosomic mice and controls fed on a NFD were compared (**Figure 3.9D, 3.10D**). No statistically significant differences in the average body weights were observed in either 8-week or 25-week old monosomic mice compared to controls (**Figure 3.9D, 3.10D**).

Finally, the DEXA analysis was also carried out on 1-year old monosomic mice and their wildtype littermates fed on a NFD. No statistically significant increase in fat percentage estimate was observed in the monosomic mice compared to controls (**Figure 3.12A**). However, a significant increase in fat mass was observed in the monosomic females compared to controls (**Figure 3.12B**). Moreover, a significant increase in lean mass and body weight was observed in the monosomic females compared to their littermate controls, while no statistically significant changes were detected between the monosomic males and controls (**Figure 3.12C, 3.12D**).

Thus it seems that the HFD is the causal factor resulting in increased fat mass and fat percentage estimate, and thus in increased fat deposition, in monosomic mice.

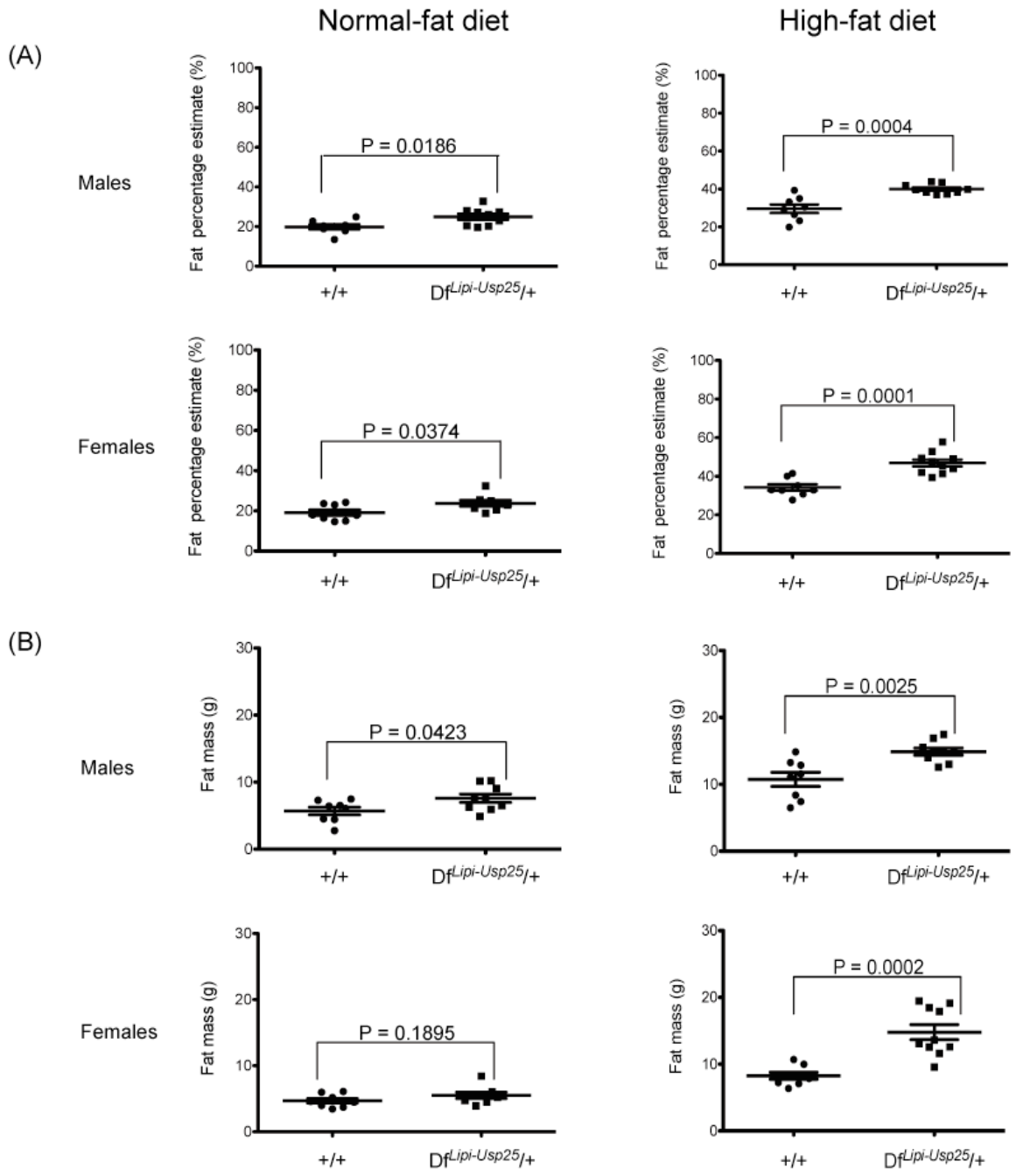
(A)
Normal-fat diet
High-fat diet
Males
Females
Fat percentage estimate (%)
P = 0.0186
P = 0.0004
P = 0.0374
P = 0.0001
+/+
Df Lipi-Usp25 /+
(B)
Fat mass (g)
P = 0.0423
P = 0.0025
P = 0.1895
P = 0.0002

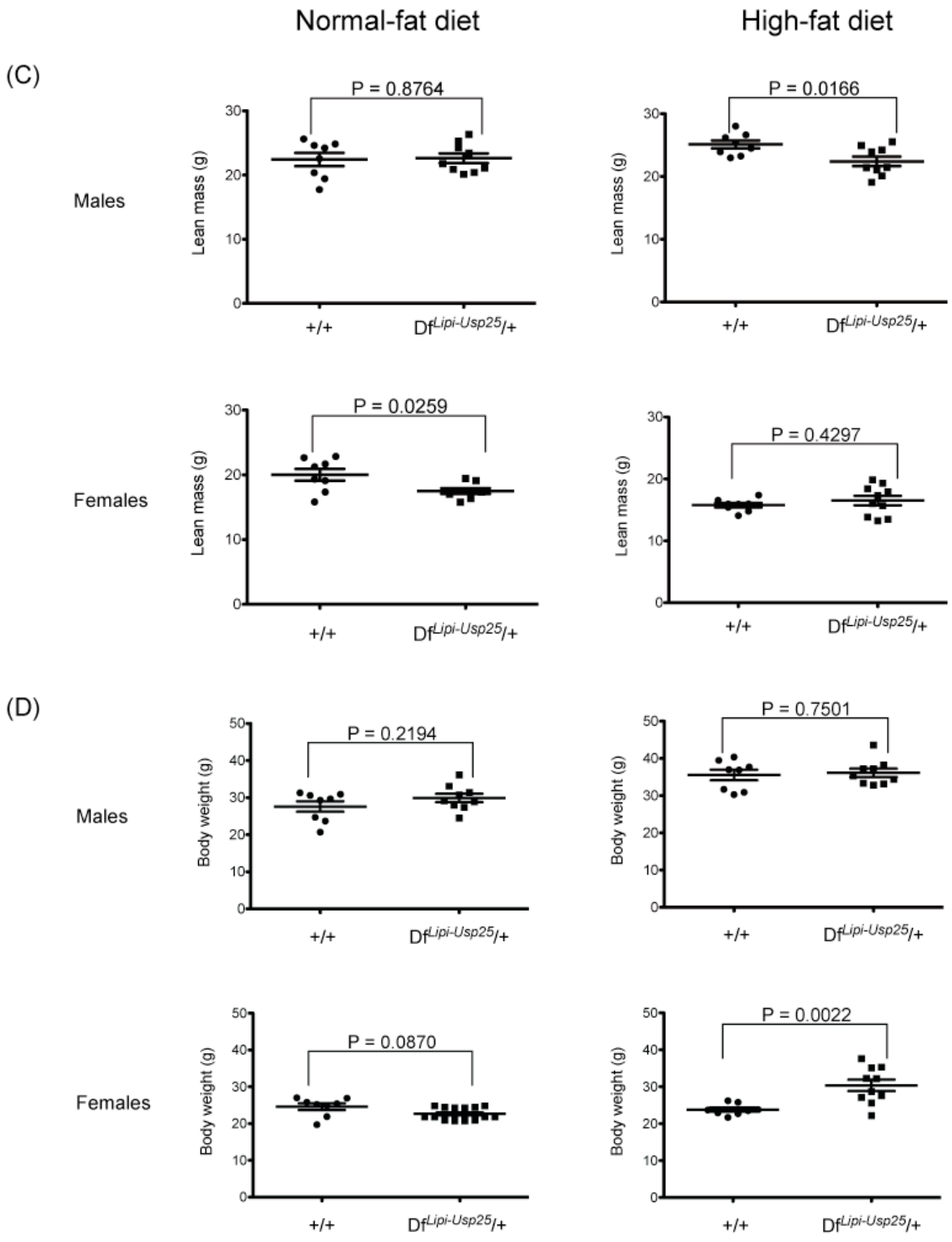

Figure 3.9. DEXA and body weight analysis of 8-week old control (+/+) and monosomic (*Df*$^{Lipi\text{-}Usp25}$/+) littermates fed either on a normal-fat or a high-fat diet. (A) DEXA results showing fat percentage estimate in male and female littermates. **(B)** DEXA results showing fat mass in male and female littermates. **(C)** DEXA results showing lean mass in male and female littermates. **(D)** Body weight results in male and female littermates. Data was statistically analysed using the two-tailed Student's *t*-test. Normal-fat diet: 9 monosomic (*Df*$^{Lipi\text{-}Usp25}$/+) males were compared with 8 control (+/+) males and 8 monosomic (*Df*$^{Lipi\text{-}Usp25}$/+) females were compared with 8 control (+/+) females. High-fat diet: 9 monosomic (*Df*$^{Lipi\text{-}Usp25}$/+) males were compared with 8 control (+/+) males and 10 monosomic (*Df*$^{Lipi\text{-}Usp25}$/+) females were compared with 8 control (+/+) females.

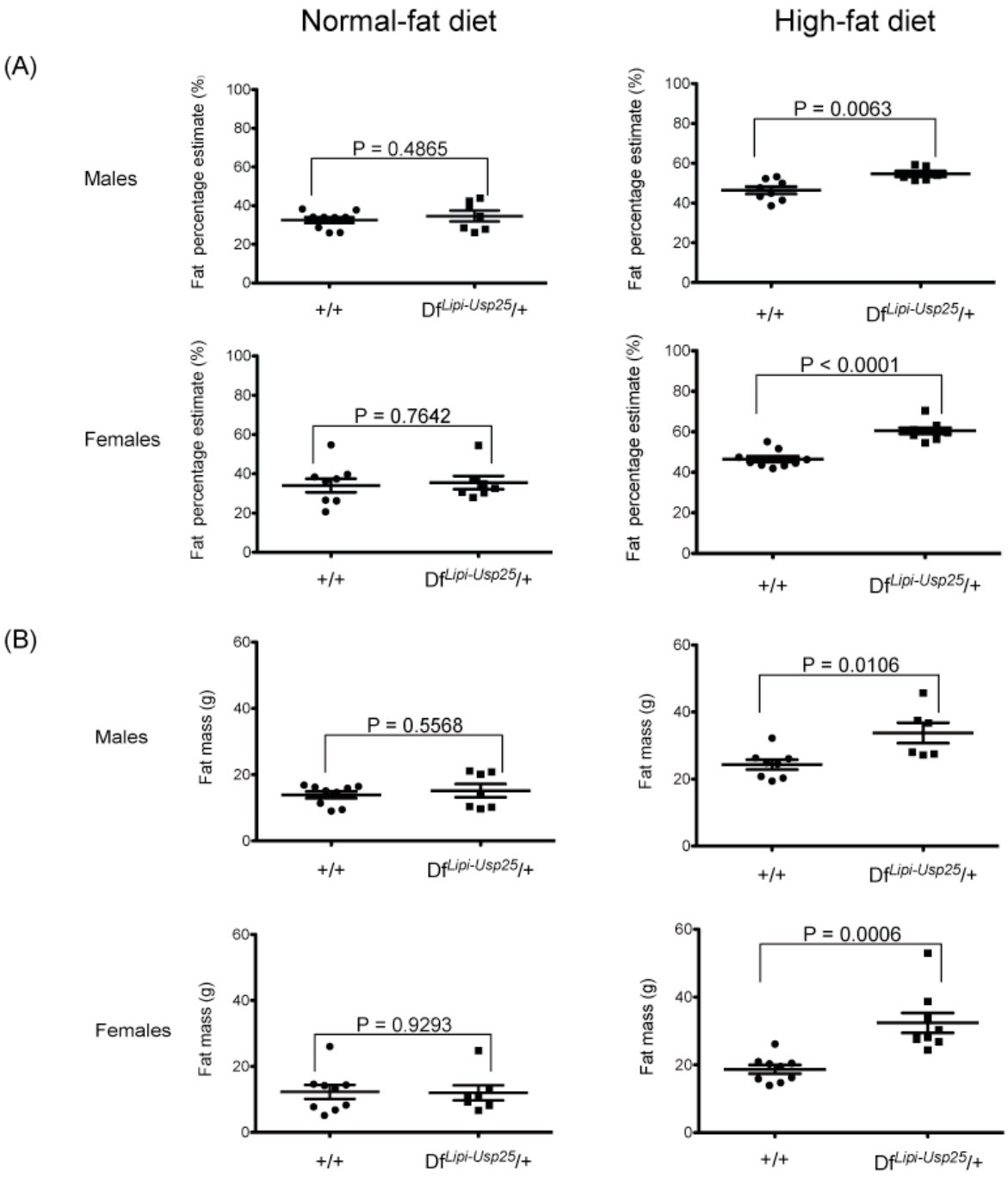
Normal-fat diet
High-fat diet
(A)
Males
Females
Fat percentage estimate (%)
P = 0.4865
P = 0.0063
P = 0.7642
P < 0.0001
(B)
Fat mass (g)
P = 0.5568
P = 0.0106
P = 0.9293
P = 0.0006
+/+
Df Lipi-Usp25 /+

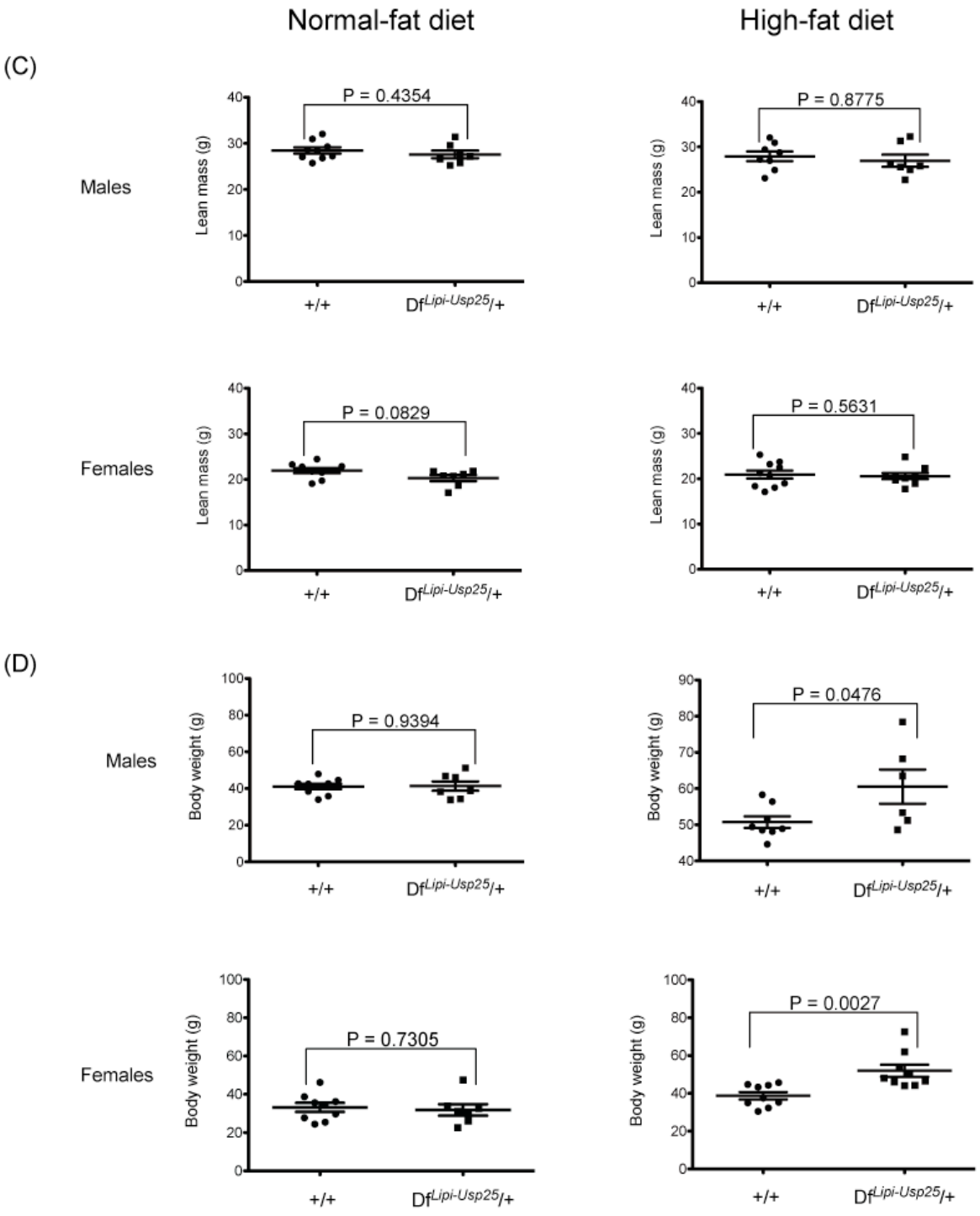

Figure 3.10. DEXA and body weight analysis of 25-week old control (+/+) and monosomic (*Df*$^{Lipi\text{-}Usp25}$/+) littermates fed either on a normal-fat or a high-fat diet. **(A)** DEXA results showing fat percentage estimate in male and female littermates. **(B)** DEXA results showing fat mass in male and female littermates. **(C)** DEXA results showing lean mass in male and female littermates. **(D)** Body weight results in male and female littermates. Data was statistically analysed using the two-tailed Student's *t*-test. Normal-fat diet: 7 monosomic (*Df*$^{Lipi\text{-}Usp25}$/+) males were compared with 9 controls (+/+) males and 7 monosomic (*Df*$^{Lipi\text{-}Usp25}$/+) females were compared with 9 control (+/+) females. High-fat diet: 7 monosomic (*Df*$^{Lipi\text{-}Usp25}$/+) males were compared with 8 controls (+/+) males and 9 monosomic (*Df*$^{Lipi\text{-}Usp25}$/+) females were compared with 10 control (+/+) females.

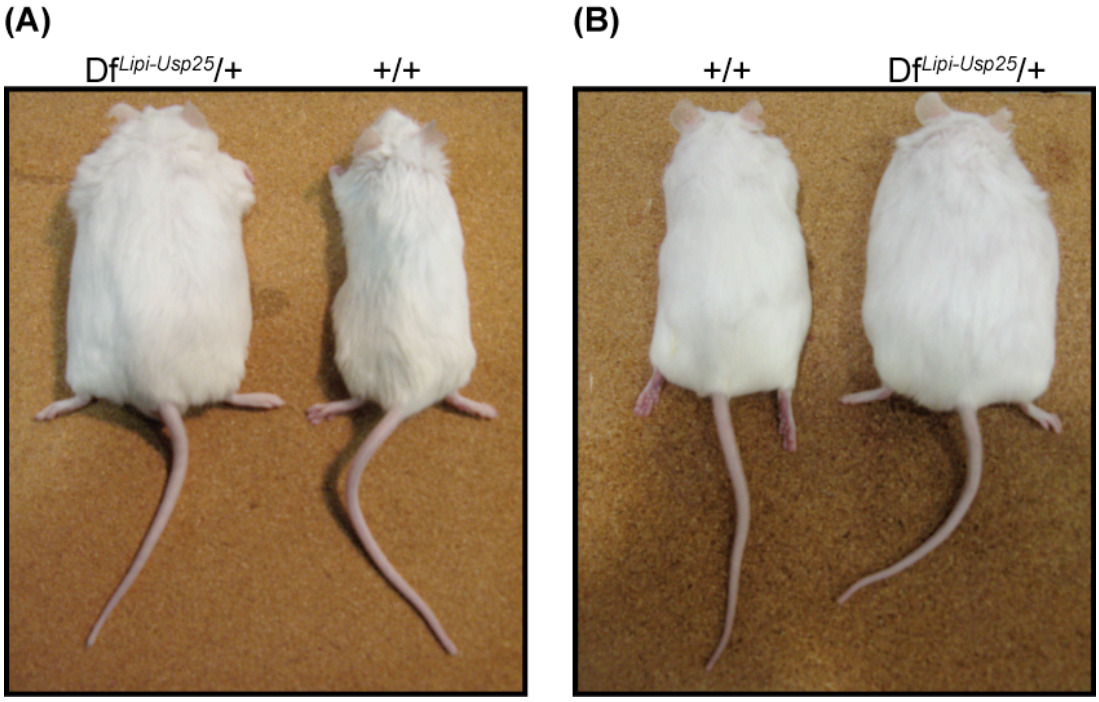

Figure 3.11. Photos of 25-week old control (+/+) and monosomic (*Df*$^{Lipi\text{-}Usp25}$/+) littermates. (A) Photo of 25-week old males fed on a high-fat diet. **(B)** Photo of 25-week old females fed on a high-fat diet.

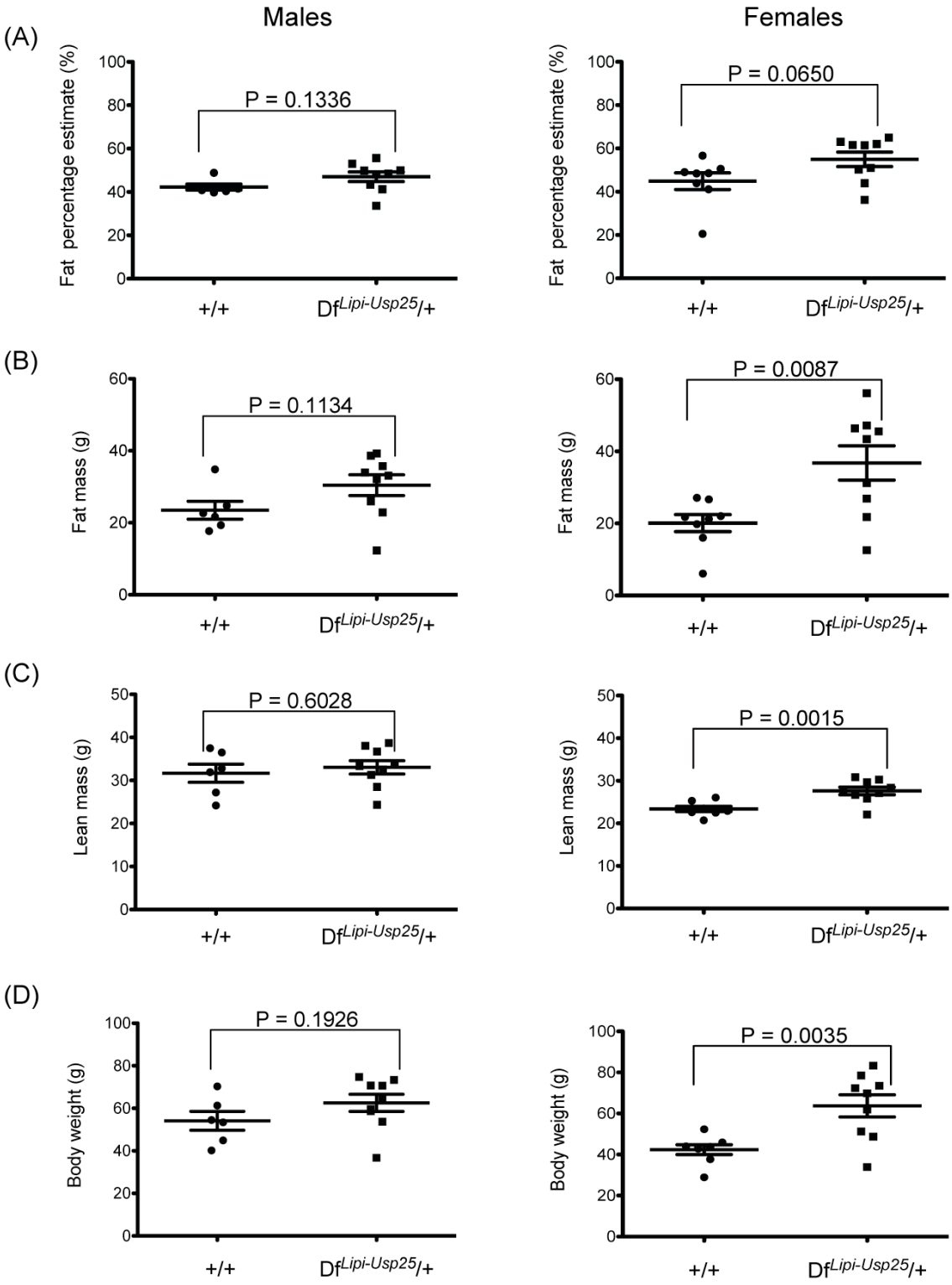

Figure 3.12. DEXA and body weight analysis of 1-year old control (+/+) and monosomic (*Df*$^{Lipi\text{-}Usp25}$/+) littermates fed on a normal-fat diet. (A) DEXA results showing fat percentage estimate in male and female littermates. **(B)** DEXA results showing fat mass in male and female littermates. **(C)** DEXA results showing lean mass in male and female littermates. **(D)** Body weight results in male and female littermates. Data was statistically analysed using the two-tailed Student's *t*-test. 9 monosomic (*Df*$^{Lipi\text{-}Usp25}$/+) males were compared with 6 control (+/+) males and 9 monosomic (*Df*$^{Lipi\text{-}Usp25}$/+) females were compared with 8 control (+/+) females.

3.3.6 INCREASED FATTY CHANGES IN THE LIVERS OF MONOSOMIC MICE FED ON A HIGH-FAT DIET

The histopathological analysis of different tissues stained with haematoxylin and eosin (H&E) of 8- and 25-week old control and monosomic mice fed on a HFD did not reveal any anatomical abnormalities of any organs, except for the presence of hepatic fatty changes in 8- and 25-week old monosomic mice (**Figure 3.13, 3.14A**) and a significantly thicker layer of subcutaneous fat (photos of all adipose sections placed on glass slides were taken under the same magnification, and subsequently the average thickness of subcutaneous adipose layer was calculated after taking three measurements of the fat layer width from each of the sections) and enlarged fat cells in 25-week old monosomic mice (**Figure 3.14B**). Specifically, the livers of 8-week old monosomic mice showed moderate fatty changes compared to mild fatty changes in the controls (**Figure 3.13**). The fatty changes in livers of the monosomic mice, as well as the controls, accelerated with age, and were regarded as severe to very severe in 25-week old monosomic mice compared to mild to moderate in the controls (**Figure 3.14A**).

The histopathological analysis of the livers stained with H&E of 8- and 25-week old monosomic mice fed on a NFD did not demonstrate the presence of any fatty changes compared to the controls (**Figure 3.13, 3.14A**). Interestingly, a broad range of fatty changes (from mild through moderate to severe) were observed in the livers of 1-year old monosomic mice and their control littermates fed on a NFD (**Figure 3.15A**). Moreover, the layer of subcutaneous fat showed differential thickness, from medium to thick, in each individual from both monosomic and control mice at 1 year of age (photos of all adipose sections placed on glass slides were taken under the same magnification, and subsequently the average thickness of subcutaneous adipose layer was calculated after taking three measurements of the fat layer width from each of the sections) (**Figure 3.15B**).

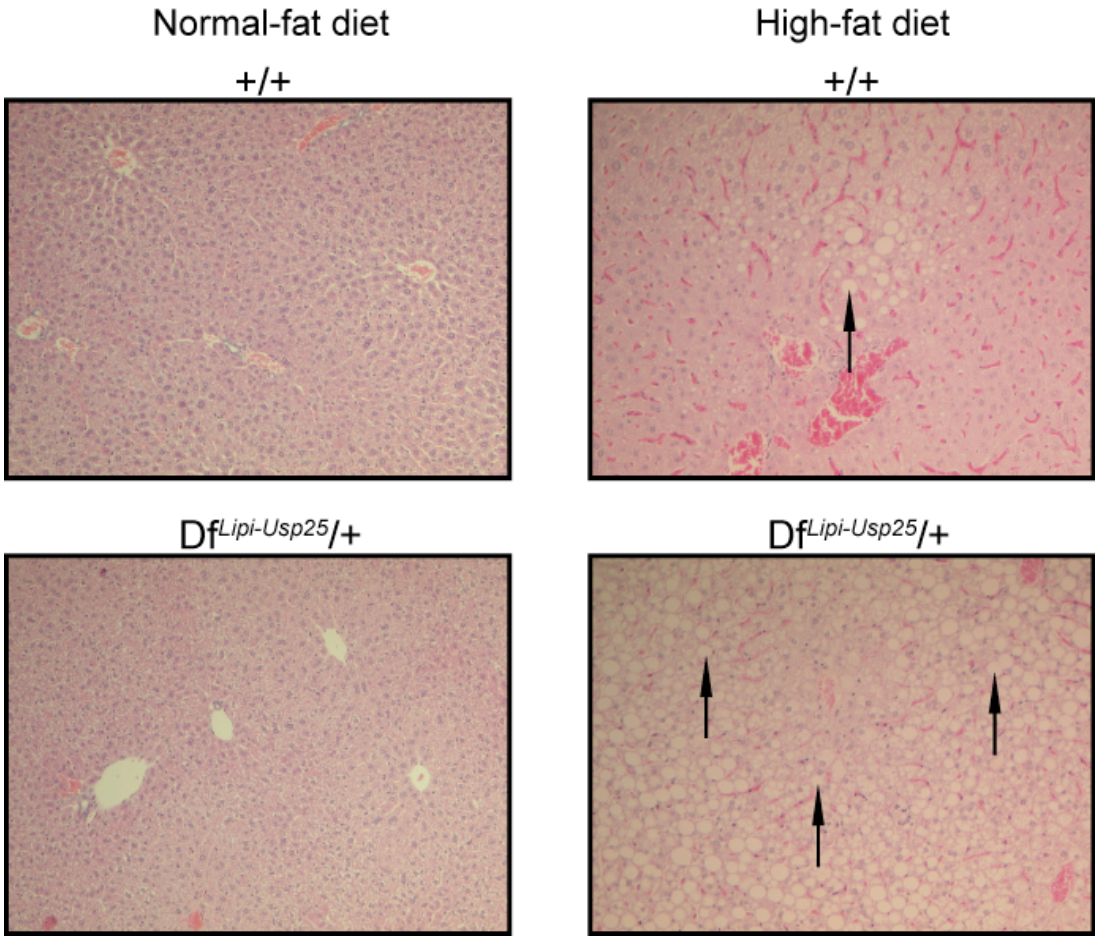

Figure 3.13. Histopathological analysis of livers collected from 8-week old control (+/+) and monosomic (*Df*$^{Lipi\text{-}Usp25}$/+) littermates fed either on a normal-fat or a high-fat diet. Haematoxylin and eosin-stained liver sections from control (+/+) and monosomic (*Df*$^{Lipi\text{-}Usp25}$/+) mice. Livers of control (+/+) and monosomic (*Df*$^{Lipi\text{-}Usp25}$/+) mice fed on a normal-fat diet showed no fatty changes. Livers of control (+/+) mice fed on a high-fat diet showed very mild fatty changes compared to moderate fatty changes in livers of monosomic (*Df*$^{Lipi\text{-}Usp25}$/+) mice. Note increased number of adipose cells (visible as white oval cells; indicated by arrows) in liver sections from monosomic (*Df*$^{Lipi\text{-}Usp25}$/+) compared to control (+/+) littermates. Images are representative and taken at x100 magnification.

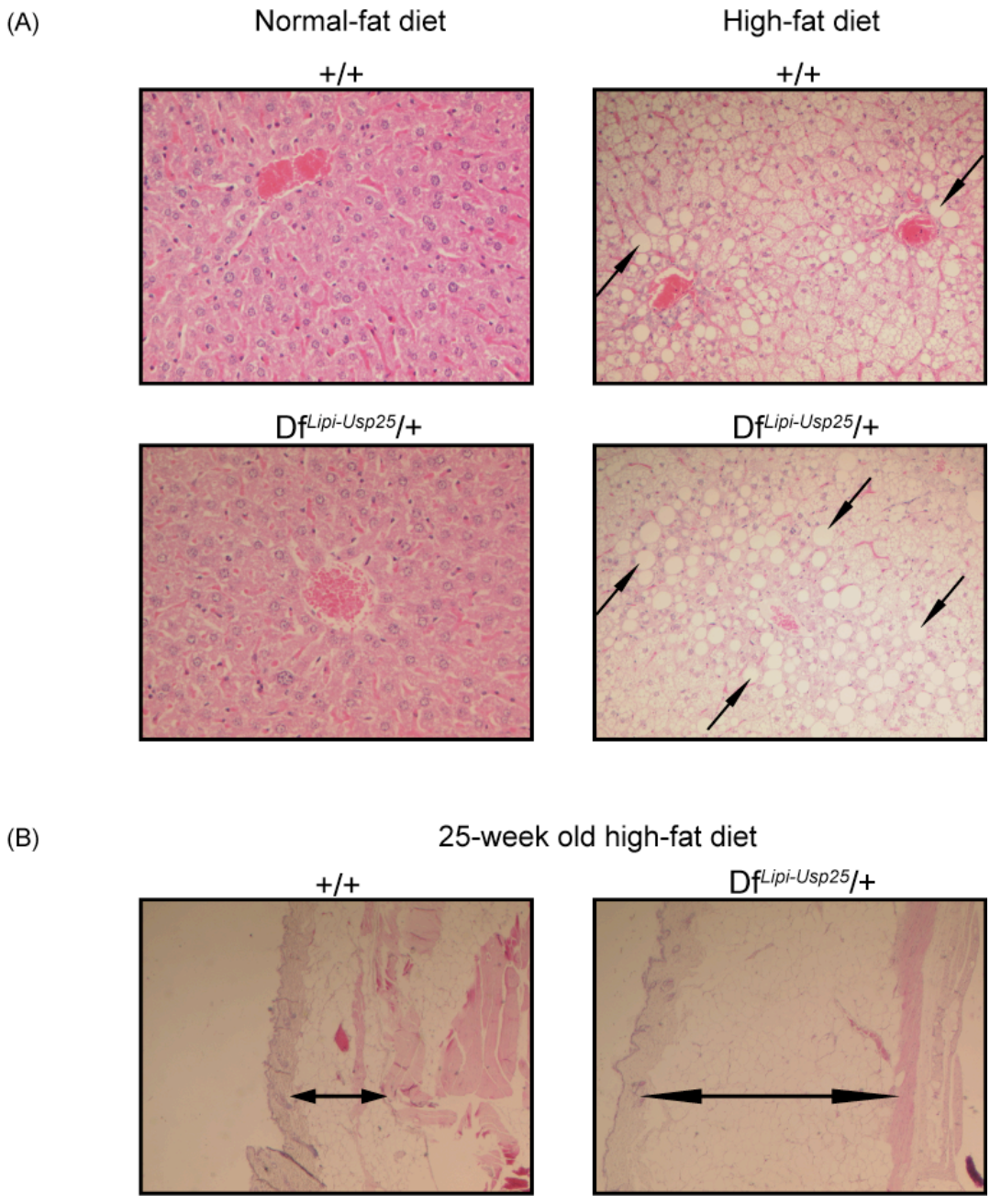

Figure 3.14. Histopathological analysis of livers and skin sections collected from 25-week old control (+/+) and monosomic (*Df*$^{Lipi\text{-}Usp25}$/+) littermates fed either on a normal-fat or a high-fat diet. (A) Haematoxylin and eosin-stained liver sections from control (+/+) and monosomic (*Df*$^{Lipi\text{-}Usp25}$/+) mice. Livers of control (+/+) and monosomic (*Df*$^{Lipi\text{-}Usp25}$/+) mice fed on a normal-fat diet showed no fatty changes. Livers of control (+/+) mice fed on a high-fat diet showed mild to moderate fatty changes compared to severe and very severe fatty changes in livers of monosomic (*Df*$^{Lipi\text{-}Usp25}$/+) mice. Note markedly increased number of adipose cells (visible as white oval cells; indicated by arrows) in liver sections from monosomic (*Df*$^{Lipi\text{-}Usp25}$/+) compared to control (+/+) littermates. Images are representative and taken at x100 magnification. **(B)** Haematoxylin and eosin-stained skin sections from control (+/+) and monosomic (*Df*$^{Lipi\text{-}Usp25}$/+) mice fed on a high-fat diet. Skin sections from monosomic (*Df*$^{Lipi\text{-}Usp25}$/+) mice have a markedly thicker fat layer (indicated by arrows) and fat cells are enlarged when compared to control (+/+) mice. Images are representative and taken at x50 magnification. One skin section was analysed per mouse and three measurements of the fat layer thickness were taken from the section. Skin sections were collected from 16 monosomic (*Df*$^{Lipi\text{-}Usp25}$/+) mice and 18 control (+/+) mice.

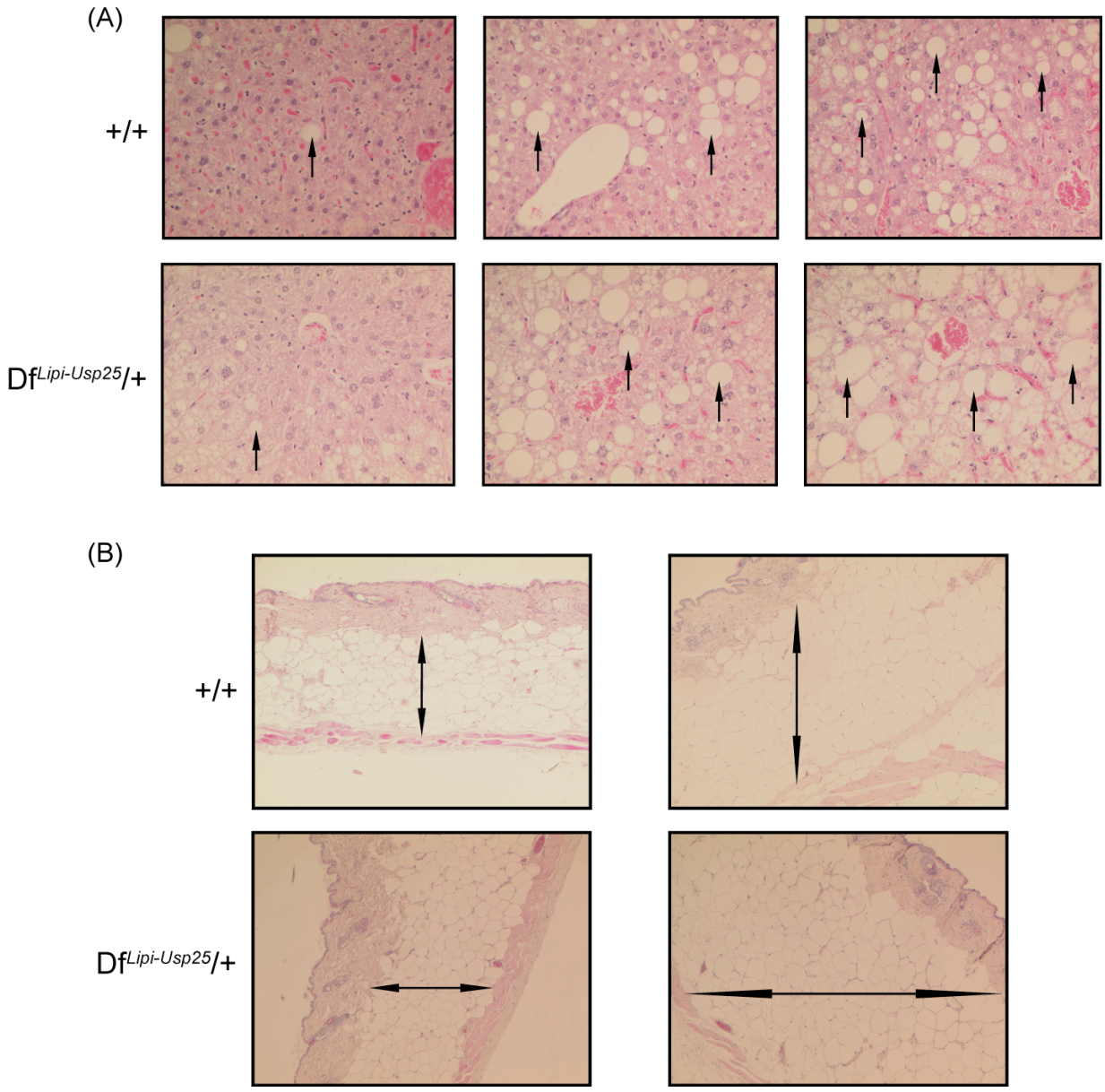

Figure 3.15. Histopathological analysis of livers and skin sections collected from 1-year old control (+/+) and monosomic (*Df*$^{Lipi\text{-}Usp25}$/+) littermates fed on a normal-fat diet. (A) Haematoxylin and eosin-stained liver sections from control (+/+) and monosomic (*Df*$^{Lipi\text{-}Usp25}$/+) mice. Livers of both control (+/+) and monosomic (*Df*$^{Lipi\text{-}Usp25}$/+) mice showed mild through moderate to severe fatty changes (from left to right; visible as white oval cells; indicated by arrows). Images are representative and taken at x200 magnification. **(B)** Haematoxylin and eosin-stained skin sections from control (+/+) and monosomic (*Df*$^{Lipi\text{-}Usp25}$/+) mice. Skin sections from both control (+/+) and monosomic (*Df*$^{Lipi\text{-}Usp25}$/+) mice showed a differential thickness of subcutaneous fat layer (indicated by arrows), from medium (left) to thick (right). Images are representative and taken at x50 magnification. One skin section was analysed per mouse and three measurements of the fat layer thickness were taken from the section. Skin sections were collected from 16 monosomic (*Df*$^{Lipi\text{-}Usp25}$/+) mice and 18 control (+/+) mice.

3.3.7 EXPRESSION ANALYSIS OF SUBCUTANEOUS ADIPOSE TISSUE IN MONOSOMIC MICE FED ON A HIGH-FAT DIET

To look at differentially expressed genes in adipocytes from monosomic and control mice fed on a high-fat diet (n=9 per genotype at 16 weeks of age), expression array analysis was performed. Analysis of the obtained data showed significantly altered expression ('raw' P values lower than 0.0015) of 30 genes (13 up-regulated, 17 down-regulated) (**Table 3.2**). However, given that the 'adjusted' p values for these genes were not significant, we performed quantitative RT-PCR (qRT-PCR) on a subset of these genes to validate our findings. Of the 15 genes analysed by qRT-PCR (selected on the basis of their rank or biological function), 2 were significantly up-regulated (*Tmem45a* and *Rbm38*; P=0.0085 and P=0.0081 respectively), and 4 were significantly down-regulated (*Plxnd1*, *Lrpap1*, *Samsn1* and *Lmna*; P=0.0047, P=0.0021, P=0.0057 and P=0.0002 respectively) (**Figure 3.16**). Moreover, *Samsn1* appears to be the only gene in the *Lipi–Usp25* deletion region to be expressed in adipose tissue and, as expected, this gene showed a significant reduction in its expression level.

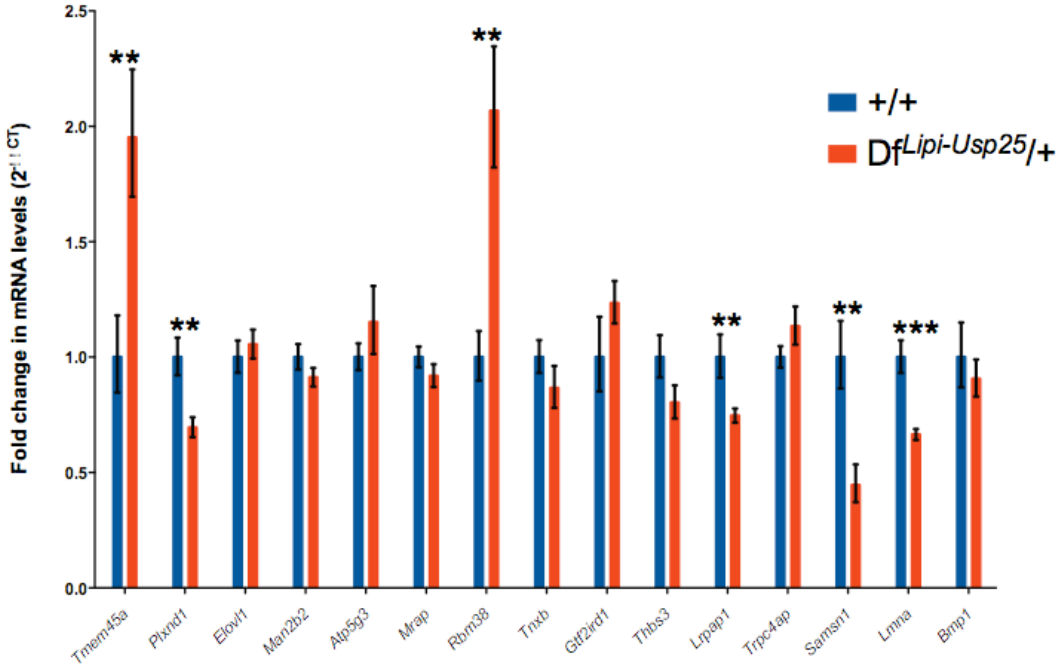

Figure 3.16. Quantitative RT-PCR (qRT-PCR) analysis of adipose tissue. qRT-PCR was performed on abdominal subcutaneous adipose tissue of 16-week old high fat diet-fed monosomic (*Df*$^{Lipi\text{-}Usp25}$/+) and control (+/+) mice (n=9 per genotype at 16 weeks). Asterisks indicate statistical significance; ** P<0.01, *** P<0.005 (two-tailed Student's *t*-test).

Table 3.2. Gene expression analysis of subcutaneous adipose tissue from monosomic (*Df*$^{Lipi\text{-}Usp25}$) and control (+/+) littermates fed on a high-fat diet. Gene expression data were obtained using RNA extracted from the subcutaneous adipose tissue of 16-week old HFD-fed monosomic and control mice (n=9 per genotype). The RNA was analysed on Illumina Mouse WG-6 v2.0 beadchips. Data were analysed and P-value adjusted (as described in the Methods) to yield a sorted list of differentially expressed genes. The differentially expressed genes with a raw P value <0.0015 are listed. Differential expression levels are shown as log fold change (LogFC) in the monosomic samples relative to the controls (a negative value indicates decreased expression). "qRT-PCR" shows whether there was a statistically significant difference in expression of the gene between the monosomic mice and controls (Yes, P<0.005; No, P>0.005; N.T., not tested). Functions/processes were based on gene ontology classifications as listed by Mouse Genome Informatics (http://www.informatics.jax.org/).

Gene	Official name	Ensembl ID (v61)	Log fold change	Average expression	Raw P value	Adjusted P value	qRT-PCR	Function/Processes (GO terms)
Tmem45a	Transmembrane protein 45a	ENSMUSG00000022754	0.245	7.0	0.0001	0.6402	Yes	Unknown
Plxnd1	Plexin D1	ENSMUSG00000030123	-0.393	8.1	0.0001	0.6402	Yes	Semaphorin receptor activity, regulation of branching involved in salivary gland morphogenesis, angiogenesis
Elovl1	Elongation of very long chain fatty acids-like 1	ENSMUSG00000006390	-0.236	9.3	0.0001	0.6402	No	Fatty acid biosynthetic processes
A	Nonagouti	ENSMUSG00000027596	0.169	6.7	0.0001	0.6402	N.T.	Melanocortin receptor binding activity, generation of precursor metabolites/energy
Man2b2	Mannosidase 2, alpha B2	ENSMUSG00000029119	-0.129	7.4	0.0002	0.6402	No	Carbohydrate metabolic processes
Atp5g3	ATP synthase, H+ transporting, mitochondrial F0 complex, subunit C3 (subunit 9)	ENSMUSG00000018770	0.213	12.8	0.0002	0.7142	No	ATP synthesis coupled proton transport
Mrap	Melanocortin 2 receptor accessory protein	ENSMUSG00000039956	-0.579	11.1	0.0004	0.7514	No	Adrenocorticotropin hormone and melanocortin receptor binding activity, brown fat cell differentiation
Rbm38	RNA binding motif protein 38	ENSMUSG00000027510	0.143	6.9	0.0005	0.7514	Yes	3'-UTR-mediated mRNA stabilization, negative regulation of cell proliferation
Zfp703	Zinc finger protein 703	ENSMUSG00000085795	-0.083	6.9	0.0005	0.7514	N.T.	Mammary gland epithelial cell differentiation & proliferation
Tnxb	Tenascin XB	ENSMUSG00000033327	-0.345	8.6	0.0006	0.7514	No	Cell-cell adhesion, extracellular matrix organization, lipid metabolic processes
Gtf2ird1	General transcription factor II I repeat domain-containing 1	ENSMUSG00000023079	0.169	7.6	0.0007	0.7514	No	DNA-dependent regulation of transcription
Ecm1	Extracellular matrix protein 1	ENSMUSG00000028108	-0.400	9.7	0.0007	0.7514	N.T.	Angiogenesis, regulation of bone mineralization
Pdk1	Pyruvate dehydrogenase kinase, isoenzyme 1	ENSMUSG00000006494	0.145	7.3	0.0007	0.7514	N.T.	Carbohydrate metabolic process
Thbs3	Thrombospondin 3	ENSMUSG00000028047	-0.121	7.0	0.0008	0.7514	No	Cell adhesion, growth plate cartilage development & ossification
Hist1h4f	Histone cluster 1, H4f	ENSMUSG00000069274	-0.260	7.3	0.0008	0.7514	N.T.	Unknown

Table 3.2 continued. Gene expression analysis of subcutaneous adipose tissue from monosomic (*Df*$^{Lipi\text{-}Usp25}$) and control (+/+) littermates fed on a high-fat diet.

Gene	Official name	Ensembl ID (v61)	Log fold change	Average expression	Raw P value	Adjusted P value	qRT-PCR	Function/Processes (GO terms)
Chchd10	Coiled-coil-helix-coiled-coil-helix domain containing 10	ENSMUSG00000049422	0.845	10.6	0.0008	0.7514	N.T.	Unknown
Lrpap1	Low density lipoprotein receptor-related protein associated protein 1	ENSMUSG00000029103	-0.337	11.4	0.0009	0.7514	Yes	Low-density lipoprotein particle receptor binding
Trpc4ap	Transient receptor potential cation channel, subfamily C, member 4 associated protein	ENSMUSG00000038324	0.110	7.9	0.0010	0.7514	No	Protein ubiquitination
Slpi	Secretory leukocyte peptidase inhibitor	ENSMUSG00000017002	-0.908	8.8	0.0010	0.7514	N.T.	Peptidase inhibitor activity
Uqcrc2	Ubiquinol cytochrome c reductase core protein 2	ENSMUSG00000030884	0.255	10.7	0.0010	0.7514	N.T.	Metal ion binding, electron transport chain
Samsn1	SAM domain, SH3 domain and nuclear localization signals, 1	ENSMUSG00000022876	-0.268	7.0	0.0010	0.7514	Yes	Unknown
Tsnax	Translin-associated factor X	ENSMUSG00000056820	0.239	9.7	0.0010	0.7514	N.T.	Cell differentiation, spermatogenesis
Diras2	DIRAS family, GTP-binding RAS-like 2	ENSMUSG00000047842	-0.358	7.3	0.0011	0.7514	N.T.	GTP catabolic processes
4930533 K18Rik	-	ENSMUSG00000047692	-0.165	7.7	0.0011	0.7514	N.T.	Unknown
Nmt1	N-myristoyltransferase 1	ENSMUSG00000020936	0.116	10.2	0.0012	0.7514	N.T.	Transferase activity, N-terminal protein myristoylation
Hist1h1c	Histone cluster 1, H1c	ENSMUSG00000036181	0.319	11.5	0.0012	0.7514	N.T.	Nucleosome assembly
Lmna	Lamin A	ENSMUSG00000028063	-0.200	7.4	0.0013	0.7514	Yes	Nucleus organization, sterol regulatory element binding protein import into nucleus, ventricular cardiac muscle cell development
Susd2	Sushi domain containing 2	ENSMUSG00000006342	-0.095	6.9	0.0013	0.7514	N.T.	Immune response, polysaccharide binding
Mtmr14	Myotubularin related protein 14	ENSMUSG00000030269	0.108	7.5	0.0014	0.7514	N.T.	Phosphatase activity
Bmp1	Bone morphogenetic protein 1	ENSMUSG00000022098	-0.374	9.1	0.0014	0.7514	No	Metalloendopeptidase activity, cartilage/bone development

3.3.8 HISTOPATHOLOGICAL ANALYSIS OF BONES OF 10-WEEK OLD MONOSOMIC MICE FED ON A NORMAL-FAT DIET SUGGESTS THAT LOSS OF ONE COPY OF THE *Lipi–Usp25* REGION MIGHT AFFECT BONE OSSIFICATION

In parallel with the phenotypic screening approach, different tissues stained with H&E collected from 10-week old control and monosomic mice fed on a NFD were subjected to detailed histopathological analysis. The examination did not reveal the existence of any anatomical changes of any organs, except tibias. Namely, decreased endochondral ossification in the cartilage of tibias was observed in the monosomic mice compared to controls (**Figure 3.17**).

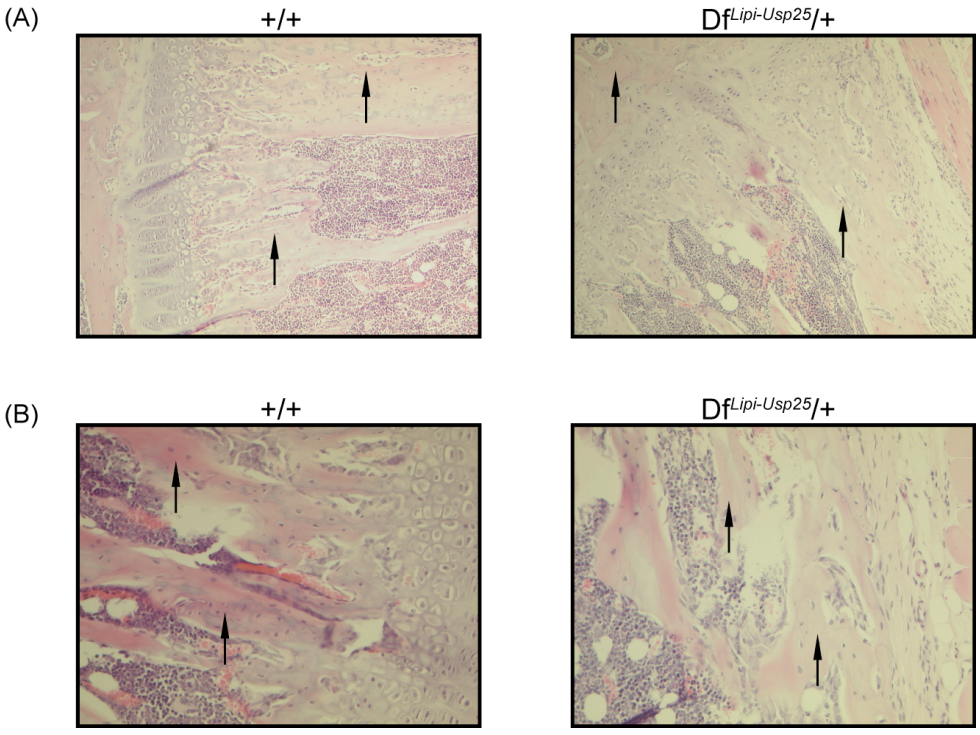

Figure 3.17. Histopathological analysis of bones collected from 10-week old control (+/+) and monosomic (*Df*$^{Lipi\text{-}Usp25}$/+) littermates fed on a normal-fat diet. (A) Haematoxylin and eosin-stained tibias sections from control (+/+) and monosomic (*Df*$^{Lipi\text{-}Usp25}$/+) males. Tibias of monosomic (*Df*$^{Lipi\text{-}Usp25}$/+) males showed lower endochondral ossification (visible as light pink staining of cartilage; indicated by arrow) compared to control (+/+) males (visible as darker pink staining of cartilage; indicated by arrow). Images are representative and taken at x100 magnification. **(B)** Haematoxylin and eosin-stained tibias sections from control (+/+) and monosomic (*Df*$^{Lipi\text{-}Usp25}$/+) females. Tibias of monosomic (*Df*$^{Lipi\text{-}Usp25}$/+) females showed lower endochondral ossification (visible as light pink staining of cartilage; indicated by arrows) compared to control (+/+) females (visible as dark pink staining of cartilage; indicated by arrows). Images are representative and taken at x200 magnification.

3.3.9 FOLLOW-UP ANALYSIS OF BONES OF 8-, 25-WEEK AND 1-YEAR OLD MONOSOMIC MICE REVEALS THAT LOSS OF ONE COPY OF THE *Lipi–Usp25* REGION DOES NOT AFFECT BONE OSSIFICATION

Following the preliminary histopathological results, suggesting that the monosomic mice fed on a NFD exhibit decreased endochondral ossification, bones of additional monosomic mice and littermate controls fed on a NFD were analysed by DEXA (to measure bone mineral density) and histopathologically (to evaluate the level of endochondral ossification of the cartilage) at additional time points, specifically at 8 and 25 weeks and 1 year of age (**Figure 3.18A, 3.18B, 3.19A, 3.19B, 3.21A, 3.21B**). No significant differences in bone mineral density were observed between control and monosomic mice at any of the time points (**Figure 3.18A, 3.19A, 3.21A**). In addition, no histopathological changes in the cartilage and/or in the cortical bone shaft of any analysed bones (tibia, femur, radius, ulna, sternum and ribs) were observed in monosomic mice at 8 and 25 weeks and 1 year of age (**Figure 3.18B, 3.19B, 3.21A**). Bones of 25-week old mice were further analysed with von Kossa staining to compare the level of calcium deposition between monosomic mice and their littermate controls. No differences in the calcium deposition were observed (**Figure 3.20**).

Thus we conclude that monosomy of the *Lipi–Usp25* region does not have an impact on endochondral ossification, bone mineral density or calcium deposition.

3.3.10 INCREASED FAT MASS IN 8- AND 25-WEEK OLD MICE DOES NOT LEAD TO THE INCREASE IN BONE MASS

The existence of the relationship between body fat mass and bone metabolism has been reported by various studies (Zhao 2008; Holecki 2010). However, it still remains unclear whether increased body fat mass has a protective effect on bone tissue, and thus causes increased bone mass, since contradicting results have been provided by these studies (Zhao 2008; Holecki 2010).

To test whether increased fat mass is linked with increased bone mass, we decided to compare the level of bone mineral density and the level of endochondral ossification in the cartilage and/or in the cortical bone shaft of monosomic and control mice fed either on a NFD or a HFD. Bones of 8- and 25-week old control and monosomic mice fed on a HFD showed no significant differences in bone mineral density, except for a decrease in bone mineral density in 8-week old monosomic males compared to controls (**Figure 3.18A, 3.19A**). In addition, no histopathological changes in the cartilage and/or in the cortical bone shaft were observed in monosomic mice at 8 and 25 weeks of age (**Figure 3.18B, 3.19B**). Furthermore, despite significant differences being observed in fat mass in both groups (**Figure 3.22A, 3.23A, 3.24A, 3.25A**), no significant differences in bone mineral density were observed between monosomic mice fed on a NFD or a HFD, or between control mice fed on a NFD or a HFD at any analysed time points (**Figure 3.22B, 3.23B, 3.24B, 3.25B**). Thus we did not observe any beneficial effects of significantly increased fat mass on bone mass in the monosomic mice compared to their littermate controls, or any correlation between significantly increased fat mass and increased bone mass in the monosomic and control mice fed on a HFD compared with those on a NFD. Altogether, our results do not support a hypothesis suggesting a protective effect of increased fat mass on bone tissue.

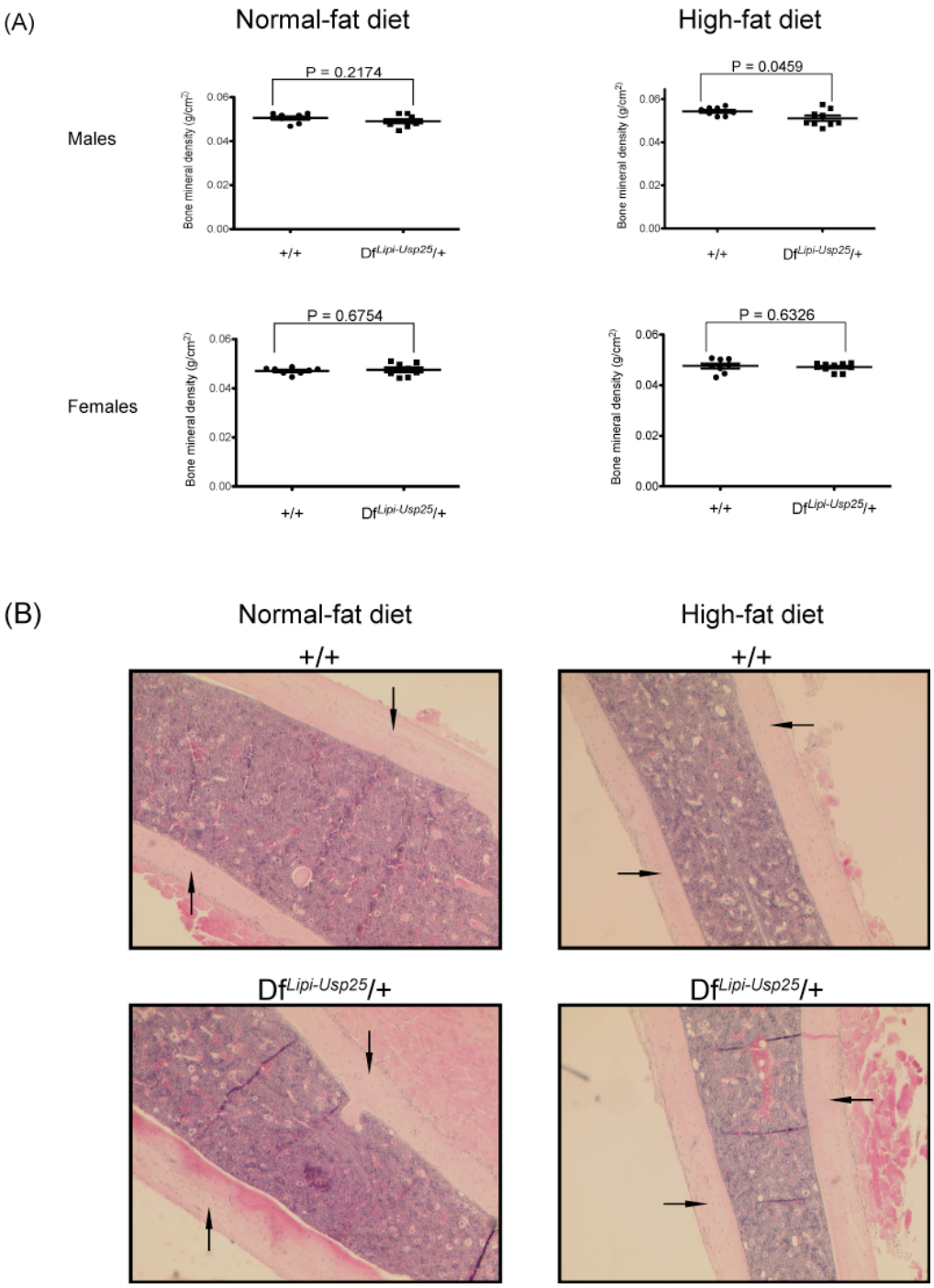

Figure 3.18. DEXA and histopathological analysis of bones collected from 8-week old control (+/+) and monosomic (*Df*$^{Lipi\text{-}Usp25}$/+) littermates fed on a normal-fat or high-fat diet. (A) DEXA results showing bone mineral density in male and female littermates fed on a normal-fat or high-fat diet. Data was statistically analysed using the two-tailed Student's *t*-test. Normal-fat diet: 9 monosomic (*Df*$^{Lipi\text{-}Usp25}$/+) males were compared with 8 control (+/+) males and 8 monosomic (*Df*$^{Lipi\text{-}Usp25}$/+) females were compared with 8 control (+/+) females. High-fat diet: 9 monosomic (*Df*$^{Lipi\text{-}Usp25}$/+) males were compared with 8 control (+/+) males and 10 monosomic (*Df*$^{Lipi\text{-}Usp25}$/+) females were compared with 8 control (+/+) females. **(B)** Haematoxylin and eosin-stained bone sections from control (+/+) and monosomic (*Df*$^{Lipi\text{-}Usp25}$/+) mice fed on a normal-fat or high-fat diet. No changes in the cortical bone ossification levels (visible as pink staining of the cortical bone shaft; indicated by arrows) were observed between the monosomic (*Df*$^{Lipi\text{-}Usp25}$/+) and control (+/+) mice. Images are representative and taken at x50 magnification.

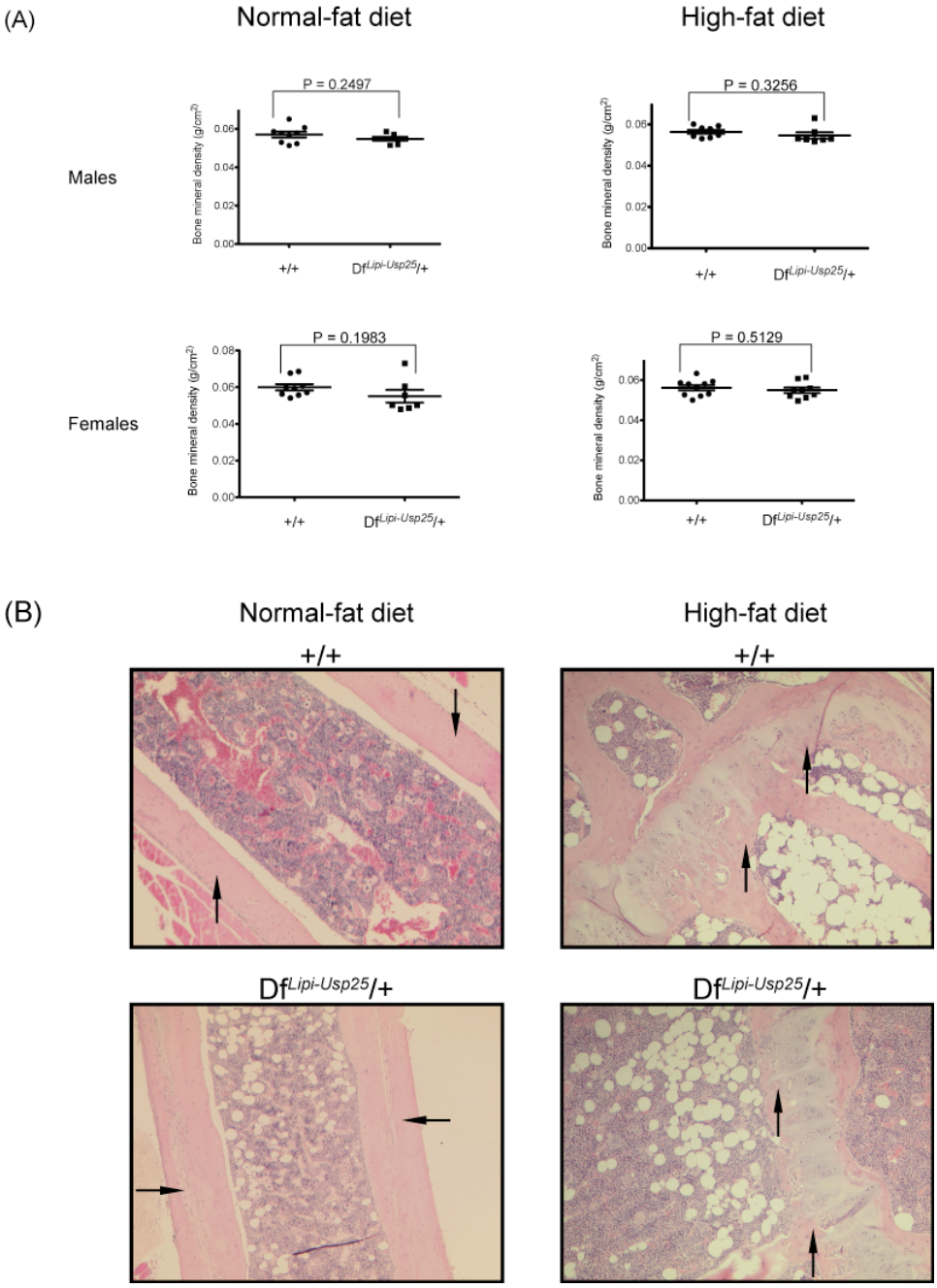

Figure 3.19. DEXA and histopathological analysis of bones collected from 25-week old control (+/+) and monosomic (*Df*$^{Lipi\text{-}Usp25}$/+) littermates fed on a normal-fat or high-fat diet. (A) DEXA results showing bone mineral density in male and female littermates fed on a normal-fat or high-fat diet. Data was statistically analysed using the two-tailed Student's *t*-test. Normal-fat diet: 7 monosomic (*Df*$^{Lipi\text{-}Usp25}$/+) males were compared with 9 controls (+/+) males and 7 monosomic (*Df*$^{Lipi\text{-}Usp25}$/+) females were compared with 9 control (+/+) females. High-fat diet: 7 monosomic (*Df*$^{Lipi\text{-}Usp25}$/+) males were compared with 8 controls (+/+) males and 9 monosomic (*Df*$^{Lipi\text{-}Usp25}$/+) females were compared with 10 control (+/+) females. **(B)** Haematoxylin and eosin-stained bone sections from control (+/+) and monosomic (*Df*$^{Lipi\text{-}Usp25}$/+) mice fed on a normal-fat or high-fat diet. No changes in the cortical bone ossification levels (left panel; visible as pink staining of the cortical bone shaft; indicated by arrows) and no changes in the endochondral ossification of the cartilage (right panel; visible as pink staining of the cartilage; indicated by arrows) and were observed between the monosomic (*Df*$^{Lipi\text{-}Usp25}$/+) and control (+/+) mice. Images are representative and taken at x50 or x100 magnification.

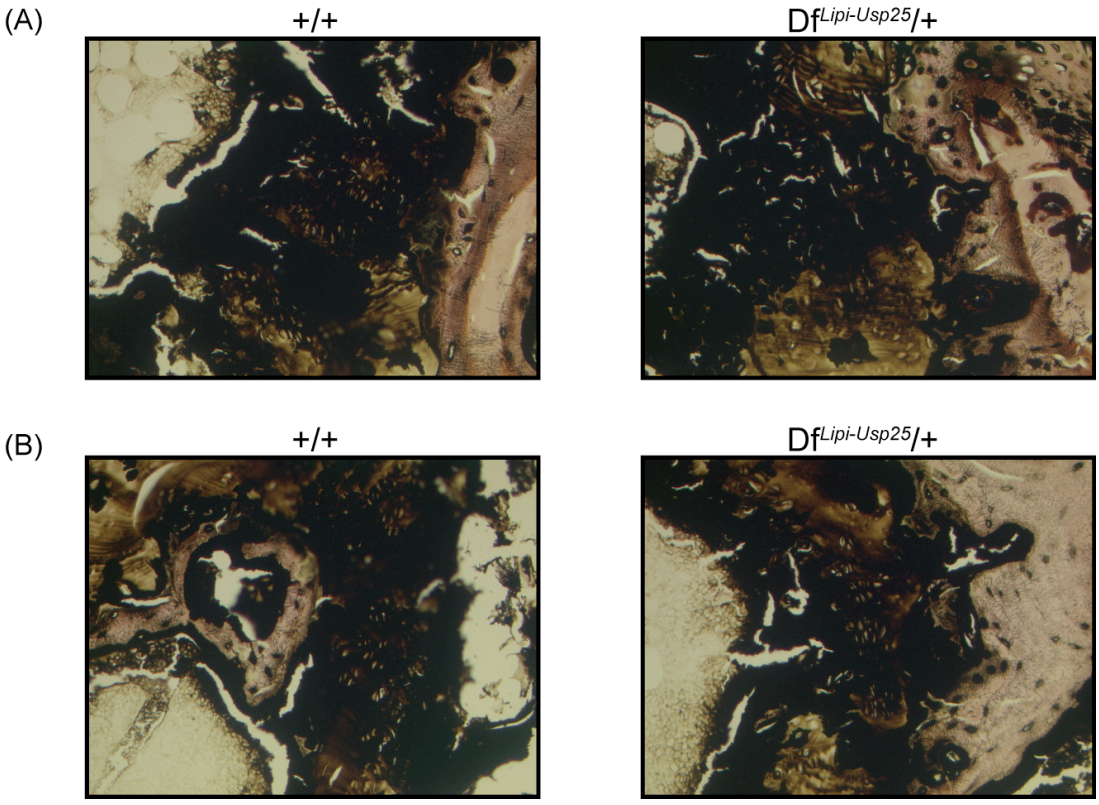

Figure 3.20. Histopathological analysis of bones collected from 25-week old control (+/+) and monosomic (*Df*$^{Lipi\text{-}Usp25}$/+) littermates fed on a normal-fat. (A) Von Kossa-stained tibia sections from control (+/+) and monosomic (*Df*$^{Lipi\text{-}Usp25}$/+) males. No changes in the calcium deposition (visible as black staining) were observed between the monosomic (*Df*$^{Lipi\text{-}Usp25}$/+) and control (+/+) males. Images are representative and taken at x200 magnification. **(B)** Von Kossa-stained tibia sections from control (+/+) and monosomic (*Df*$^{Lipi\text{-}Usp25}$/+) females. No changes in the calcium deposition (visible as black staining) were observed between the monosomic (*Df*$^{Lipi\text{-}Usp25}$/+) and control (+/+) females. Images are representative and taken at x200 magnification.

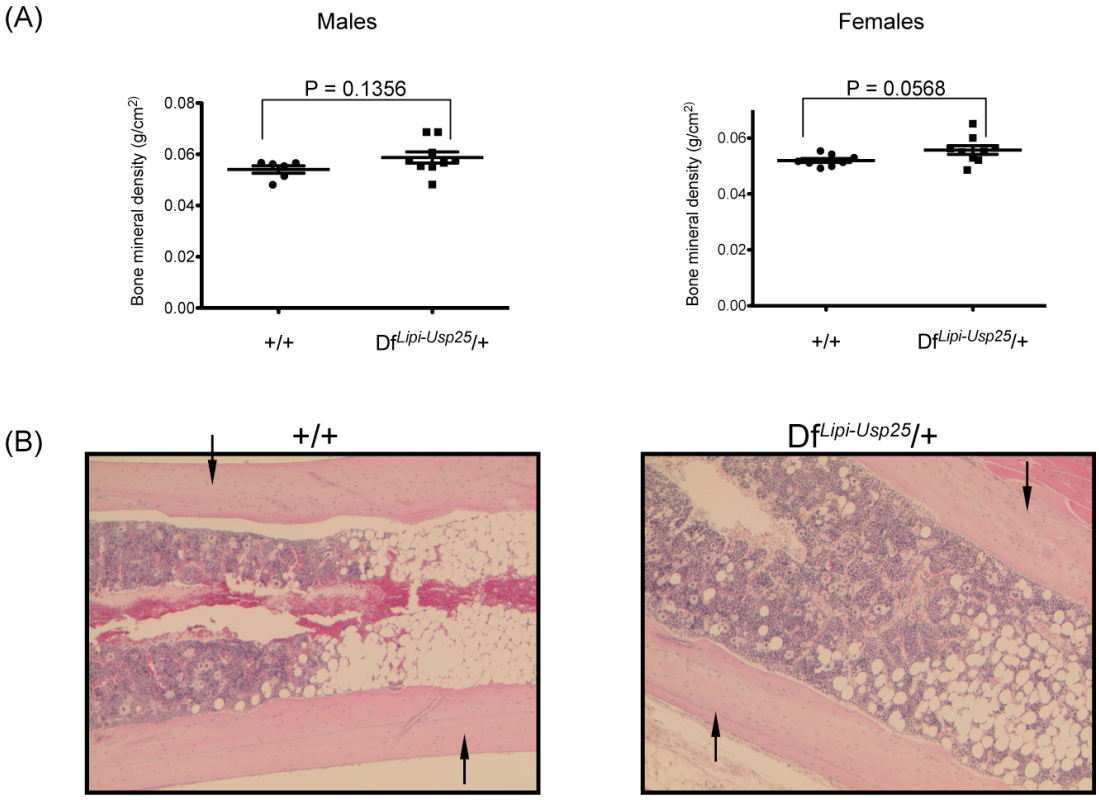

Figure 3.21. DEXA and histopathological analysis of bones collected from 1-year old control (+/+) and monosomic (*Df*$^{Lipi\text{-}Usp25}$/+) littermates fed on a normal-fat diet. **(A)** DEXA results showing bone mineral density in male and female littermates. Data was statistically analysed using the two-tailed Student's *t*-test. 9 monosomic (*Df*$^{Lipi\text{-}Usp25}$/+) males were compared with 6 control (+/+) males and 9 monosomic (*Df*$^{Lipi\text{-}Usp25}$/+) females were compared with 8 control (+/+) females. **(B)** Haematoxylin and eosin-stained bone sections from control (+/+) and monosomic (*Df*$^{Lipi\text{-}Usp25}$/+) mice. No changes in the cortical bone ossification levels (visible as pink staining of the cortical bone shaft) were observed between the monosomic (*Df*$^{Lipi\text{-}Usp25}$/+) and control (+/+) mice. Images are representative and taken at x50 magnification.

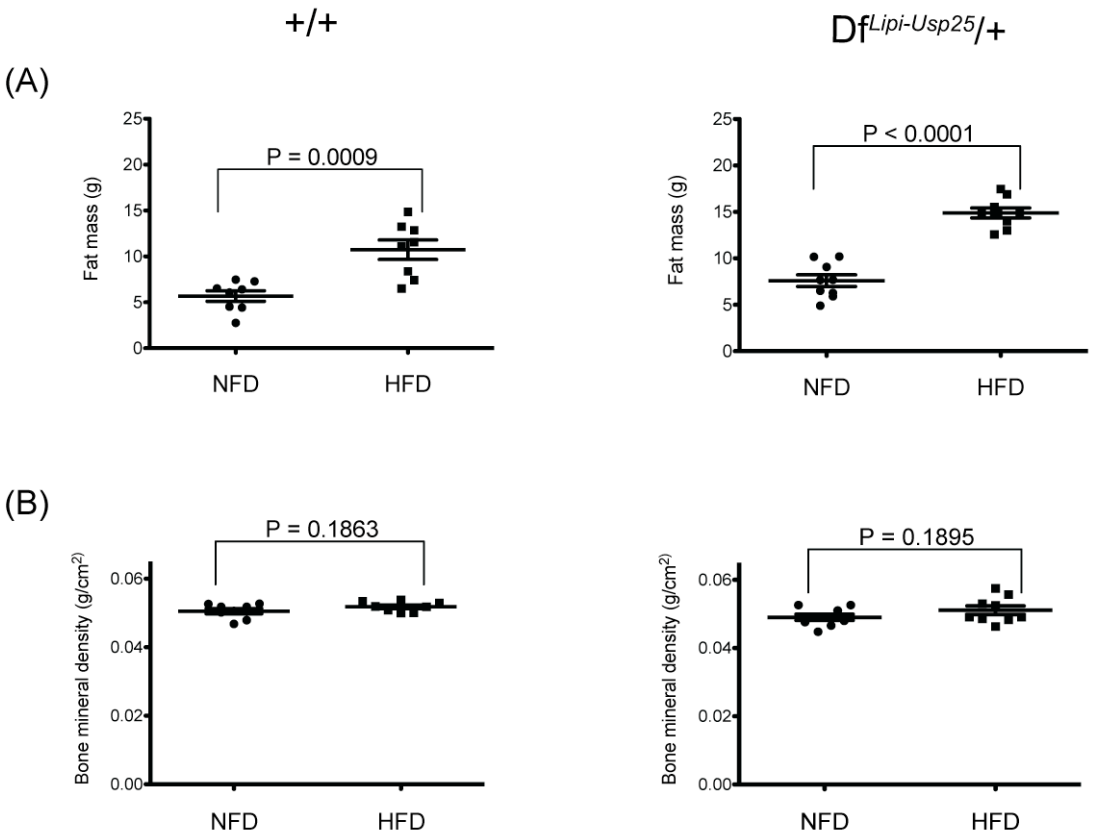

Figure 3.22. DEXA analysis of 8-week old control (+/+) and monosomic (*Df*$^{Lipi\text{-}Usp25}$/+) male littermates fed on a normal-fat or high-fat diet (group 1). (A) DEXA results showing fat mass in control (+/+) and monosomic (*Df*$^{Lipi\text{-}Usp25}$/+) male littermates fed on a normal-fat or high-fat diet. **(B)** DEXA results showing bone mineral density in control (+/+) and monosomic (*Df*$^{Lipi\text{-}Usp25}$/+) male littermates fed on a normal-fat or high-fat diet. Data was statistically analysed using the two-tailed Student's *t*-test. Normal-fat diet: 9 monosomic (*Df*$^{Lipi\text{-}Usp25}$/+) males were compared with 8 control (+/+) males. High-fat diet: 9 monosomic (*Df*$^{Lipi\text{-}Usp25}$/+) males were compared with 8 control (+/+) males. NFD - normal fat diet, HFD - high fat diet.

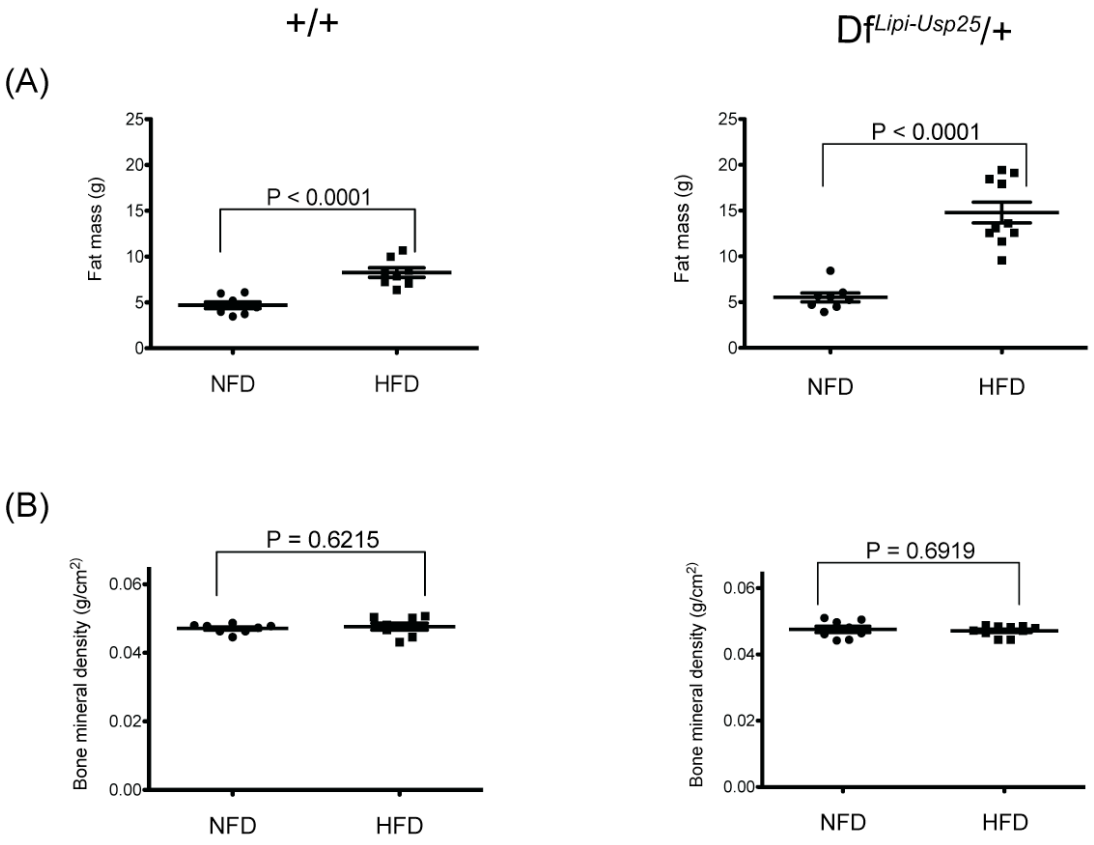

Figure 3.23. DEXA analysis of 8-week old control (+/+) and monosomic (*Df*$^{Lipi\text{-}Usp25}$/+) female littermates fed on a normal-fat or high-fat diet (group 2). (A) DEXA results showing fat mass in control (+/+) and monosomic (*Df*$^{Lipi\text{-}Usp25}$/+) female littermates fed on a normal-fat or high-fat diet. **(B)** DEXA results showing bone mineral density in control (+/+) and monosomic (*Df*$^{Lipi\text{-}Usp25}$/+) female littermates fed on a normal-fat or high-fat diet. Data was statistically analysed using the two-tailed Student's *t*-test. Normal-fat diet 8 monosomic (*Df*$^{Lipi\text{-}Usp25}$/+) females were compared with 8 control (+/+) females. High-fat diet: 10 monosomic (*Df*$^{Lipi\text{-}Usp25}$/+) females were compared with 8 control (+/+) females. NFD - normal fat diet, HFD - high fat diet.

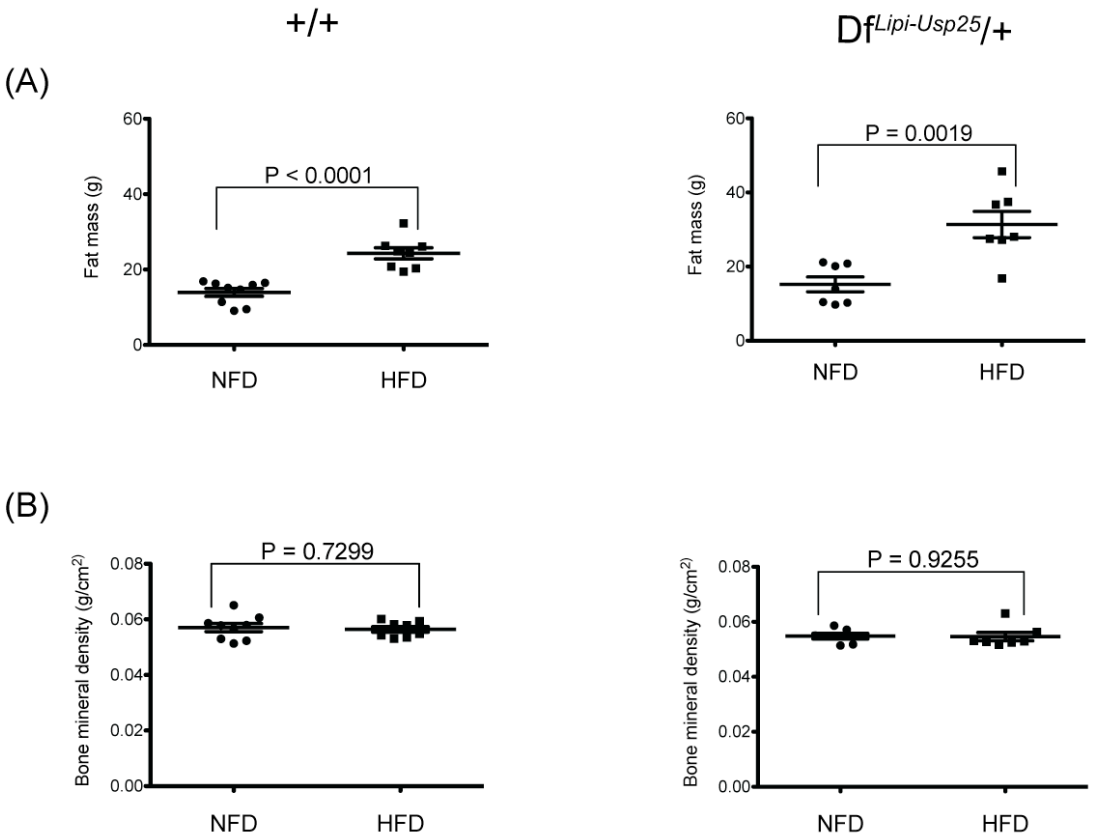

Figure 3.24. DEXA analysis of 25-week old control (+/+) and monosomic (*Df*$^{Lipi\text{-}Usp25}$/+) male littermates fed on a normal-fat or high-fat diet (group 3). (A) DEXA results showing fat mass in control (+/+) and monosomic (*Df*$^{Lipi\text{-}Usp25}$/+) male littermates fed on a normal-fat or high-fat diet. **(B)** DEXA results showing bone mineral density in control (+/+) and monosomic (*Df*$^{Lipi\text{-}Usp25}$/+) male littermates fed on a normal-fat or high-fat diet. Data was statistically analysed using the two-tailed Student's *t*-test. Normal-fat diet: 7 monosomic (*Df*$^{Lipi\text{-}Usp25}$/+) males were compared with 9 controls (+/+) males. High-fat diet: 7 monosomic (*Df*$^{Lipi\text{-}Usp25}$/+) males were compared with 8 controls (+/+) males. NFD - normal fat diet, HFD - high fat diet.

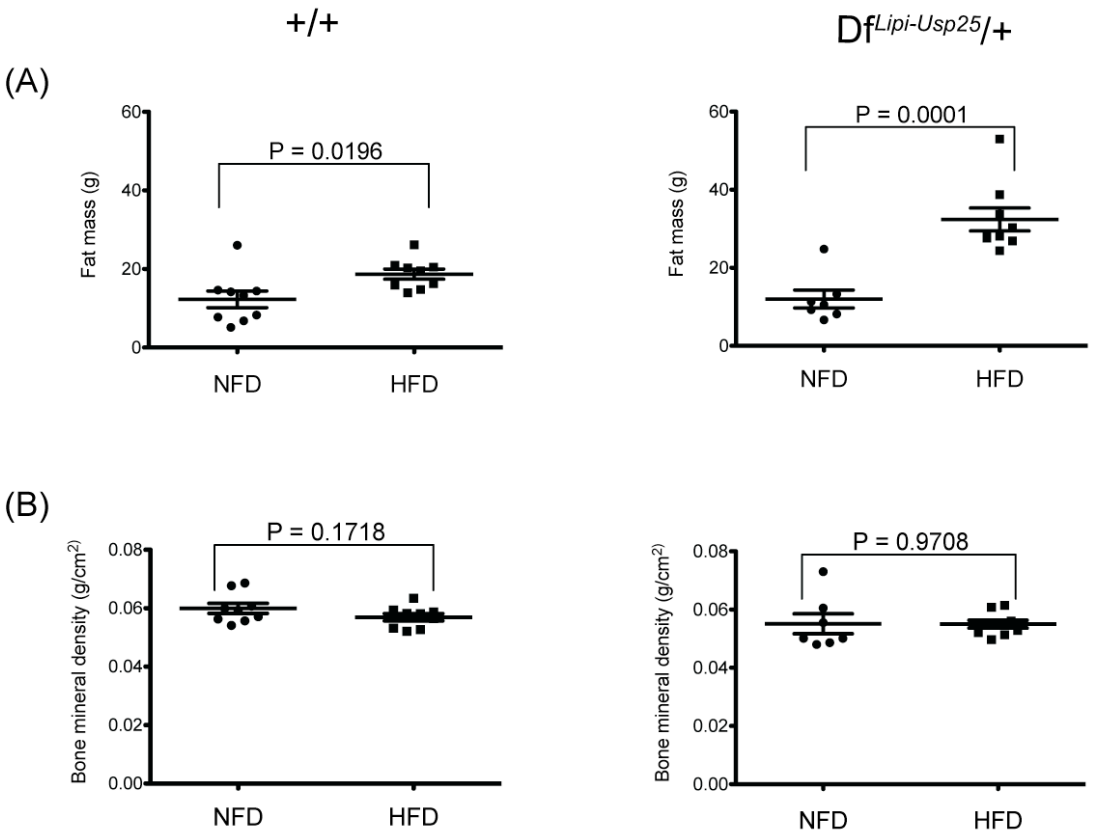

Figure 3.25. DEXA analysis of 25-week old control (+/+) and monosomic *(Df*$^{Lipi\text{-}Usp25}$*/+)* female littermates fed on a normal-fat or high-fat diet (group 4). (A) DEXA results showing fat mass in control (+/+) and monosomic (*Df*$^{Lipi\text{-}Usp25}$/+) female littermates fed on a normal-fat or high-fat diet. **(B)** DEXA results showing bone mineral density in control (+/+) and monosomic (*Df*$^{Lipi\text{-}Usp25}$/+) female littermates fed on a normal-fat or high-fat diet. Data was statistically analysed using the two-tailed Student's *t*-test. Normal-fat diet: 7 monosomic (*Df*$^{Lipi\text{-}Usp25}$/+) females were compared with 9 control (+/+) females. High-fat diet: 9 monosomic (*Df*$^{Lipi\text{-}Usp25}$/+) females were compared with 10 control (+/+) females. NFD - normal fat diet, HFD - high fat diet.

3.3.11 DIFFERENTIAL RESPONSES OF MONOSOMIC FEMALES TO INFECTION WITH *CITROBACTER RODENTIUM* LUX MIGHT HAVE BEEN CAUSED BY SUBTLE CHANGES IN THE MICROENVIRONMENT

To determine whether monosomic *Df*$^{Lipi\text{-}Usp25}$ mice show differences in the susceptibility to bacterial infections, 8 monosomic and 8 control males fed on a NFD were infected with *Salmonella* Typhimurium TET C, while 8 monosomic and 8 control females fed on a NFD were infected with *Citrobacter rodentium* lux.

No differences in the susceptibility to infection with *Salmonella* Typhimurium TET C were identified between control and monosomic mice. Specifically, no significant differences were observed in bacterial enumeration of spleens, livers and caecal contents (**Figure 3.26**), and upon histopathological analysis of spleens and livers between control and monosomic mice. Also, no significant changes were identified by enzyme-linked immunosorbent assay (ELISA) (**Figure 3.26**).

In contrast, a significant decrease in the amount of viable bacteria present in faecal samples (bacterial shedding) was observed between control and monosomic female mice infected with *Citrobacter rodentium* lux on day 13 and 17 post infection (P=0.0237 and P=0.0265 respectively) (**Figure 3.27**). No significant changes were detected in bacterial enumeration of spleens, livers, caecal patches, caecums, distal colons and ceacal contents (**Figure 3.28**), and upon histopathological analysis of spleens, livers, caecums and distal colons between control and monosomic female mice (**Figure 3.29**). The observed significant difference in the number of enumerated bacteria from faecal samples suggests the monosomic females might be resistant to the infection with *Citrobacter rodentium* lux. To confirm this finding, we infected another group of control and monosomic females (n=8 per genotype) with *Citrobacter rodentium* lux. Surprisingly, not only did we not observe any significant difference in the number of enumerated bacteria from faecal samples, but we also noticed that the amount of bacteria present in faecal samples was increased in the monosomic females compared to controls (**Figure 3.30**). After obtaining this contradicting result, we decided to carry

out the infection with *Citrobacter rodentium* lux in a third group of mice (n=8 per genotype). On this occasion, we did not observe a significant difference in the number of enumerated bacteria from faecal samples but we did notice that the amount of bacteria present in faecal samples was decreased in the monosomic females compared to the controls, concomitant with the analysis from the first group (**Figure 3.31**). Thus, in conclusion, analysis of the results from the second and third batch of monosomic females and their wildtype female littermates did not confirm the resistance of the monosomic females to the infection with *Citrobacter rodentium* lux. We can only speculate what may have been responsible for the observed differences in the responses to the infection with *Citrobacter rodentium* lux. It has been observed that even very subtle changes in the microenvironment in which mice are bred and kept, can affect the subsequent response to the bacterial infection (Simon Clare, personal communication). In our experiments, even though all three batches of mice were bred and kept in the same room prior to testing, they were bred at different time-points and kept on different racks, and thus were potentially exposed to slightly different microenvironments.

(A)

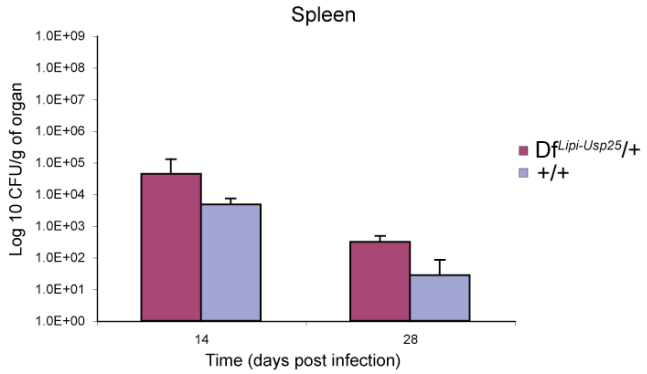

(B)

(C)

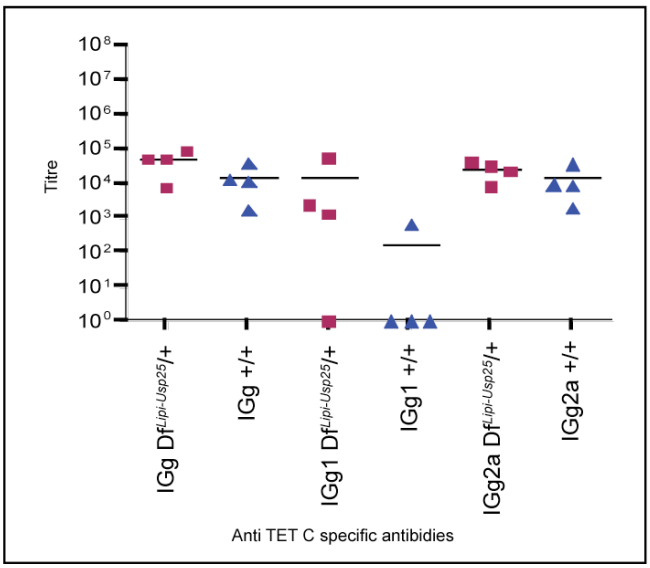

Figure 3.26. Bacterial enumeration and ELISA results for monosomic (*Df*$^{Lipi\text{-}Usp25}$/+) and control (+/+) male littermates infected with *Salmonella* Typhimurium TET C. **(A)** Bacterial counts from spleens collected from monosomic (*Df*$^{Lipi\text{-}Usp25}$/+) and control (+/+) littermates. **(B)** Bacterial counts from livers collected from monosomic (*Df*$^{Lipi\text{-}Usp25}$/+) and control (+/+) littermates. Data was statistically analysed using the two-tailed Mann-Whitney test. At each time-point 4 males per genotype were analysed. **(C)** ELISA assay results for IGg, IGg1 and IGg2a antibodies for monosomic (*Df*$^{Lipi\text{-}Usp25}$/+) and control (+/+) littermates. At each time-point 4 males per genotype were analysed.

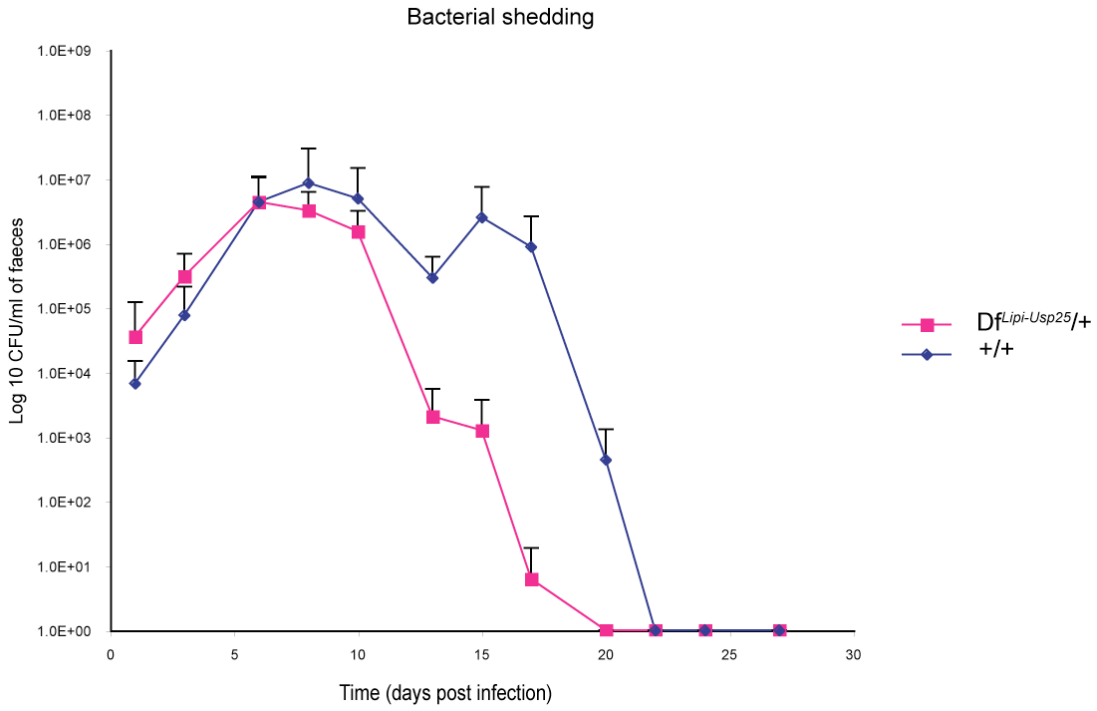

Figure 3.27. Bacterial shedding results for the first group of monosomic (*Df*$^{Lipi\text{-}Usp25}$/+) and control (+/+) female littermates infected with *Citrobacter rodentium* lux. Bacterial counts from faeces collected from monosomic (*Df*$^{Lipi\text{-}Usp25}$/+) and control (+/+) littermates. Data was statistically analysed using the two-tailed Mann-Whitney test. 8 females per genotype were analysed at collection days 0 – 13, while 4 females per genotype were analysed at collection days 14 – 28.

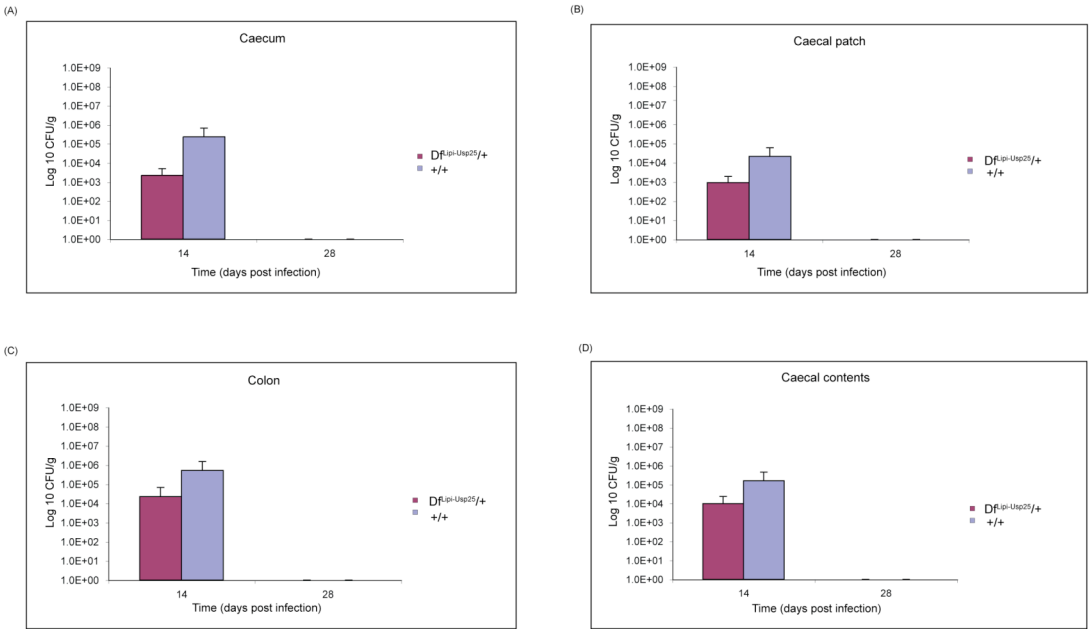

Figure 3.28. Bacterial enumeration results for monosomic (*Df*$^{Lipi\text{-}Usp25}$/+) and control (+/+) female littermates infected with *Citrobacter rodentium* lux. (A) Bacterial counts from caecums collected from monosomic (*Df*$^{Lipi\text{-}Usp25}$/+) and control (+/+) littermates. **(B)** Bacterial counts from caecal patches collected from monosomic (*Df*$^{Lipi\text{-}Usp25}$/+) and control (+/+) littermates. **(C)** Bacterial counts from colons collected from monosomic (*Df*$^{Lipi\text{-}Usp25}$/+) and control (+/+) littermates. **(D)** Bacterial counts from caecal contents collected from monosomic (*Df*$^{Lipi\text{-}Usp25}$/+) and control (+/+) littermates. Data was statistically analysed using the two-tailed Mann-Whitney test. At each time-point 4 females per genotype were analysed.

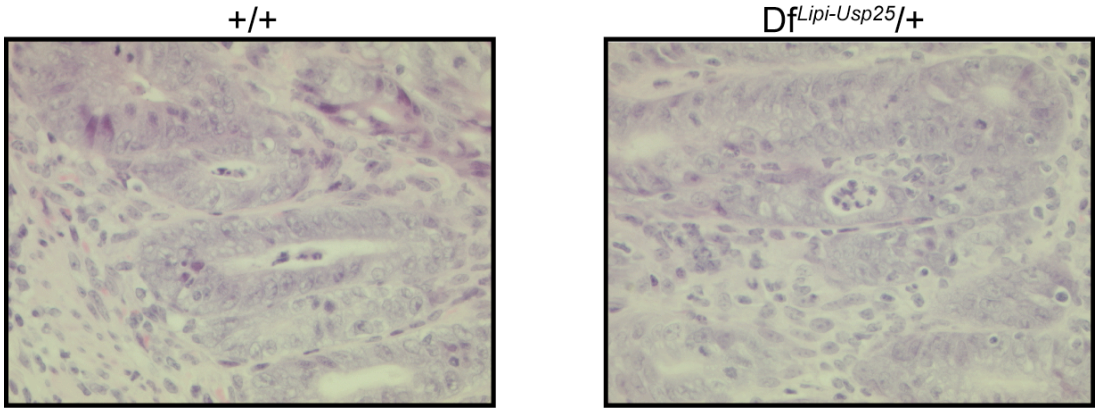

Figure 3.29. Histopathological analysis of caecums collected from control (+/+) and monosomic (*Df*$^{Lipi\text{-}Usp25}$/+) female littermates infected with *Citrobacter rodentium* lux. Haematoxylin and eosin-stained ceacum sections from control (+/+) and monosomic (*Df*$^{Lipi\text{-}Usp25}$/+) littermates. No changes were observed between ceacum sections collected from control (+/+) and monosomic (*Df*$^{Lipi\text{-}Usp25}$/+) littermates. Images are representative and taken at x400 magnification.

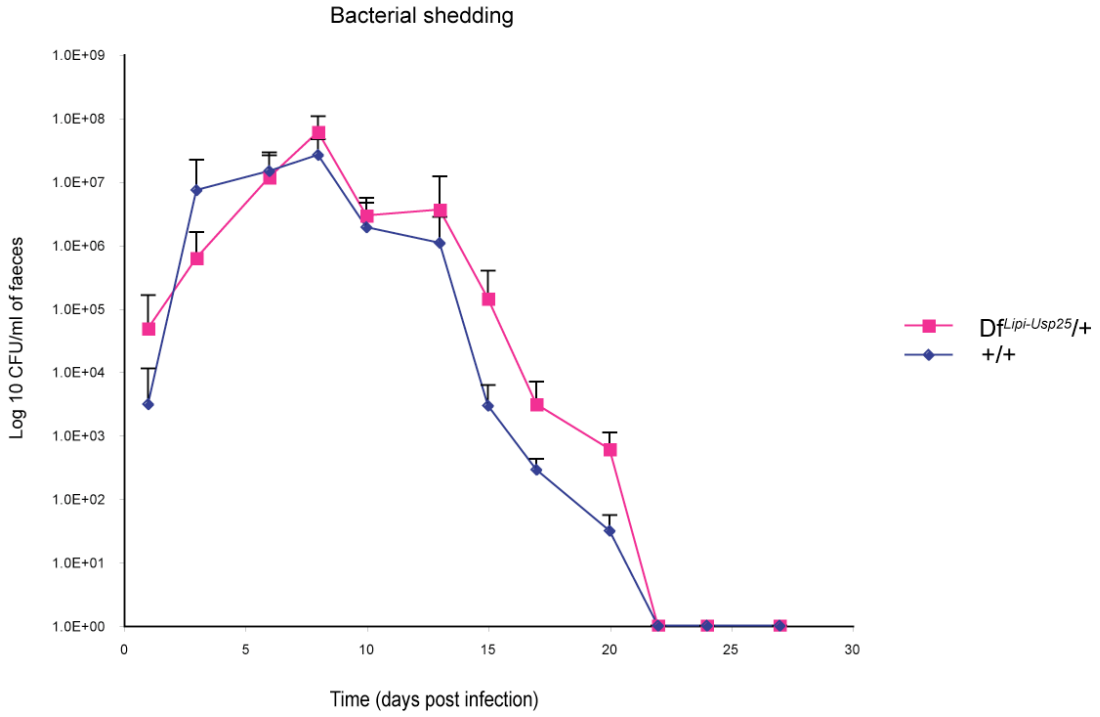

Figure 3.30. Bacterial shedding results for the second group of monosomic (*Df*$^{Lipi\text{-}Usp25}$/+) and control (+/+) female littermates infected with *Citrobacter rodentium* lux. Bacterial counts from faeces collected from monosomic (*Df*$^{Lipi\text{-}Usp25}$/+) and control (+/+) littermates. Data was statistically analysed using the two-tailed Mann-Whitney test. 8 females per genotype were analysed at collection days 0 – 13 were analysed, while 4 females per genotype were analysed at collection days 14 – 28.

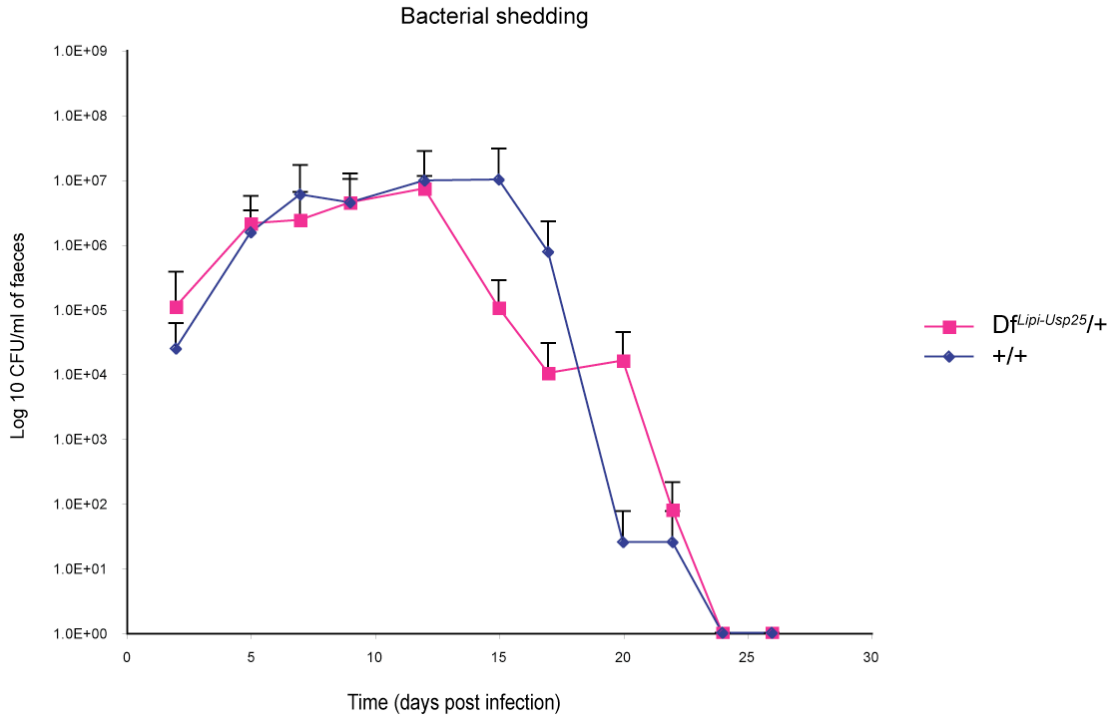

Figure 3.31. Bacterial shedding results for the third group of monosomic (*Df*$^{Lipi\text{-}Usp25}$/+) and control (+/+) female littermates infected with *Citrobacter rodentium* lux. Bacterial counts from faeces collected from monosomic (*Df*$^{Lipi\text{-}Usp25}$/+) and control (+/+) littermates. Data was statistically analysed using the two-tailed Mann-Whitney test. 8 females per genotype were analysed at collection days 0 – 13 were analysed, while 4 females per genotype were analysed at collection days 14 – 28.

3.3.12 AGEING STUDY SUGGESTS AN INCREASED PREDISPOSITION TO TUMOUR FORMATION IN MONOSOMIC MICE

In order to check whether the monosomic and/or nullisomic deletion of the *Lipi–Usp25* region in mice results in an increased predisposition to cancer, monosomic ($Df^{Lipi\text{-}Usp25}$/+) mice were crossed with Bloom's syndrome protein deficient ($Blm^{m3/m3}$) mice to generate a cohort for an ageing study. We used $Blm^{m3/m3}$ mice in our study to increase the chance of obtaining a nullisomic deletion in some cells of the monosomic mice. This is because *Blm*-deficient ES cells have a high rate of mitotic recombination (Guo 2004) and thus the generation of homozygous mutations is significantly elevated in ES cells maintained on a *Blm*-deficient background (Guo 2004). Also, *Blm*-deficient mice show increased susceptibility to cancer, as 29% of *Blm*-deficient mice develop tumours (lymphomas, carcinomas and sarcomas) by 20 months of age (Luo 2000). From all the mice obtained, we selected and further analysed only mice with the following genotypes: $Df^{Lipi\text{-}Usp25}$/+;$Blm^{m3/m3}$ (n=30), $Df^{Lipi\text{-}Usp25}$/+;$Blm^{+/+}$ (n=20), and $Df^{+/+}$;$Blm^{m3/m3}$ (n=10).

The data presented below summarizes the results obtained from this study up until the end of July 2011. At this time, 23 $Df^{Lipi\text{-}Usp25}$/+;$Blm^{m3/m3}$ (77%), 9 $Df^{Lipi\text{-}Usp25}$/+;$Blm^{+/+}$ (45%) and 10 $Blm^{m3/m3}$ (100%) mice had been culled due to illness or found dead.

The most frequent reason mice had to be culled was on humane grounds due to excessive skin ulceration. Specifically, mice from all 3 cohorts developed severe ulceration of their backs, ears, necks, penises or eyes, and were therefore culled (**Table 3.3, Figure 3.32A, 3.32B**). Histopathological analysis of the tissues from these mice showed no pathological changes except increased extramedullary haematopoiesis in the spleen (**Figure 3.32C, 3.32D**), which is a physiological reaction to bleeding from the ulcerated areas. In addition, there were also cases of mice showing severe inflammation and hyperactive bone marrow or multiple abscesses in the kidney (multiple colonies of bacteria surrounded by neutrophils). However, in some cases, when mice were culled due to signs of morbidity (pale extremities, hunched posture and piloerection) or were found dead (**Table 3.3**), histopathological

analysis either did not reveal any pathology or only showed moderate fatty changes in the liver (**Figure 3.33**), similar to that observed in the livers of healthy 1-year-old monosomic mice fed on a normal-fat diet (**Figure 3.12A**). Thus the cause of sickness/death in these mice remains unknown. Macroscopic observations and histopathological diagnosis from all these mice are detailed in **Table 3.3**.

Interestingly, in many cases histopathological analysis showed the presence of cancer (**Table 3.3**). Although mice from all 3 cohorts developed tumours, the incidence was slightly higher in $Df^{Lipi\text{-}Usp25}/+;Blm^{m3/m3}$ (11/23 mice; 48%) than in $Df^{Lipi\text{-}Usp25}/+;Blm^{+/+}$ (3/9 mice; 33%) and $Blm^{m3/m3}$ (2/10 mice; 20%) mice. Of all cancers, lymphoma was the most prevalent, being found in 7/11 $Df^{Lipi\text{-}Usp25}/+;Blm^{m3/m3}$ (63%), 1/3 $Df^{Lipi\text{-}Usp25}/+;Blm^{+/+}$ (33%) and 2/2 $Blm^{m3/m3}$ (100%) mice (**Table 3.3**). The other cancers detected in $Df^{Lipi\text{-}Usp25}/+;Blm^{m3/m3}$ and $Df^{Lipi\text{-}Usp25}/+;Blm^{+/+}$ mice included hepatocellular carcinoma (3 mice), invasive adenocarcinoma of the kidneys and pancreas (1 mouse), adenocarcinoma of the small intestine (1 mouse), undifferentiated carcinoma of the uterus (1 mouse), bone osteosarcoma (1 mouse), and squamous skin carcinoma (1 mouse) (**Table 3.3**).

In order to check for loss of the second *Lipi–Usp25* region in tumour samples collected from $Df^{Lipi\text{-}Usp25}/+;Blm^{m3/m3}$ mice, FISH analysis was performed in the tissue sections mounted on glass slides. In all analysed samples, no homozygous loss of the *Lipi–Usp25* region was detected (**Figure 3.35D, 3.35E, 3.41C, 3.42C**), which is perhaps not so surprisingly given the small sample size (n=3). Interestingly, in the $Df^{Lipi\text{-}Usp25}/+;Blm^{m3/m3}$ mouse diagnosed with invasive adenocarcinoma of the kidney and pancreas, the triplication of the chromosome carrying the deletion of the *Lipi–Usp25* region was observed in 10% of the cells located in the tumour area (kidney and pancreas) (**Figure 3.35E**). Thus, in total for this mouse, 10% of the cells located in the tumour area of the kidney and pancreas had only one wildtype chromosome and four chromosomes with the deletion of the *Lipi–Usp25* region, and so the potential influence of these cells on tumour development and/or progression cannot be ruled out.

Table 3.3. Summary of the histopathological findings observed in culled or dead mice subjected to ageing study that did not develop tumour.

Histopathological findings	Cohort
No histopathological changes	*Df*$^{Lipi\text{-}Usp25}$*/+;Blm*$^{m3/m3}$ *Df*$^{Lipi\text{-}Usp25}$*/+;Blm*$^{+/+}$ *Blm*$^{m3/m3}$
Extramedullary haematopoiesis in the spleen (**Figure 3.32C, 3.32D**)	*Df*$^{Lipi\text{-}Usp25}$*/+;Blm*$^{m3/m3}$ *Df*$^{Lipi\text{-}Usp25}$*/+;Blm*$^{+/+}$ *Blm*$^{m3/m3}$
Moderate fatty changes in the liver (**Figure 3.33**)	*Df*$^{Lipi\text{-}Usp25}$*/+;Blm*$^{m3/m3}$ *Df*$^{Lipi\text{-}Usp25}$*/+;Blm*$^{+/+}$
Inflammation, including: • severe acute inflammation of the bladder, prostate and kidneys in a pattern of a pyelonephritis • severe acute inflammation in the cornea of an eye with the squamous epithelium of the cornea being occupied by neutrophils (**Figure 3.34A**) • severe acute and chronic inflammation in the surface of the heart (**Figure 3.34B**)	*Df*$^{Lipi\text{-}Usp25}$*/+;Blm*$^{m3/m3}$
Multiple abscesses in the kidney; multiple colonies of bacteria surrounded by neutrophils in the kidney	*+/+;Blm*$^{m3/m3}$
Lymphoma, including: • low grade lymphoma in the liver (big foci) (**Figure 3.35A, 3.35B**), and in the spleen and lungs (small foci) • low grade lymphoma in the liver, spleen and lung (**Figure 3.36A, 3.36B**); lymph node with low grade lymphoma in the pancreas • low grade lymphoma in the lungs (big foci), and in the liver, pancreas and salivary glands (small foci) • low grade lymphoma in the liver • low grade lymphoma in the liver and intestine • low grade lymphoma in the kidneys (big foci) (**Figure 3.37A, 3.37B**) and in the pancreas, liver and salivary glands (small foci) • high grade lymphoma in the mesentery of the intestine (**Figure 3.38A**); lymphoma spread into the spleen • high grade lymphoma in the spleen, liver, kidney and abdominal fat • high grade lymphoma in the spleen, thymus, fat, surface of the heart and lungs (**Figure 3.39A, 3.39B**); abdominal lymph node with high grade lymphoma • high grade lymphoma in the liver and kidney (small foci); abdominal lymph node with high grade lymphoma (**Figure 3.40A, 3.40B)**	*Df*$^{Lipi\text{-}Usp25}$*/+;Blm*$^{m3/m3}$ *Df*$^{Lipi\text{-}Usp25}$*/+;Blm*$^{+/+}$ *Blm*$^{m3/m3}$

Table 3.3 continued. Summary of the histopathological findings observed in culled or dead mice subjected to ageing study that developed tumour.

Histopathological findings	Cohort
Adenocarcinoma, including: • invasive adenocarcinoma of the kidneys (**Figure 3.41A, 3.41B**) and pancreas (**Figure 3.41C**) • adenocarcinoma with a moderate level of dysplasia of the small intestine (**Figure 3.42A, 3.42B**)	*Df*$^{Lipi\text{-}Usp25}$*/+;Blm*$^{m3/m3}$
Hepatocellular carcinoma (Figure 3.38B; Figure 3.43A, 3.43B; Figure 3.44A, 3.44B)	*Df*$^{Lipi\text{-}Usp25}$*/+;Blm*$^{m3/m3}$
Invasive malignant undifferentiated carcinoma of the uterus invading into the uterus wall (Figure 3.45A) and fat (Figure 3.45B)	*Df*$^{Lipi\text{-}Usp25}$*/+;Blm*$^{m3/m3}$
Bone osteosarcoma in the tibia and femur (Figure 3.46B), metastatic osteosarcoma in the spleen, kidney, small intestine and liver (Figure 3.46C)	*Df*$^{Lipi\text{-}Usp25}$*/+;Blm*$^{+/+}$
Squamous skin carcinoma invading into the fat (Figure 3.47A, 3.47B)	*Df*$^{Lipi\text{-}Usp25}$*/+;Blm*$^{+/+}$

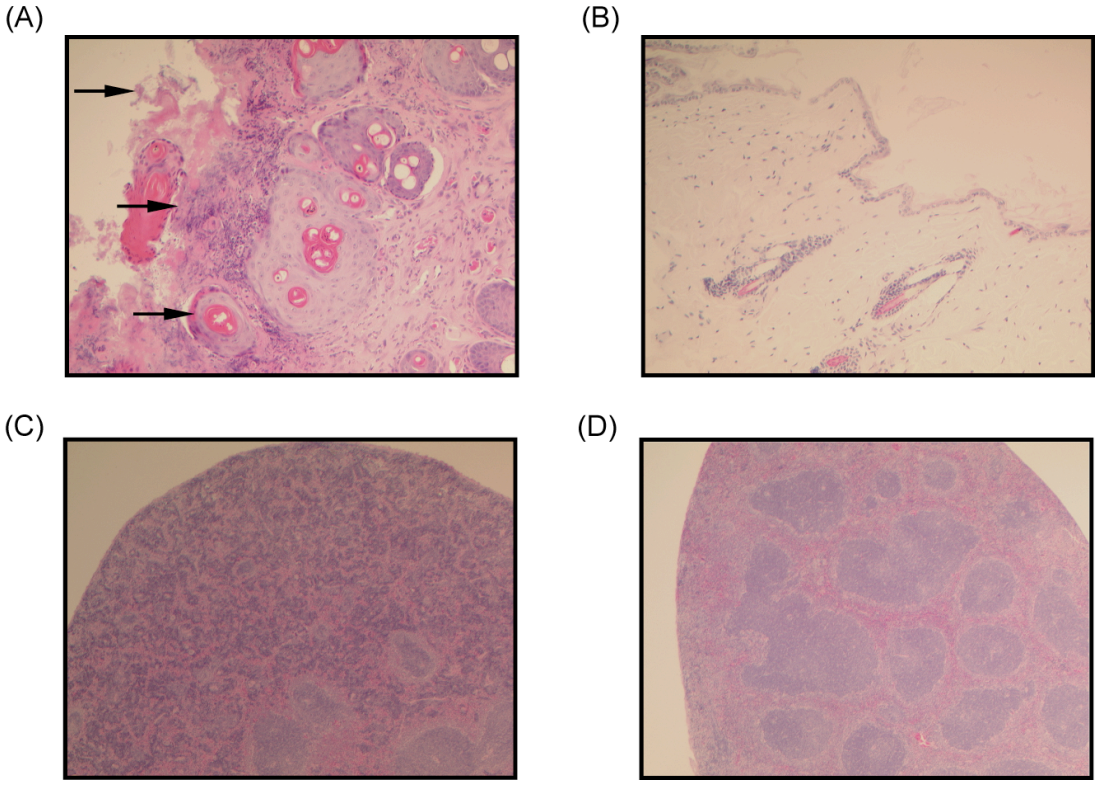

Figure 3.32. Histopathological analysis of haematoxylin and eosin-stained skin sections collected from *Df*$^{Lipi\text{-}Usp25}$/+;*Blm*$^{m3/m3}$, *Df*$^{Lipi\text{-}Usp25}$/+;*Blm*$^{+/+}$ and +/+;*Blm*$^{m3/m3}$ mice that were culled due to severe ulceration. **(A)** Skin ulcer section collected from the *Df*$^{Lipi\text{-}Usp25}$/+;*Blm*$^{m3/m3}$ mouse. The discontinuity of the skin, loss of outer skin layers and inflammation of the tissue can be observed (indicated by arrows). Image is representative and taken at x100 magnification. **(B)** Normal appearance of the skin section collected from the same *Df*$^{Lipi\text{-}Usp25}$/+;*Blm*$^{m3/m3}$ mouse. Sample was collected from a place adjacent to the ulcer. Images are representative and taken at x100 magnification. **(C)** Spleen collected from the *Df*$^{Lipi\text{-}Usp25}$/+;*Blm*$^{m3/m3}$ mouse. Increased extramedullary haematopoiesis can be observed (visible as dark puple staining). Image is representative and taken at x25 magnification. **(D)** Normal appearance of the spleen section collected from a different *Df*$^{Lipi\text{-}Usp25}$/+;*Blm*$^{m3/m3}$ mouse that did not have any skin ulceration. Image is representative and taken at x25 magnification.

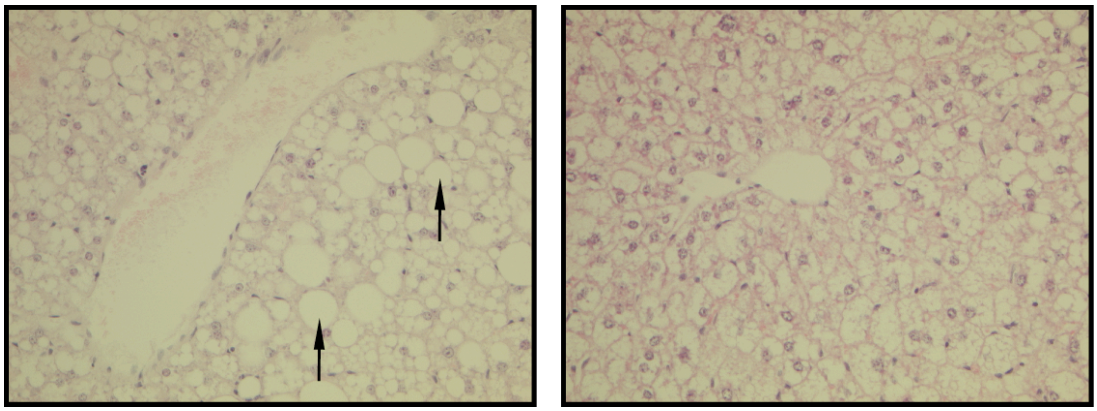

Figure 3.33. Histopathological analysis of haematoxylin and eosin-stained livers collected from *Df*$^{Lipi\text{-}Usp25}$/+;*Blm*$^{m3/m3}$ and *Df*$^{Lipi\text{-}Usp25}$/+;*Blm*$^{+/+}$ mice that were found dead or culled as they looked pale or had hunched piloerection. Livers of some *Df*$^{Lipi\text{-}Usp25}$/+;*Blm*$^{m3/m3}$ and *Df*$^{Lipi\text{-}Usp25}$/+;*Blm*$^{+/+}$ mice showed moderate fatty changes (left side; visible as white oval cells; indicated by arrows) compared to no fatty changes in livers of other *Df*$^{Lipi\text{-}Usp25}$/+;*Blm*$^{m3/m3}$ and *Df*$^{Lipi\text{-}Usp25}$/+;*Blm*$^{+/+}$ mice (right side). Images are representative and taken at x200 magnification.

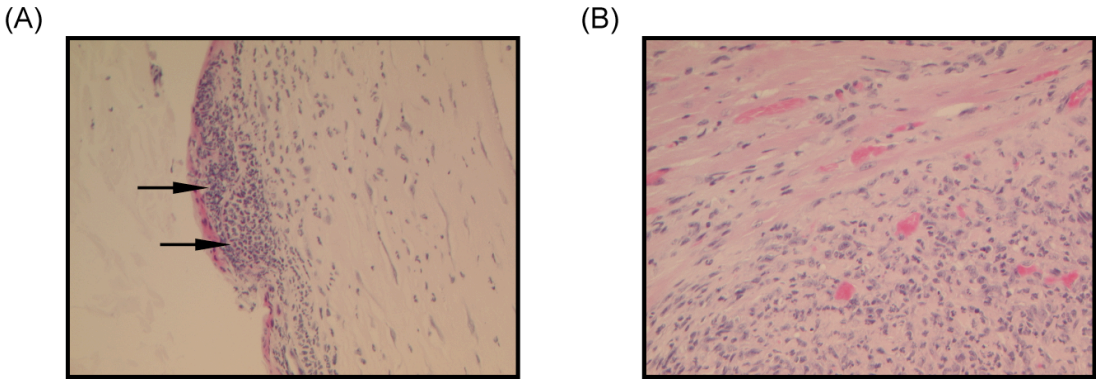

Figure 3.34. Histopathological analysis of haematoxylin and eosin-stained bladder and bone collected from *Df*$^{Lipi\text{-}Usp25}$/+;*Blm*$^{m3/m3}$ mice that were culled sick. (A) Eye section showing the signs of severe acute inflammation in the cornea (indicated by arrows). **(B)** Heart section showing the signs of severe acute and chronic inflammation on its surface. Images are representative and taken at x200 magnification.

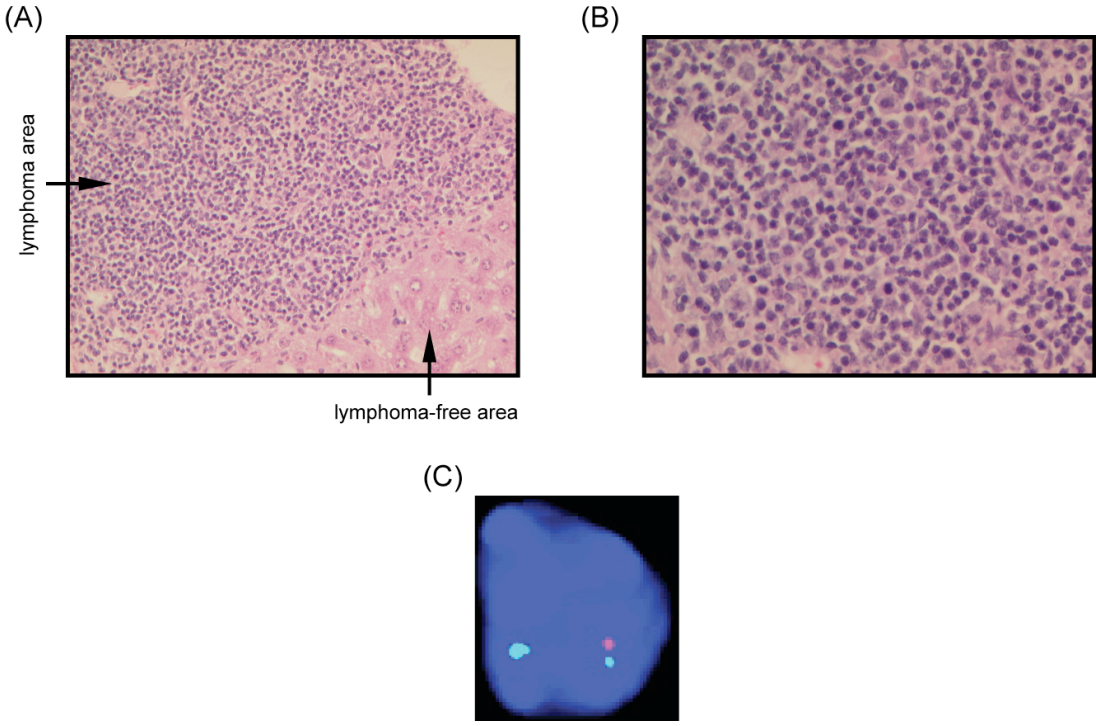

Figure 3.35. Analysis of liver collected from *Df*$^{Lipi\text{-}Usp25}$/+;*Blm*$^{m3/m3}$ mouse. **(A)** Histopathological analysis of haematoxylin and eosin stained liver section showing high grade lymphoma. Arrows show tumour and tumour-free area of liver. Image is representative and taken at x200 magnification. **(B)** Histopathological analysis of haematoxylin and eosin stained section showing lymphoma infiltration into liver. Image is representative and taken at x400 magnification. **(C)** FISH analysis with BAC probes that mapped in the region of the deletion (red) and outside (green) conducted on the tumour area of kidney section. 100% of the cells showed two green and one red signal (normal monosomic cells).

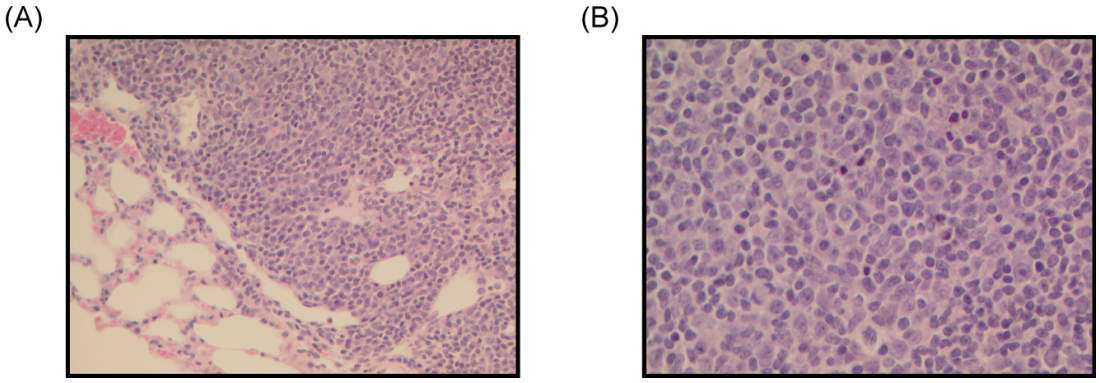

Figure 3.36. Analysis of lungs collected from *Df*$^{Lipi\text{-}Usp25}$/+;*Blm*$^{m3/m3}$ mouse. **(A)** Histopathological analysis of haematoxylin and eosin stained lung section showing low grade lymphoma. Image is representative and taken at x200 magnification. **(B)** Histopathological analysis of haematoxylin and eosin stained lung section showing low grade lymphoma. Image is representative and taken at x400 magnification.

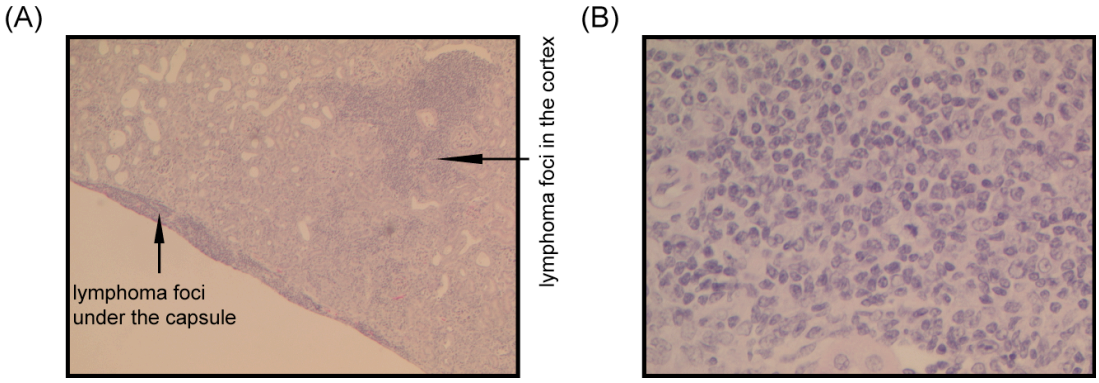

Figure 3.37. Analysis of kidney collected from *Df*$^{Lipi\text{-}Usp25}$/+;*Blm*$^{+/+}$ mouse. (A) Histopathological analysis of haematoxylin and eosin stained kidney section showing high grade lymphoma changes under the capsule and in the cortex. Image is representative and taken at x50 magnification. **(B)** Histopathological analysis of haematoxylin and eosin stained section showing high grade lymphoma in the kidney. Image is representative and taken at x400 magnification.

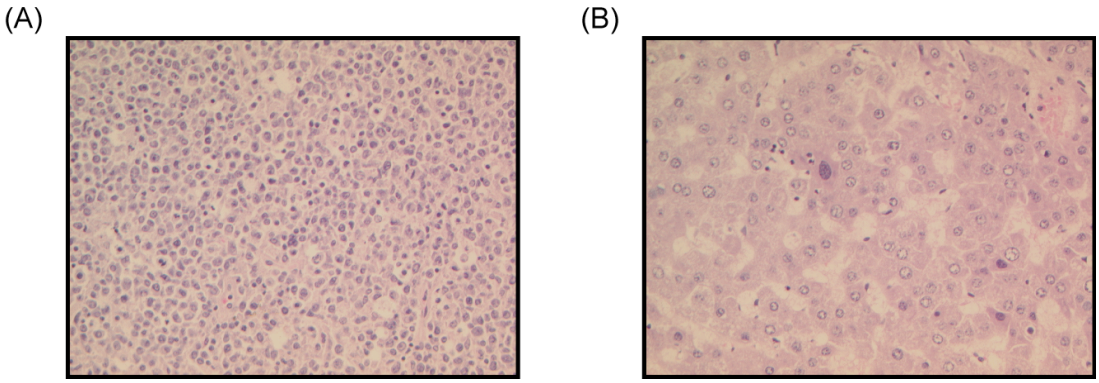

Figure 3.38. Analysis of abdominal lymph node and liver collected from *Df*$^{Lipi\text{-}Usp25}$/+;*Blm*$^{m3/m3}$ mouse. (A) Histopathological analysis of haematoxylin and eosin stained abdominal lymph node section showing high grade lymphoma. Image is representative and taken at x200 magnification. **(B)** Histopathological analysis of haematoxylin and eosin stained section showing hepatocellular carcinoma. Image is representative and taken at x200 magnification.

(A) (B)

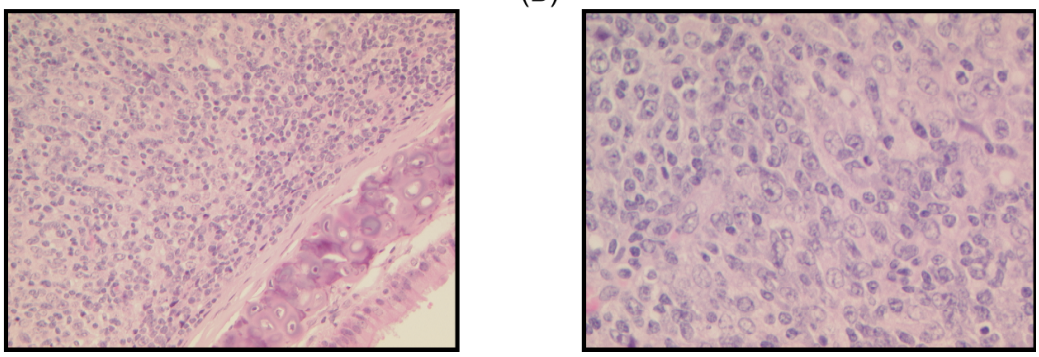

Figure 3.39. Analysis of lungs collected from +/+;*Blm*$^{m3/m3}$ mouse. (A) Histopathological analysis of haematoxylin and eosin stained lung section showing high grade lymphoma in the lung. Image is representative and taken at x200 magnification. **(B)** Histopathological analysis of haematoxylin and eosin stained lung section showing high grade lymphoma in the lung. Image is representative and taken at x400 magnification.

(A) (B)

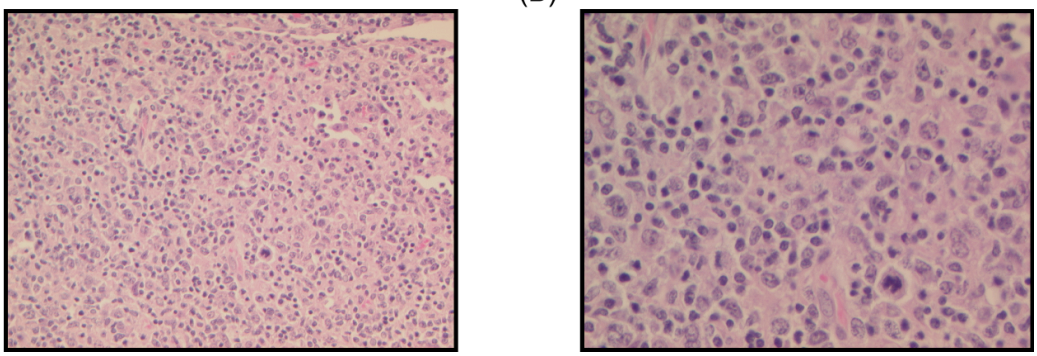

Figure 3.40. Analysis of abdominal lymph node collected from +/+;*Blm*$^{m3/m3}$ mouse. (A) Histopathological analysis of haematoxylin and eosin stained abdominal lymph node section showing high grade lymphoma. Image is representative and taken at x200 magnification. **(B)** Histopathological analysis of haematoxylin and eosin stained abdominal lymph node section showing high grade lymphoma. Image is representative and taken at x400 magnification.

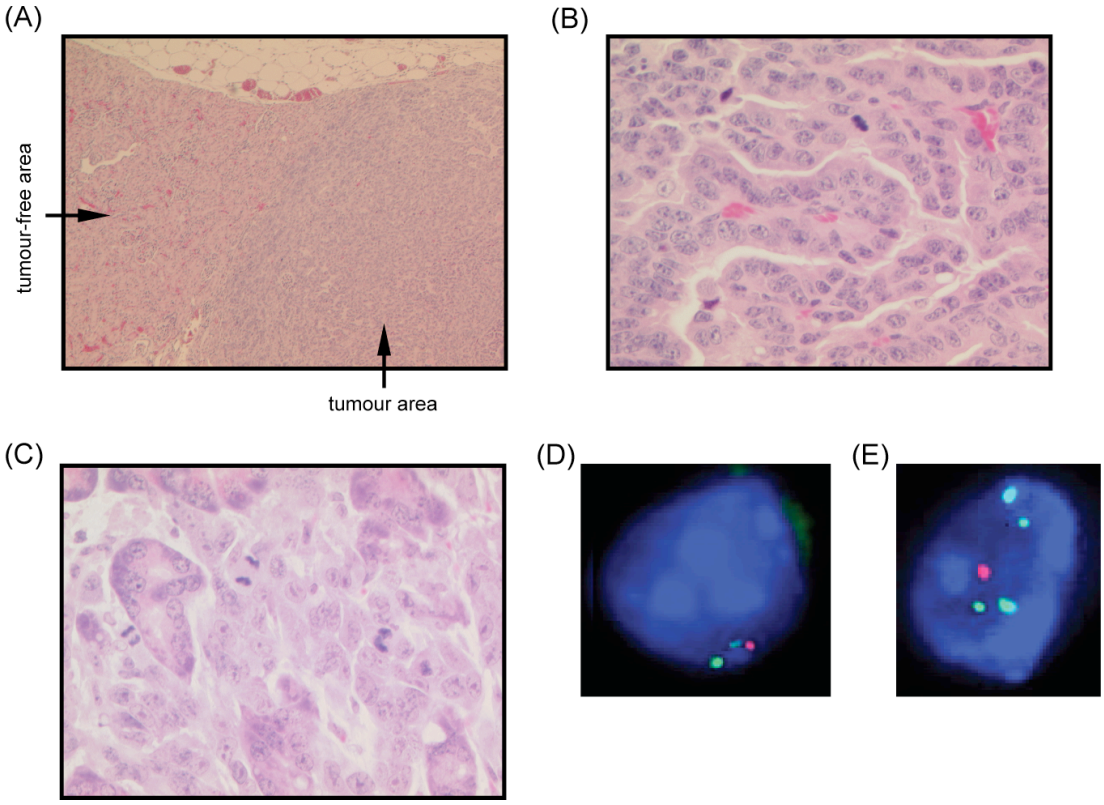

Figure 3.41. Analysis of kidneys and pancreas collected from *Df*$^{Lipi\text{-}Usp25}$/+;*Blm*$^{m3/m3}$ mouse. (A) Histopathological analysis of haematoxylin and eosin stained kidney section showing invasive adenocarcinoma. Arrows show tumour and tumour-free area of kidney. Image is representative and taken at x50 magnification. **(B)** Histopathological analysis of haematoxylin and eosin stained kidney section showing invasive adenocarcinoma changes. Image is representative and taken at x400 magnification. **(C)** Histopathological analysis of haematoxylin and eosin stained pancreas section showing invasive adenocarcinoma changes. Image is representative and taken at x400 magnification. **(D), (E)** FISH analysis with BAC probes that mapped in the region of the deletion (red) and outside (green) conducted on the tumour area of a kidney section. 90% of the cells showed two green and one red signal (normal monosomic cells) **(D)**. Interestingly, 10% of the cells showed four green and one red signal (abnormal cells) **(E)**, thus showing the existence of two additional monosomic chromosomes in the cell.

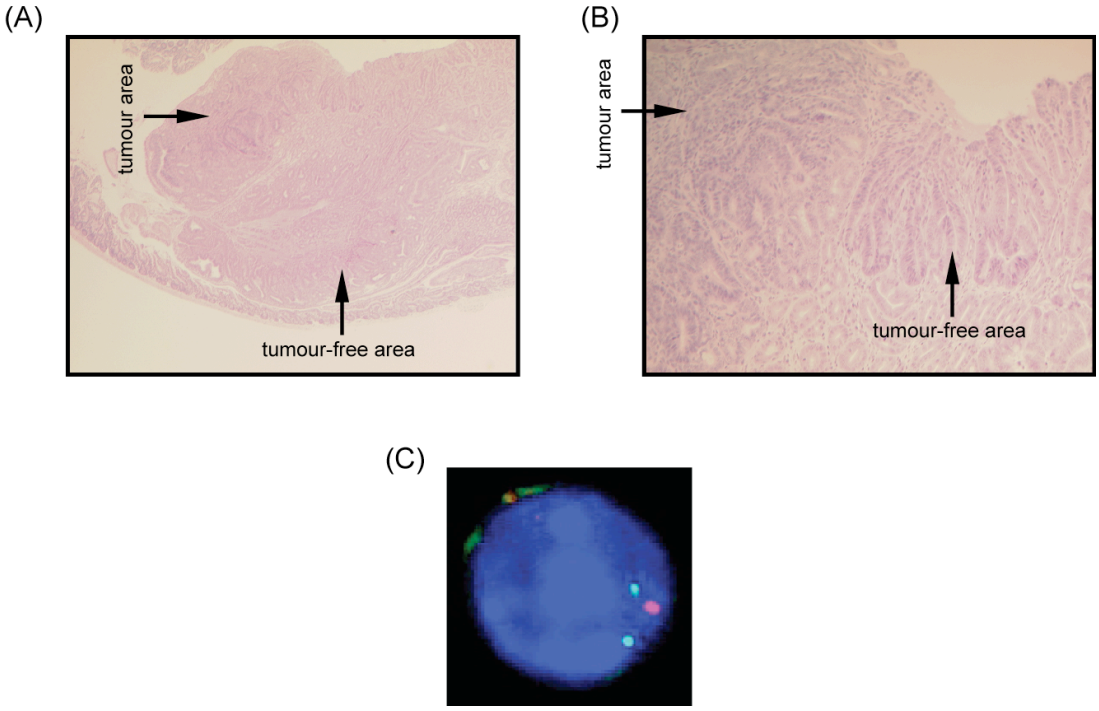

Figure 3.42. Analysis of small intestine collected from *Df*$^{Lipi\text{-}Usp25}$/+;*Blm*$^{m3/m3}$ mouse. **(A)** Histopathological analysis of haematoxylin and eosin stained small intestine section showing adenocarcinoma. Arrows show tumour and tumour-free area of small intestine. Image is representative and taken at x25 magnification. **(B)** Histopathological analysis of haematoxylin and eosin stained small intestine section showing adenocarcinoma changes. Image is representative and taken at x100 magnification. **(C)** FISH analysis with BAC probes that mapped in the region of the deletion (red) and outside (green) conducted on the tumour area of kidney section. 100% of the cells showed two green and one red signal (normal monosomic cells).

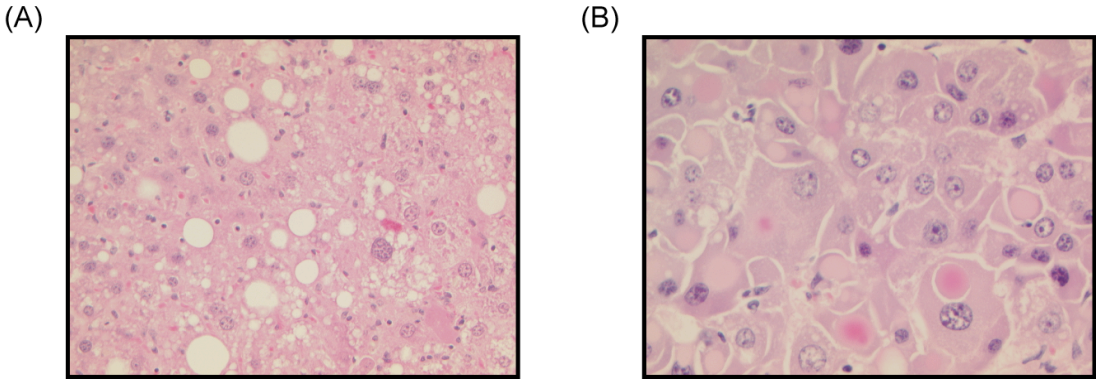

Figure 3.43. Analysis of liver collected from *Df*$^{Lipi\text{-}Usp25}$/+;*Blm*$^{m3/m3}$ mouse. **(A)** Histopathological analysis of haematoxylin and eosin stained liver section showing hepatocellular carcinoma. Image is representative and taken at x200 magnification. **(B)** Histopathological analysis of haematoxylin and eosin stained liver section showing hepatocellular carcinoma. Image is representative and taken at x400 magnification.

(A) (B)

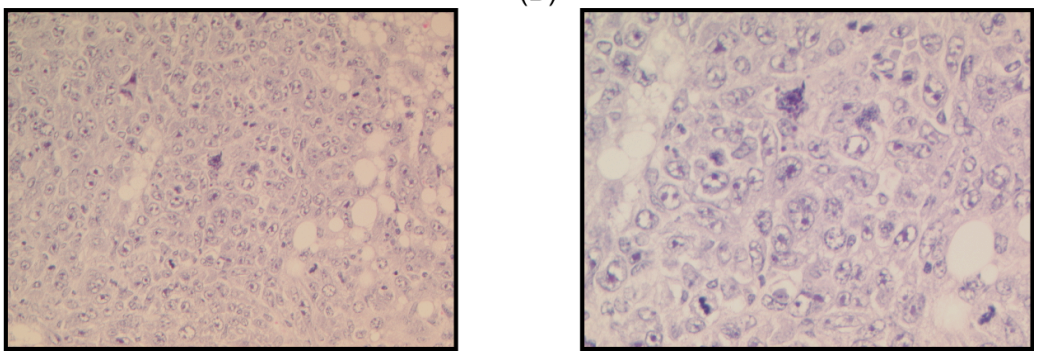

Figure 3.44. Analysis of liver collected from *Df*$^{Lipi\text{-}Usp25}$/+;*Blm*$^{m3/m3}$ mouse. **(A)** Histopathological analysis of haematoxylin and eosin stained liver section showing poorly differentiated hepatocellular carcinoma invading into the fat. Image is representative and taken at x200 magnification. **(B)** Histopathological analysis of haematoxylin and eosin stained liver section showing poorly differentiated hepatocellular carcinoma invading into the fat. Image is representative and taken at x400 magnification.

(A) (B)

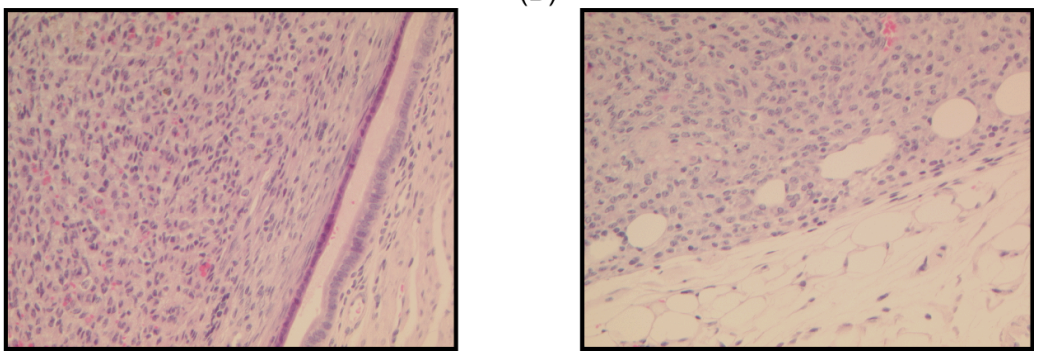

Figure 3.45. Analysis of uterus collected from *Df*$^{Lipi\text{-}Usp25}$/+;*Blm*$^{m3/m3}$ mouse. **(A)** Histopathological analysis of haematoxylin and eosin stained uterus section showing undifferentiated carcinoma invading into the uterus wall. Image is representative and taken at x200 magnification. **(B)** Histopathological analysis of haematoxylin and eosin stained uterus section showing undifferentiated carcinoma invading into the fat. Image is representative and taken at x200 magnification.

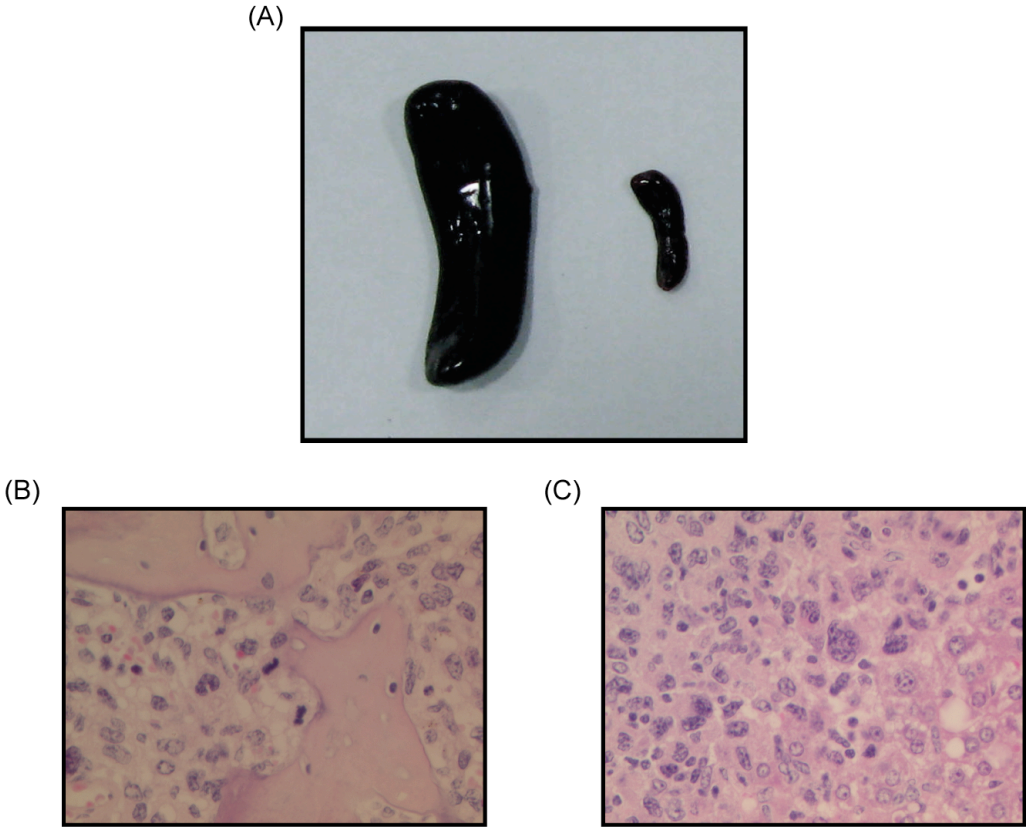

Figure 3.46. Analysis of spleen, bone and liver collected from *Df*$^{Lipi\text{-}Usp25}$/+;*Blm*$^{+/+}$mouse. **(A)** Photo showing greatly enlarged spleen collected from this mouse (left side) compared to a normal spleen (right side) collected from a healthy mouse. **(B)** Histopathological analysis of haematoxylin and eosin stained bone section showing osteosarcoma. Image is representative and taken at x400 magnification. **(C)** Histopathological analysis of haematoxylin and eosin stained liver section showing metastatic osteosarcoma. Image is representative and taken at x400 magnification.

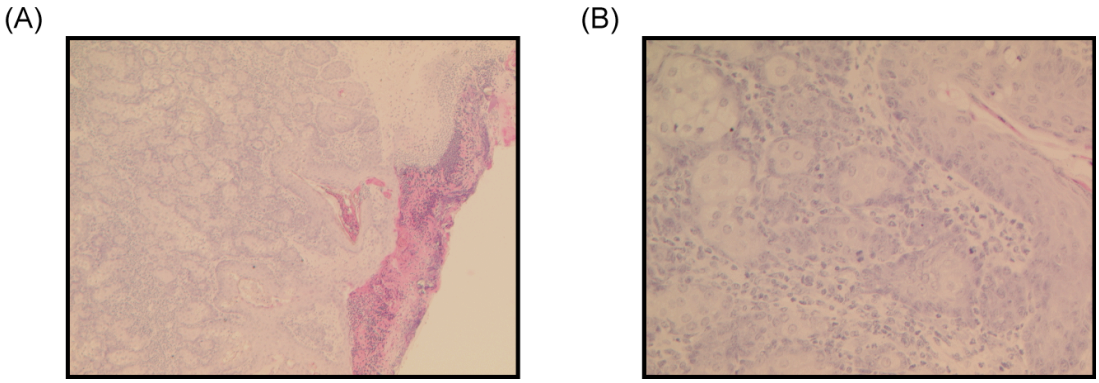

Figure 3.47. Analysis of skin section collected from *Df*$^{Lipi\text{-}Usp25}$/+;*Blm*$^{+/+}$ mouse. **(A)** Histopathological analysis of haematoxylin and eosin stained skin section showing squamous skin carcinoma invading into fat. Image is representative and taken at x50 magnification. **(B)** Histopathological analysis of haematoxylin and eosin stained skin section showing squamous skin carcinoma changes. Image is representative and taken at x400 magnification.

3.4 DISCUSSION

We generated and phenotypically characterized the *Df*$^{Lipi\text{-}Usp25}$ mouse, a monosomic model for the 1.6 Mb *Lipi–Usp25* region. The deleted region is syntenic to the centromeric part of the human chromosome 21, and contains six genes that are conserved between human and mouse.

Homozygous deletion of the region (nullisomy) resulted in mid-gestational embryonic lethality mostly due to neural tube degeneration with evidence of prominent apoptosis, suggesting that at least one of the genes in the *Lipi–Usp25* region is required for the development and maintenance of the neural tube. However, as all six genes in this region are normally expressed in the developing brain of the mouse embryo at both E9.5 and E10.5 (Reymond 2002), and have not been reported to be involved in apoptosis and/or neural tube development, it is difficult to speculate which genes might be responsible. However, two genes, namely *Samsn1* and *Nrip1*, are unlikely to be potential candidates for the observed embryonic lethality, as homozygous null *Samsn1* and *Nrip1* mice are viable (White 2000; Wang 2010).

Detailed phenotypical analysis of monosomic *Df*$^{Lipi\text{-}Usp25}$ mice found them to be viable, fertile and displaying no obvious differences from controls (wildtype littermates) in terms of morphology, motor skills, haematology and clinical chemistry. They did, however, show deficits in long-term memory retention in a socially relevant testing paradigm. Social recognition is hippocampus-dependent (Kogan 2000) and has been used for learning and memory testing (Richter 2005; Engelmann 2011) and for assessing cognitive impairment in mice (Mitsui 2009). The ability of retaining long-term memory is crucial for any learning process and any abnormalities in memory retention can affect learning capacity. Indeed, the observed deficit in long-term memory retention in monosomic *Df*$^{Lipi\text{-}Usp25}$ mice had a significant impact on their learning abilities, as monosomic mice were incapable of distinguishing a familiar stimulus animal from an unfamiliar one 24 hours after the initial training was conducted. As intellectual disability and learning difficulties are identified in all Monosomy 21 patients carrying “centromeric” deletions (Wakui

2002; Tinkel-Vernon 2003, Lyle 2008; Roberson 2010; Lindstrand 2010), it is tempting to speculate that the deficit in long-term memory retention might be at least in part responsible for a decline in learning abilities in Monosomy 21 individuals and thus that haploinsufficiency of a gene (or genes) mapped within the *Lipi–Usp25* deletion may contribute to the intellectual disability/learning impairment of humans with Monosomy 21. However, as all six genes in this region are normally expressed in the developing brain of the mouse embryo (Reymond 2002), and as four of these genes (*Hspa13*, *Samsn1*, *Nrip1* and *Usp25*) are normally expressed in the adult mouse brain, it is hard to speculate which genes might be responsible for observed impairment in learning and long-term memory retention. To date, only the mouse models for the *Samsn1* and *Nrip1* genes have been generated (White 2000; Wang 2010). However, the cognitive abilities of the homozygous and heterozygous *Samsn1* and *Nrip1* mice were not analysed and so these genes cannot be excluded from a list of potential candidates for learning and long-term memory impairment.

Although these monosomic mice did not model the other clinical phenotypes commonly seen in Monosomy 21 patients, given that all currently known Monosomy 21 patients with the “centromeric” deletions span much larger regions of HSA21 than represented in our monosomic mice, we cannot rule out the possibility that genes in the *Lipi–Usp25* region work in synergy with other genes mapped to the “centromeric” region of HSA21, and that only loss of all of these genes together would give the clinical phenotypes observed. In addition, there are 2 genes in the 21q11.2–q21.1 region of HSA21 for which there are no mouse orthologs, namely *ABCC13* and *AF165138.7*. Thus our model does not account for the possible roles that these genes may play in the phenotype.

Monosomic $Df^{Lipi\text{-}Usp25}$ mice fed on a HFD showed a significantly increased fat percentage estimate at 8-, 14-, and 25-weeks of age compared to the controls. However, significant increases in fat percentage estimates over controls were not observed when the monosomic mice were fed a NFD, except at 8-weeks of age. Considering the fact that the overall fat percentage estimate was much higher in both groups of mice on a HFD (containing

21% crude fat) compared to a NFD (containing 9% crude fat), the HFD can be regarded as an environmental factor that increases fat percentage estimates in the mice. Nevertheless, given that monosomic mice showed significantly higher percentage fat estimates than controls, it is clear there is also a genetic factor affecting this phenotypic change. Although the interaction between genetic susceptibility loci and environmental factors in the development of obesity have been shown in different analyses performed both in humans and mice (Poehlman 1986; Bouchard 1990; Heitmann 1995; Asnicar 2001; Luan 2001; Nieters 2002; Sato 2010), to our knowledge this interaction has not been shown before in patients with deletions encompassing the 21q11.2–q21.1 region.

Although four studies have reported on the presence or absence of obesity in Monosomy 21 patients with deletions encompassing the 21q11.2–q21.1 region (Roland 1990; Korenberg 1991; Ahlbom 1996; Tinkel-Vernon 2003), only a study by Roland *et al* found a positive correlation (two cases that showed mild intellectual disability, some facial abnormalities and obesity (Roland 1990)). Unfortunately, without knowledge of the type of a diet of these individuals, we can only speculate as to whether the observed obesity in these patients was caused by the interaction between the genetic component (deletion of the 21q11.2–q21.3 region) and the environmental factor (consumption of food highly-enriched in fat). Thus studies of other obese patients with deletions of/or encompassing the 21q11.2–q21.1 region are required to identify a possible interaction between deletions of this region and a high-fat diet, and to understand a possible link of both genetic and environmental factors with increased fat deposition.

There are six genes in the *Lipi–Usp25* region: *Lipi*, *Rbm11*, *Hspa13*, *Samsn1*, *Nrip1* and *Usp25*. To date, the mouse models for *Samsn1* and *Nrip1* genes have been generated and neither of them showed signs of obesity (White 2000; Wang 2010). Homozygous *Samsn1*-knockout (*Samsn1*$^{-/-}$) mice are viable, fertile and display enhanced adaptive immunity compared to their wildtype littermates (Wang 2010). However, no phenotypic data is available for *Samsn1+/-* mice (Wang 2010). Homozygous *Nrip1*-knockout (*Nrip1*$^{-/-}$) mice are viable but 15–20% smaller than their heterozygous and wildtype

littermates (White 2000). Moreover, *Nrip1*$^{-/-}$ females are infertile due to ovulatory dysfunction, while heterozygous *Nrip1*-knockout (*Nrip1*$^{+/-}$) females are partially infertile (White 2000). In addition, Nrip1 can affect the function of adipose tissue by blocking both mitochondrial respiration and energy uncoupling, as well as preventing expression of key regulatory genes in white adipose tissue (WAT), including the uncoupling protein 1 (*Ucp1*) gene. *Nrip1*$^{-/-}$ mice fed a NFD showed a 20% reduction in body weight compared with wildtype controls, and remained leaner than controls even when fed a HFD (Leonardsson 2004). On average, the body weight of *Nrip1*$^{-/-}$ mice increased by 3.8%, while the body weight of their wildtype littermates increased by 14.5%. The histopathological analysis of WAT showed that adipose cells were much smaller in *Nrip1*$^{-/-}$ mice fed on either diet compared to their wildtype littermates. Histopathological analysis of livers from *Nrip1*$^{-/-}$ mice showed they were resistant to both age-induced hepatic steosis and HFD-induced fatty changes in the liver. The resistance to HFD-induced obesity and hepatic steosis in *Nrip1*$^{-/-}$ mice might be explained by both the increased expression of genes in energy expenditure and mitochondrial uncoupling, and the decreased expression of some genes encoding lipogenic enzymes (Leonardsson 2004). However, it is not known whether the heterozygous deletion of *Nrip1* would provide resistance to HFD-induced obesity and hepatic steatosis, as only *Nrip1-/-* mice were evaluated for their resistance to HFD-induced obesity and hepatic steatosis (Leonardsson 2004). As none of the other genes in the *Lipi–Usp25* region are known to be involved in lipid and carbohydrate metabolism or maintenance of energy homeostasis, it is difficult to hypothesize which missing genes cause the development of HFD-induced increase in fat deposition and fatty changes in the livers of our monosomic mice.

To investigate potential molecular mechanisms leading to the HFD-induced increase in fat deposition in the monosomic mice, we performed microarray expression analysis and found significant differential gene expression in adipocytes between control and monosomic *Df*$^{Lipi\text{-}Usp25}$ mice. qRT-PCR analysis on a subset of these genes found six of them to show significantly altered expression in the monosomic mice relative to controls: transmembrane protein 45a (*Tmem45a*) was upregulated in the monosomic

mice whilst plexin D1 (*Plxnd1*), low density lipoprotein receptor-related protein associated protein 1 (*Lrpap1*), SAM domain, SH3 domain and nuclear localization signals, 1 (*Samsn1*) and lamin A (*Lmna*) were down-regulated.

Of these six genes, knockout mice have been generated for each of the four down-regulated genes (Willnow 1995; Sullivan 1999; Umans 1999; Gitler 2004; Yang 2005; Fong 2006; Davies 2008; Wang 2010). As stated above, *Samsn1*$^{-/-}$ mice are viable, fertile and displayed enhanced adaptive immunity compared to their wildtype littermates (Wang 2010). Homozygous *Plxnd1*-knockout (*Plxnd1*$^{-/-}$) mice all die within the first 24 hours due to abnormal atrial development, congenital heart abnormalities (including defects of cardiac outflow tract and aortic branchial arch), and reduced amount of differentiated smooth muscle cells around arch arteries (Gitler 2004). However, no phenotypic data is available for *Plxnd1*$^{+/-}$ mice (Gitler 2004). Two homozygous *Lrpap1*-knockout (*Lrpap1*$^{-/-}$) mouse models have been generated so far (Willnow 1995; Umans 1999). *Lrpap1*$^{-/-}$ mice were phenotypically identical to their wildtype littermates, expressed a normal level of low-density lipoprotein (LDL) receptor in the liver and brain but showed abnormal activity of lipoprotein receptor-related protein (LRP) expression in the liver and brain due to significant reduction of functional LRP. The reduced activity of functional LRP in the liver resulted in defected clearance of α2-macroglobulin from plasma (Willnow 1995). Umans *et al* confirmed observations made by Willnow *et al* but also reported that nearly 50% of pups died at or shortly after birth (Umans 1999). They found that the expression of both LRP and LDL receptor was significantly increased in pregnant *Lrpap1*$^{-/-}$ females compared to their wildtype littermates, and showed that both LRP and LDL receptor are required for maintenance of a normal lipid metabolism during pregnancy but did not find an explanation for the increased perinatal lethality of *Lrpap1*$^{-/-}$ mice (Umans 1999). No phenotypic data is available for *Lrpap1*$^{+/-}$ mice (Willnow 1995; Umans 1999). Several *Lmna*-knockout (*Lmna*$^{-/-}$) mouse models have been generated up to date to examine the function of lamin A and C, and their involvement in a range of human disorders (Sullivan 1999; Yang 2005; Fong 2006; Davies 2008; Davies 2010). Sullivan *et al* generated *Lmna*$^{-/-}$ mice that lacked the expression of both lamin A and C (Sullivan 1999). At birth *Lmna*$^{-/-}$ mice were identical to both their heterozygous

and wildtype littermates. However, by 4 weeks of age they showed severe growth retardation, and a significant reduction in body weight (around 50% decreased compared to their heterozygous and wildtype littermates) and fat stores. Also, *Lmna*$^{-/-}$ mice displayed an abnormal gait, and their posture showed progressive signs of scoliosis/kyphosis, and none survived past 8 weeks of age. Histopathological analysis of these mice showed absence of WAT, thymic atrophy, reduction in spleen size, and striking evidence of muscular dystrophy. *Lmna*$^{-/-}$ mice also showed changes in the nuclear envelope integrity and mislocalization of emerin in the cardiac and skeletal muscles; such a phenotype resembles Emery-Dreifuss muscular dystrophy (EDMD) (Sullivan 1999). In contrast, *Lmna*$^{+/-}$ mice did not show any phenotypic or histopathological abnormalities, and did not die prematurely (Sullivan 1999). Fong *et al* generated *Lmna*-knockout (*Lmna*^{LCO}) mice that lacked the expression of lamin A only (Fong 2006). Both *Lmna*$^{LCO/+}$ and *Lmna*$^{LCO/LCO}$ mice were phenotypically normal, showed no evidence of growth retardation or muscular dystrophy, and showed no changes in the nuclear shape and envelope integrity or localization of emerin (Fong 2006). Both Yang *et al* and Davies *et al* generated *Lmna*-knock-in mice (*Lmna*$^{HG/+}$ and *Lmna*$^{ggHG/+}$ respectively) that lacked the expression of lamin C and expressed a truncated version of lamin A, commonly known as progerin (Yang 2005; Davies 2008). These two mouse models differed only at one amino acid position, namely methionine in the CaaX motif in the *Lmna*$^{HG/+}$ allele (mice expressed progerin terminating with a farnesylcysteine) was replaced with a leucine *Lmna*$^{ggHG/+}$ allele (mice expressed progerin terminating with a geranylgeranylcysteine). Both *Lmna*$^{HG/+}$ and *Lmna*$^{ggHG/+}$ mouse models expressed progerin, a protein that is synthetized instead of normal prelamin A in humans with Hutchinson-Gilford progeria syndrome (HGPS), a very rare genetic disorder that is characterized by a variety of ageing-like phenotypes, such as osteoporosis, premature atherosclerosis alopecia, cardiovascular problems, loss of eye sight and hair (Yang 2005; Davies 2008). Both *Lmna*$^{HG/+}$ and *Lmna*$^{ggHG/+}$ mouse models displayed a variety of phenotypes. However, neither of them showed changes in body weight and fat stores. In particular, *Lmna*$^{HG/+}$ mice showed growth retardation, and developed a bone-disease phenotype (bone fragility) before 4 months of age (Yang 2005). In

contrast, *Lmna*$^{ggHG/+}$ mice developed a milder bone-disease phenotype and lived longer compared to *Lmna*$^{HG/+}$ mice (Davies 2008). Davies *et al* also generated another homozygous *Lmna*-knock-in mouse (*Lmna*$^{nPLAO/nPLAO}$) that expressed only non-farnesylated prelamin A (Davies 2010). *Lmna*$^{nPLAO/nPLAO}$ mice had normal weight and did not exhibit a bone-disease phenotype (bone fragility). They showed apparently normal development up to 20 weeks of age when premature mortality started to be evident due to a dilated cardiomyopathy. No phenotypic data was available on *Lmna*$^{nPLAO/+}$ mice (Davies 2010).

Taken altogether, out of the currently available mouse models for the *Plxnd1*, *Lrpap1*, *Samsn1* and *Lmna* genes, only *Lmna*$^{-/-}$ mice showed changes in body weight and fat stores, namely they exhibited significant reduction in body weight and fat stores (Sullivan 1999). No changes in body weight and fat stores were observed in heterozygous *Lmna*-knockout and knock-in mouse models, meaning that these mice retained some level of lamin A and/or C expression (Sullivan 1999; Yang 2005; Fong 2006; Davies 2008). As *Lmna* expression was significantly decreased but still detectable in our monosomic mice, which resembles *Lmna* expression observed in heterozygous *Lmna*-knockout and knock-in mice, we believe that decreased *Lmna* expression may have had no influence on changes in fat percentage in our monosomic *Df*$^{Lipi\text{-}Usp25}$ mice.

Interestingly, point mutations in the lamin A or C gene result in familial partial lipodystrophy of the Dunnigan type 2 (FPLD2 OMIM ID: 151660), which is an autosomal dominant disorder characterized by loss of subcutaneous adipose tissue in the limbs and buttocks from puberty, accumulation of fat in the neck and face, liver steosis, and insulin resistance (Wojtanik 2009). FPLD-transgenic mice expressed in their adipose tissue one copy of either human lamin A or C containing the most common R482Q mutation. FPLD-transgenic mice displayed many features that are observed in human patients with FPLD2, including insulin resistance, fatty livers, and lack of subcutaneous adipose tissue accumulation starting several weeks postnatally related to defects in preadipocytes differentiation into functional adipocytes (Wojtanik 2009). Thus abnormal distribution and differentiation of adipose tissue in FPLD2 patients prompts the question of a possible association

between common single nucleotide polymorphisms (SNPs) in *LMNA* and increased risk of obesity. Indeed, an association between the *LMNA* 1908T/C SNP and elevated plasma leptin concentration, and increased obesity-related indices, including body mass index (BMI), body fat percentage and ratio of waist-to-hip circumference was identified in 306 adult nondiabetic aboriginal Canadian Oji-Cree population (Hegele 2000). The association between the *LMNA* 1908T/C SNP and obesity-related indices was subsequently replicated in 186 adult nondiabetic aboriginal Canadian Inuits (Hegele 2001). However, no association between the *LMNA* 1908T/C SNP and obesity-related indices was found in 255 adult Pima Indians (Weyer 2001). Instead, an association between the *LMNA* 1908T/C SNP and smaller age-, sex- and body fat percentage-adjusted mean subcutaneous abdominal adipocyte size was identified (Weyer 2001). Thus further studies are required to confirm the association between the *LMNA* 1908T/C SNP and obesity-related indices.

Monosomy 21 is a rare human disease with variable clinical appearances due to differing gene dosage errors on chromosome 21 resulting in variable severity and expressivity of major phenotypic features, including intellectual disability, dysmorphism, and cardiac and/or renal abnormalities (Chettouh 1995; Riegel 2005; Lyle 2008; Lindstrand 2010; Roberson 2010). Attempts to generate genotype-phenotype correlations in this disease are complicated by both the small number of patients available for study (there is a lack of informative sets of partial Monosomy 21 patients (Lyle 2008)) and the fact that some patients with Monosomy 21 also carry anomalies involving other human chromosomes, such as segmental trisomies and deletions (Lyle 2008; Katzenstein 2009). We show here that haploinsufficiency of a gene (or genes) in the *Lipi–Usp25* region of MMU16, syntenic to the human 21q11.2–q21.1 region, results in a deficit in memory retention and high-fat diet-induced increase in fat deposition in monosomic mice. These partially monosomic mice have contributed new insights into genes involved in Monosomy 21-associated intellectual disability and will play a critical role in future studies of genotype-phenotype correlations in Monosomy 21 patients and unraveling of the molecular mechanisms underlying this phenotype. Moreover, some changes in gene expression in subcutaneous fat of the

monosomic mice were identified, including down-regulation of *Samsn1* (one of the deleted genes in this region) and *Lmna*, although there is complex genetic regulation of fat metabolism and deposition contributing to obesity, involving gene expression in the central nervous system, liver, central and peripheral fat amongst other places. Thus further studies will be required to understand the molecular causes of increased fat deposition.

Detailed histopathological analysis of monosomic $Df^{Lipi\text{-}Usp25}$ mice found no anatomical abnormalities of any organs. Initial results, suggesting the existence of decreased endochondral ossification in the cartilage of tibias of 10-week old monosomic mice fed on a NFD, were not replicated in further studies. Specifically, normal levels of bone mineral density (BMD) and cartilage endochondral ossification were observed in 8-, 25-week and 1-year old monosomic mice, and no differences in the level of calcium deposition were detected between a 25-week old control and monosomic mice. Thus we concluded that a deletion of the *Lipi–Usp25* region does not play a role in bone development and metabolism. We also decided to test a hypothesis linking increased fat mass with increased bone mass, thus suggesting a protective effect of fat mass on bone tissue (Zhao 2008; Holecki 2010). However, we did not observe any differences in the level of BMD at 8 or 25 weeks of age between control and monosomic mice fed on either a NFD or a HFD. Thus altogether our results do not support the hypothesis of a beneficial effect of increased fat mass on bone tissue.

Analysis of monosomic $Df^{Lipi\text{-}Usp25}$ males showed no changes in the susceptibility to infection with *Salmonella* Typhimurium TET C. Although initial results suggested a decrease in the susceptibility of the monosomic females to infection with *Citrobacter rodentium* lux, this finding was not replicated in further studies. We speculate that our inability to confirm the resistance of the monosomic females to the infection with *Citrobacter rodentium* lux in our further analysis might be related to subtle differences in the microenvironment (e.g. breeding and keeping different batches of mice on different racks), to which different batches of tested mice were exposed, as even small changes in the microenvironment has been reported to influence murine responses to the bacterial infection (Simon Clare; personal communication).

The tumour watch study consisting of 30 *Df*$^{Lipi\text{-}Usp25}$*/+;Blm*$^{m3/m3}$, 20 *Df*$^{Lipi\text{-}Usp25}$*/+;Blm*$^{+/+}$ and 10 *+/+; Blm*$^{m3/m3}$ mice was set up to validate whether monosomic and/or nullisomic deletion of the *Lipi–Usp25* region increases a risk of developing cancer, as partial loss of the proximal end of the long arm of human chromosome 21 has been found in several types of solid tumours, including cancers of the ovary, stomach, breast, oral cavity and bone (Cliby 1993; Ohgaki 1998; Yamamoto 2003; Aoki 2005; Chen 2005; dos Santos Aguiar 2007), and heterozygous deletions spanning the chromosomal region 21q11.2–q21.1 have been detected in 50 cancer cell lines (see dataset released by the Cancer Genome Project; http://www.sanger.ac.uk/cgi-bin/genetics/CGP/cghviewer/CghHome.cgi). At the point of writing this thesis (the end of July 2011), the tumour watch study is still ongoing, as 7 *Df*$^{Lipi\text{-}Usp25}$*/+;Blm*$^{m3/m3}$ (23% of the cohort) and 11 *Df*$^{Lipi\text{-}Usp25}$*/+;Blm*$^{+/+}$ (55% of the cohort) mice are still alive. Nevertheless, histopathological analysis of the mice that have been culled or found dead, revealed the presence of cancer in 11 *Df*$^{Lipi\text{-}Usp25}$*/+;Blm*$^{m3/m3}$ (48%), 3 *Df*$^{Lipi\text{-}Usp25}$*/+;Blm*$^{+/+}$ (33%) and 2 *Blm*$^{m3/m3}$ (20%) mice. The tumours found in *Df*$^{Lipi\text{-}Usp25}$*/+;Blm*$^{m3/m3}$ mice included 7 lymphomas and 6 carcinomas (including 3 hepatocellular carcinomas, 1 invasive adenocarcinoma of the kidneys and pancreas, 1 adenocarcinoma of the small intestine, and 1 undifferentiated carcinoma of the uterus). 1 lymphoma, 1 bone osteosarcoma and 1 squamous skin carcinoma were among the tumours found in *Df*$^{Lipi\text{-}Usp25}$*/+;Blm*$^{+/+}$ mice, while 2 lymphomas were detected in *Blm*$^{m3/m3}$ mice. Although these findings are preliminary, the development of tumours in *Df*$^{Lipi\text{-}Usp25}$*/+;Blm*$^{+/+}$ mice and higher incidence of tumours in *Df*$^{Lipi\text{-}Usp25}$*/+;Blm*$^{m3/m3}$ mice compared to *Blm*$^{m3/m3}$ alone suggests that a gene (or genes) mapped within the *Lipi–Usp25* region plays a role in cancer development and/or progression.